Master of Science

Hydrothermal synthesis of carbon dot and their uses in fluorescence sensor

The Graduate School of University of Ulsan

School of Chemical Engineering

Hye Jin Lee

Hydrothermal synthesis of carbon dot and their uses in fluorescence sensor

Supervisor: Professor Seung Hyun Hur

A Dissertation

Submitted to

the Graduate School of the University of Ulsan

In partial Fulfillment of the Requirements

for the Degree of

Master

by

Lee, Hye Jin

School of Chemical Engineering

University of Ulsan, Korea

February 2021

Hydrothermal synthesis of carbon dot and their uses in fluorescence sensor

This certifies that the master's thesis

of Hye Jin Lee is approved.

Committee Chair Prof. Won Mook Choi

Committee Member Prof. Seung Hyun Hur

Committee Member Prof. Jin Suk Chung

School of Chemical Engineering

University of Ulsan, Korea

February 2021

Acknowledgement

For over three years including life when I was undergraduate student, I'm not sure it is really good choice or not in terms of general opinion from my family and relative. My father doesn't like this university and firstly not allow me to study for a long time. But, now, he said me "I hope you don't stop studying and study harder and harder". So, I'm really grad to hear this sentence.

I want to express my appreciation to my supervisor Seung Hyun Hur because I obtained valuable experience about both social community and research. And, to be honestly, I really love my professor as a teacher. I hope my professor also think me his excellent pupil.

I appreciate three committee members, prof. Seung Hyun Hur, prof. Won Mook Choi and prof. Jin Suk Chung, because they spend valuable and expensive time for reviewing my master's thesis.

Finally, I'm thankful for my lab member, very smart teacher, Dr. Jayasmita Jana, Linh, Linlin, Sui, Phuc, Diem. I also thankful for Khoi who is studied carbon dot and firstly teach me how to synthesize the carbon dot. I really hope they get a good job and they have much happier life. Thank you.

Abstract in Korean

탄소 동소체 중 하나로 알려진 탄소 양자점은 비독성, 높은 흡광 계수와 양자 효율로 인해 많은 관심을 받아왔으며, 특히 형광 센서 로서의 응용이 많이 연구되어 온 바가 있다.

형광 센서는 감응 속도에서의 이점과 적은 농도만 이용하더라도 센서로 응용이 가능하여 비용 측면에서 유리하다는 점 등 다른 방법들에 비해 많은 장점을 가지고 있다.

그러나 먼저, 탄소 양자점의 경우 형광 센서로서 가져야 하는 기본 성능인 광학적 성질에 대한 규명이 정확히 이루어지지 않았으며 이를 형성하는 원리 또한 밝혀져 있지 않다는 한계를 가지고 있었다.

또한, 양자를 기반으로 하는 형광 센서의 경우, 형광 센서 성능의 지표가 될 수 있는 감도(Sensitivity)에 강하게 영향을 미치는 전자 전달(Electron transfer)에 대한 많은 수학적 모델이 개선되었음에도 불구하고 여전히 한계를 가지고 있었다.

본 연구에서는 탄소 양자점 합성 기법 가운데 가장 많이 연구된 수열 합성이라는 방법을 기반으로 다양한 전구 물질(Precursor)를 이용하여 전구 물질 디자인에 이바지하고자 하였고 또한 형광 센서의 원리로 이용되는 Inner-filter effect 에 대한 수학적 모델을 도입하여 형광 센서 발전에 있어 도움이 되고자 한 바가 있다.

Abstract in English

Carbon dots (CDs) are one of the carbon allotropes that consist of sp^2 carbon atoms, such as graphene, carbon nanotube (CNT), and fullerene. They have generated a lot of interest because of their non-toxicity, high extinction coefficient, and quantum yield. These CDs have been used in fluorescence sensors to detect hazardous Fe^{3+} and Hg^{2+} ions.

The fluorescence sensors have a rapid response because of their short lifetime (μs ~ ns), which normally decreases within the analytes. In addition, only trace amounts of fluorescent material needs to be detected, which save the cost of the manufacturing process. The detection mechanism is being studied in the fields of supramolecular chemistry and organic dyes. Therefore, the mechanism can be explained easily by traditional spectroscopy theory.

However, the actual formation and fluorescence mechanisms of the CDs have not been determined and have been always controversial because of the quantum mechanics involved. Therefore, a rational design of the CDs is difficult.

The most important feature of a sensor is its sensitivity. The sensitivity strongly depends on the electron transfer, which is regarded as the main mechanism of the fluorescence sensors. Although there are improved mathematical models of the fluorescence sensors, the actual model has not been developed.

In this study, we fabricated the CDs using various precursors to systematically investigate the design of the precursors. We introduced a mathematical model for the inner-filter effect, one of the quenching mechanisms, for application in developing a fluorescence sensor based on the CDs.

Contents

Chapter 3. Fabrication of dual emission carbon dots and its use in highly sensitive thioamide detection

Chapter 4. Uncovering the actual inner-filter effect between highly efficient carbon dots and nitroaromatics

Figure list

Table list

Chapter 1. Introduction

1.1. Carbon dots

The carbon allotropes are composed of sp^2 and sp^3 carbon atoms, whose ratios determine their properties. These carbon allotropes are classified as 0D that includes fullerenes, onion-like carbons (OLC) structures, carbon dots (CDs), and nanodiamonds; 1D that which includes carbon nanotubes (CNTs), carbon nanofibers; and 2D that includes graphene, graphene nanoribbons, and few-layer graphenes [1].

CD is a comprehensive term for various nanosized carbon materials [2]. Therefore, the CDs can be defined based on two conditions, that is, a transmission electron microscopy (TEM) image that shows an almost spherical shape and an elemental analysis showing a high ratio of carbon atoms. It is not fully understood whether the sp^2 cluster exists in the carbon core or not. This makes it different from other carbon allotropes. Meanwhile, atomic resolution imaging shows that graphene has a hexagonal structure [3], unlike CDs. However, it is difficult to obtain atomic resolution images of the CDs because organic compounds are easily burnt by an accelerated electron beam. Typically, the CDs are regarded as carbonaceous nanoparticles synthesized using bottom-up synthesis, which is the assembly of small molecules to form large products. However, some researchers use the term bottom-up synthesis for polymer dots [2,4]. Consequently, it is difficult to determine the actual mechanism for the formation of CDs despite several previous attempts [5–7]. To our knowledge, no researcher knows whether the actual CDs exist or not.

Despite this knowledge gap, the CDs have generated a lot of interest because of their superior optical properties, such as high extinction coefficient and high quantum yield [8–9]. Further popularity can result from easier understanding of the meaning of CDs. The photostability of

the CDs is also not fully understood because the data are not presented in papers. Moreover, the CDs show little difference in cytotoxicity, hence a cell viability test is required [10].

The CDs can be synthesized by pyrolysis [5,11], hydrothermal [6–7], microwave [12], sonochemical synthesis (ultrasonication) [13], and reflux heating [14]. The term "graphene quantum dot" is also used because the CDs were not defined in the early 2010s [6,11], although they were synthesized using the bottom-up approach. Nowadays, researchers generally use the term "carbon dot."

The hydrothermal method is the most popular method for the synthesis of the CDs. This is a mature technology that has been used to determine controllable factors, such as temperature, heating ratio, and reaction time [6–7, 15–16]. Many precursors can be adjusted during the synthesis of the CDs by the hydrothermal method. The highest quantum yield (94 %) of the CDs has been reported using the hydrothermal method [6]. Meanwhile, microwave-assisted synthesis negatively affects biological systems [17], although it has a short reaction time [12] that is conducive for effective production systems. Pyrolysis also has a shorter reaction time than the hydrothermal method; however, its lower quantum yield is of concern [11].

The purification of CDs is necessary for effective manufacture of the CDs. Dialysis tubes are generally used for 24–48 h; however, they are expensive and take a long time [16]. Magnetic separation and ethanol precipitation have been developed [18–19]; however, they can only be used in special cases.

Scientists who will work on carbon dots in the future are strongly warned that proving the formation and photoluminescence mechanisms of the CDs is difficult, so is determining the fundamental principle behind these phenomena because of the comprehensive term, carbon dot.

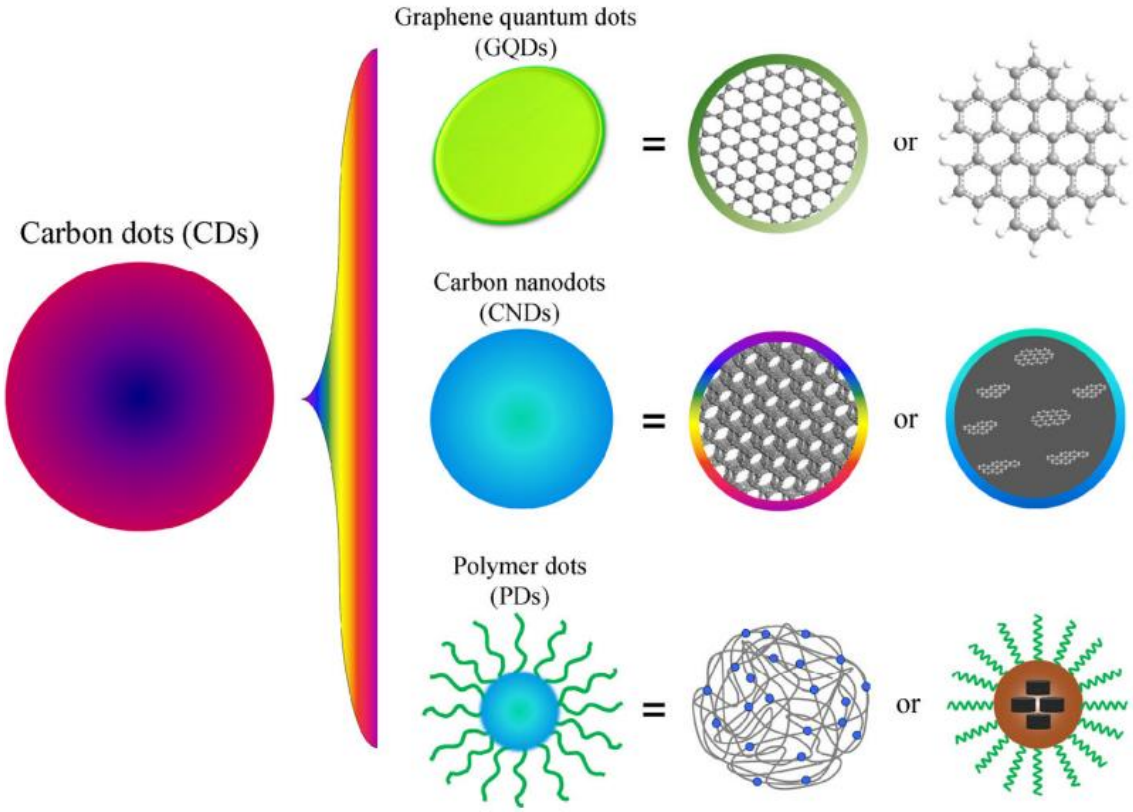

Fig 1.1. Three types of fluorescent CDs: graphene quantum dots (GQDs), carbon nanodots (CNDs), and polymer dots (PDs)

1.2. Fluorescence sensor

The most important advantages of fluorescence sensors are their rapid response from a short lifetime [20] and fast light velocity. Consequently, signaling exploits fluorescence, not phosphorescence, except in specific cases, such as distinguishing signals from autofluorescence in biological systems [21] and complex security systems for counterfeit detection [22]. Furthermore, the lifetime of fluorescence is typically longer when the fluorescent materials interact with analytes (dynamic quenching) [23]. However, the lifetime does not always decrease, as referred to by the terms, static quenching and inner-filter effect [24].

The fluorescence sensors do not always correctly detect various hazardous compounds and diseases [25]. This is because their sensitivity (the most important factor in sensing performance) has a strong relationship with the electron transfer or the electron path.

For example, electron transfer is caused by voltage while photoinduced electron transfer (PET) is driven by light energy. The energy source causes a difference in the electron population resulting in electron transfer and different electron pathways [26]. This is observed as a change in conductivity and intensity. In other words, there is one effective method for each analyte or disease. In addition, different signals can be obtained in specific systems [27].

1.3. Quenching mechanism

Quenching mechanism is important because literature related to fluorescence sensors refers to quenching as the main signaling method [28]. The quenching power has a strong relationship with sensitivity, one of the most important factors that affect sensing performance. The quenching mechanism is separated into PET, intramolecular charge transfer (ICT), metal–ligand charge transfer (MLCT), twisted intramolecular charge transfer (TICT), electronic energy transfer (EET), fluorescence resonance energy transfer (FRET), and excimer/exciplex formation [29]. One of the most common mechanism is photoinduced electron transfer (PET).

One of the most common mechanisms is PET. To evaluate whether this mechanism is applicable, the Gibbs energy (ΔG_{cs}) is calculated by [30]:

$$\Delta G_{cs} = E_{ox} - E_{red} - E_{0,0} + C$$

However, this equation is fundamentally limited by cyclic voltammetry because electrons move to acceptors when they are excited; however, the oxidation and reduction potentials are obtained from the voltage (electrochemical energy).

The FRET is normally used to explain the quenching dynamics in biological systems, such as protein dynamics. This is because these dynamics depend on the distance between the fluorophores and quencher [20]. This occurs when the emission band of the fluorophores overlaps with the absorption band of the quencher [29].

The inner-filter effect is different from the two aforementioned mechanisms. This mechanism does not involve molecular interactions; hence, there is no change in its lifetime [24]. This effect depends on the florescence field, which is highly affected by the beam angle [31], whose quenching power can be optimized by the fluorescence field condition.

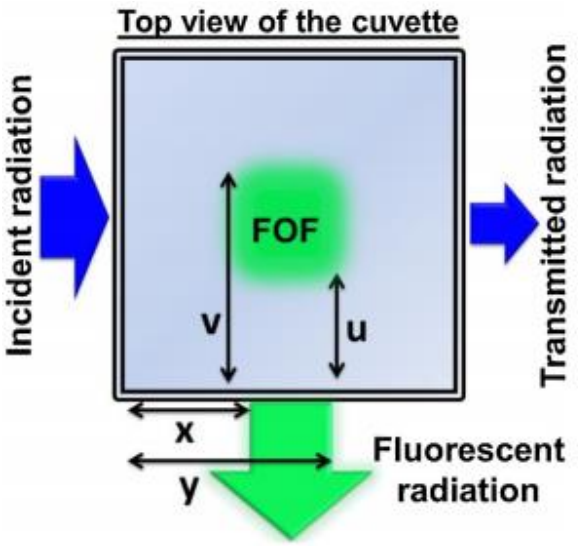

Fig 1.2. Schematic depiction of top view of the cuvette with the fluorescence observation field (FOF)

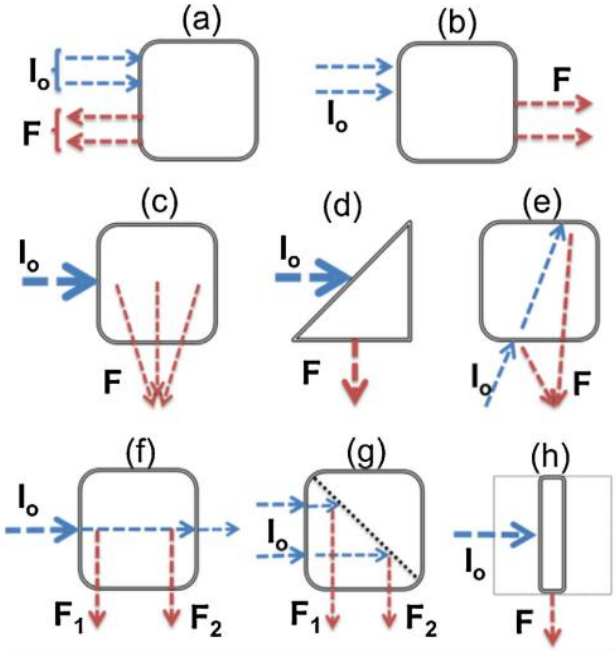

Fig 1.3. Various cuvette cell configurations used for fluorescence measurements. I_0 is incident radiation and F is observed fluorescence

References

[1] V. Georgakilas, J.A. Perman, J. Tucek, R. Zboril, Broad Family of Carbon Nanoallotropes: Classification, Chemistry, and Applications of Fullerenes, Carbon Dots, Nanotubes, Graphene, Nanodiamonds, and Combined Superstructures, Chem. Rev. 115 (2015) 4744−4822

[2] S. Zhu, Y. Song, X. Zhao, J. Shao, J. Zhang, B. Yang, The photoluminescence mechanism in carbon dots (graphene quantum dots, carbon nanodots, and polymer dots): Current state and future perspective, Nano Research 8 (2015) 355–381

[3] A.W. Robertson, J.H. Warner, Atomic resolution imaging of graphene by transmission electron microscopy, Nanoscale 5 (2013) 4079-4093

[4] S. Liu, J. Tian, L. Wang, Y. Zhang, X. Qin, Y. Luo, A. M. Asiri, A.O. Al-Youbi, X. Sun, Hydrothermal Treatment of Grass: A Low-Cost, Green Route to Nitrogen-Doped, Carbon-Rich, Photoluminescent Polymer Nanodots as an Effective Fluorescent Sensing Platform for Label-Free Detection of Cu(II) Ions, Adv. Mater. 24 (2012) 2037–2041

[5] Y. Song, S. Zhu, S. Zhang, Y. Fu, L. Wang, X. Zhao, B. Yang, Investigation from chemical structure to photoluminescent mechanism: a type of carbon dots from the pyrolysis of citric acid and an amine, J. Mater. Chem. C 3 (2015) 5976-5984

[6] D. Qu, M. Zheng, L. Zhang, H. Zhao, Z. Xie, X. Jing, R.E. Haddad, H. Fan, Z. Sun, Formation mechanism and optimization of highly luminescent N-doped graphene quantum dots, Scientific Reports 4 (2014) Article number: 5294

[7] T. Ogi, K. Aishima, F.A. Permatasari, F. Iskandar, E. Tanabe, K. Okuyama, Kinetics of nitrogen-doped carbon dot formation via hydrothermal synthesis, New J. Chem. 40 (2016) 5555-5561

[8] S.Y. Lim, W. Shen, Z. Gao, Carbon quantum dots and their applications, Chem. Soc. Rev. 44 (2015) 362-381

[9] H. Li, Z. Kang, Y. Liu, S.T. Lee, Carbon nanodots: synthesis, properties and applications, J. Mater. Chem. 22 (2012) 24230-24253

[10] M. Havrdova, Katerina Hola, Josef Skopalik, K. Tomankova, Martin Petr, Klara Cepe, Katerina Polakova, J. Tucek, A.B.Bourlinos, R. Zboril, Toxicity of carbon dots – Effect of surface functionalization on the cell viability, reactive oxygen species generation and cell cycle, Carbon 99 (2016) 238-248

[11] Y. Dong, J. Shao, C. Chen, H. Li, R. Wang, Y. Chi, X. Lin, G. Chen, Blue luminescent graphene quantum dots and graphene oxide prepared by tuning the carbonization degree of citric acid, Carbon 50 (2012) 4738-4743

[12] J. Jiang, Y. He, S. Li, H. Cui, Amino acids as the source for producing carbon nanodots: microwave assisted one-step synthesis, intrinsic photoluminescence property and intense chemiluminescence enhancement, Chem. Commun. 48 (2012) 9634–9636

[13] R. Kumar, V.B. Kumar. A. Gedanken, Sonochemical synthesis of carbon dots, mechanism, effect of parameters, and catalytic, energy, biomedical and tissue engineering applications, Ultrasonics Sonochemistry 64 (2020) Article number: 105009

[14] S. Liu, J. Tian, L. Wang, Y. Luo, J. Zhai, X. Sun, Preparation of photoluminescent carbon nitride dots from CCl_4 and 1,2-ethylenediamine: a heat-treatment-based strategy, J. Mater. Chem. 21 (2011) 11726-11729

[15] M.J. Krysmann, A. Kelarakis, P. Dallas, E.P. Giannelis, Formation Mechanism of Carbogenic Nanoparticles with Dual Photoluminescence Emission, J. Am. Chem.Soc. 134

(2012) 747−750

[16] S. Zhu, Q. Meng, L. Wang, J. Zhang, Y. Song, H. Jin, K. Zhang, H. Sun, H. Wang, B. Yang, Highly Photoluminescent Carbon Dots for Multicolor Patterning, Sensors, and Bioimaging, Angew. Chem. Int. Ed. 2013, 52, 3953 –3957

[17] D.I. McRee, Environmental Aspects of Microwave Radiation, Environ. Health Perspect. 2 (1972), 41-53

[18] S. Mohapatra, S. Sahu, S. Nayak, S.K. Ghosh, Design of Fe3O4@SiO2@Carbon Quantum Dot Based Nanostructure for Fluorescence Sensing, Magnetic Separation, and Live Cell Imaging of Fluoride Ion, Langmuir 31 (2015) 8111−8120

[19] J. Zhan, R. Peng, S. Wei, J. Chen, X. Peng, B. Xiao, Ethanol-Precipitation-Assisted Highly Efficient Synthesis of Nitrogen-Doped Carbon Quantum Dots from Chitosan, ACS Omega 4 (2019) 22574−22580

[20] C. Albrecht, Joseph R. Lakowicz, Principles of Fluorescence Spectroscopy (3rd edition), Springer (2007)

[21] A. Jimenez-Banzo, X. Ragas, P. Kapusta, S. Nonell, Time-resolved methods in biophysics. 7. Photon counting vs. analog time-resolved singlet oxygen phosphorescence detection, Photochem. Photobiol. Sci. 7 (2008) 1003–1010

[22] K. Jiang, L. Zhang, J. Lu, C. Xu, C. Cai, H. Lin, Triple-Mode Emission of Carbon Dots: Applications for Advanced Anti-Counterfeiting, Angew. Chem. Int. Ed. 55 (2016) 7231 –7235

[23] L.K. Fraiji, D.M. Hayes, T. C. Werner, Static and Dynamic Fluorescence Quenching Experiments for the Physical Chemistry Laboratory, Journal of Chemical Education 69 (1992)

424-428

[24] F. Zu, F. Yan, Z. Bai, J. Xu, Y. Wang, Y. Huang, X. Zhou, The quenching of the fluorescence of carbon dots: A review on mechanisms and applications, Microchimica Acta 184 (2017) 1899–1914

[25] S.B. Nimse, M.D. Sonawane, K.S. Song, T. Kim, Biomarker detection technologies and future directions, Analyst 141 (2016) 740-755

[26] P. Suppan, E. Vauthey, The energy balance of photoinduced electron transfer reactions, J. Photochem. Photobiol. A 49 (1989) 239-248

[27] X. Wu, L. Wu, X. Cao, Y. Li, A. Liu, S. Liu, Nitrogen-doped carbon quantum dots for fluorescence detection of Cu2+ and electrochemical monitoring of bisphenol A, RSC Adv. 8 (2018) 20000-20006

[28] X. Sun, Y. Lei, Fluorescent carbon dots and their sensing applications, Trends Anal. Chem 89 (2017) 163-180

[29] J. Wu, W. Liu, J. Ge, H. Zhang, P. Wang, New sensing mechanisms for design of fluorescent chemosensors emerging in recent years, Chem. Soc. Rev. 40 (2011) 3483–3495

[30] S. Doose, H. Neuweiler, M. Sauer, Fluorescence Quenching by Photoinduced Electron Transfer: A Reporter for Conformational Dynamics of Macromolecules, ChemPhysChem 10 (2009) 1389-1398

[31] S.K. Panigrahi, A.K. Mishra, Inner filter effect in fluorescence spectroscopy: as a problem and as a solution, J. Photochem. Photobiol. C-Photochem. Rev. 41 (2019) Article number: 100318

Chapter 2. The effect of solvent polarity on emission properties of carbon dots and their uses in colorimetric sensors for water and humidity

2.1. Introduction

Carbon dots (CDs) are widely used as active materials for the fluorescent sensors of pH, biomolecules, environmental contaminants and metal ions because of their outstanding properties, such as high photoluminescence (PL), photostability, and cost effectiveness [1–4]. Z. Zhang et al. synthesized CDs surface-modified with glycine and applied on detection of human-transferrin, universal iron carriers [3]. H. Soni et al. synthesized CDs using triflic acid and palm shell powder which was the economical green materials and applied on detection of nitrophenols [4]. Until now, there are a lot of attempts to control photoluminescence of CDs and apply on sensors. However, the desired optical properties are still in high demand, because the actual PL mechanism of CDs is not clearly verified, even though researchers have suggested several hypotheses about potential PL mechanisms [5,6].

Recently, multicolor-emitting CDs were reported by controlling precursors and fabrication conditions [7–13]. Jiang et al. synthesized CDs that have red, green, and blue emissions and successfully fabricated a full-color PVA-composite film [9]. Wang et al. synthesized CDs whose emission peaks were 511, 525, 545, 554, 568, 602, and 615 nm. CDs showed excitation wavelength-independent and solvent-dependent behavior [10]. Lin et al. synthesized CDs that have the solvatochromatic phenomenon from para-phenylenediamine and ortho-phenylenediamine. Their emissions cover the range of yellow-orange according to the various surrounding molecules [11]. Zhang et al. synthesized CDs based on p-phenylenediamine by means of solvothermal treatment in different solvents including water, ethanol, DMF (dimethylformamide), cyclohexane, and toluene. They studied the effect of solvents as both

reaction mediums and surrounding environments [12]. Chao et al. obtained CDs with ortho-phenylenediamine that showed the solvent dependent emission and fabricated the nanoprobe for water detection in organic solvents [13].

Detection of water in organic solvents is very important in the chemical industries, especially in multiple-step organic synthesis. Water impurity can cause undesirable reactions, lower the yield of products, and cause explosions. Fluorescent nanoprobes have several advantages in terms of high sensitivity, simplicity, and fast response. Recent studies showed that CDs can be effective base materials for the quantitation of water in organic solvents [14–18]. Wang et al. employed CDs for the detection of water at low concentration. They attached an imidazole ring at the surface of CDs, and their emissions were increased by the water molecules because of photoinduced electron transfer (PET) [16]. Ye et al. synthesized CDs from resorcinol and fabricated a paper-based sensor strip for water detection in a real sample [17]. Wei et al. obtained CDs that had a yellow emission by solvothermal treatment with sodium citrate, carbamide, and cobalt chloride as precursors and used them for quantitative analysis of water content in organic solvents [18].

Herein, we successfully fabricated CDs from para-phenylenediamine (p-PD) and nitrilotriacetic acid (NTA) as novel precursors. The CDs fabricated in this study showed excitation wavelength-independent behavior and solvent-dependent multicolor emission. The relation between polarity of solvents and optical properties of CDs was systematically studied by using various organic solvents. The CDs fabricated in this study exhibited strong solvatochromatic properties, which were then applied in the quantitative analysis of many different amounts of water in the various organic solvents. In addition, a prototype of a paper-strip humidity sensor was successfully fabricated.

2.2. Experimental

2.2.1. Chemicals and instruments

NTA, p-PD, ortho-phenylenediamine (o-PD), meta-phenylenediamine (m-PD), Cobalt chloride ($CoCl_2$) were purchased from SigmaAldrich Co., Ltd (USA). Ethyl alcohol anhydrous was purchased from Samchun Pure Chemical Co., Ltd. (Republic of Korea). Ethyl acetate, acetonitrile, N,N-dimethylformamide (DMF), potassium chloride (KCl), lithium chloride anhydrous (LiCl), and magnesium chloride anhydrous ($MgCl_2$) were purchased from Daejung Chemicals & Metals Co., Ltd. (Republic of Korea). Methyl alcohol was purchased from Avantor Performance Materials LLC (USA). was purchased from Yakuri Pure Chemicals Co., Ltd. (Japan). Sodium bromide (NaBr) was purchased from Junsei Chemical Co., Ltd. (Japan). Lead (II) nitrate ($Pb(NO_3)_2$) was purchased from Samchun Pure Chemical Co., Ltd. (Republic of Korea). All the reagents were used without further purification.

The morphology and size distribution of CDs were investigated by field-emission transmission electron microscope (FE-TEM, JEL-2100 F, JEOL, Japan). X-ray Diffraction (XRD, ULTIMA 4, Rigaku, Japan) was done investigating characterization of CDs. UV–vis absorbance measurement was done using a Specord 210 Plus (Analytik Jena, Germany). Fluorescence measurement was done with a Cary Eclipse Fluorescence Spectrophotometer G9800AA (Agilent Technologies, USA). The elemental composition was found by X-ray photoelectron spectroscopy (XPS, K-alpha, Thermo Fisher Scientific, USA). Fourier-transform infrared spectroscopy (FT-IR; Nicolet iS5 FTIR Spectrometer, Thermo Fisher Scientific, USA) was used to collect surface functional groups.

2.2.2 Synthesis of CDs

As illustrated in Fig 2.1, CDs were fabricated using NTA and p-PD by solvothermal synthesis. First, 382 mg of NTA and 54 mg of p-PD were dispersed in 20 ml ethyl alcohol. Then the solution was stirred until p-PD was completely dissolved in the ethanol. The solution was transferred to the Teflon-lined stainless-steel autoclave for six hours at 160 ℃. After reaction, the solution was centrifuged at 10,000 rpm for 20 min to remove the residual reagents. We could obtain a clear solution of CDs without any complicated purification method. We diluted the resulting solution to pure solvent, including ethyl acetate, acetonitrile, DMF, ethyl alcohol, methyl alcohol, and D.I. water with a dilution ratio of CDs to them of 1: before PL measurement.

2.2.3. Detection of water in organic solvents

First, 10, 20, 30, 40, 50, 60, 70, 80, 90, and 100 vol.% of water containing solutions of acetonitrile, DMF, and ethyl alcohol were prepared. Then the CDs solution was added to the above solutions with a dilution ratio of CDs to them of 1:80 while stirring with a magnetic bar for a few min. The fluorescence spectra were collected ten times for each experiment. Accuracy (R^2) and sensitivity of the sensor were calculated for the 95% confidence interval and considering the standard deviation.

2.2.4. The paper-based humidity sensors

Common filter paper was immersed in the CDs solution overnight. Then, the paper was dried in room-temperature air. Specific saturated salt solutions that can control the water vapor in equilibrium were used to obtain the specific humidity. Saturated aqueous solutions of LiCl, $MgCl_2$, NaBr, $CoCl_2$, KCl, and $Pb(NO_3)_2$ were put in the vials to achieve approximate 11.31%, 33.07%, 59.14%, 67%, 85.11%, and 98% of RH levels at 20 ℃ [19,20]. Then the CDs-coated

papers were put in the vials with a saturated solution of salt, and they were covered with a lid to keep the specific humidity. The humidity levels were estimated according to the paper color under UV illumination.

2.2.5. Quantum yield measurements

The quantum yield was determined by secondary method which rely on comparison of the fluorescence spectra of the standard and the sample. Quinine bisulfate (0.1N H_2SO_4, ϕ=0.54) is selected by reference material for all range of the emissions. Excitation wavelength is 350nm for all solvents. Fluorescence spectra was collected on condition that excitation slit bandwidth is 2.5 nm and emission slit bandwidth is 5 nm. The following equation is used to determine the quantum yields.

$$\phi_x = \phi_s \frac{A_s}{A_x} \frac{F_x}{F_s} (\frac{n_x}{n_s})^2$$

The subscript of "χ" means the sample and "s" means the reference material. ϕ is quantum yield, A is absorbance at the excitation wavelength, F is the integrated emission area across the band and n is refractive index of solvents, which correct the change of intensity which is caused by difference of the refraction in different solvents. The absorbance was kept below 0.1 and the measurement was done at room temperature.

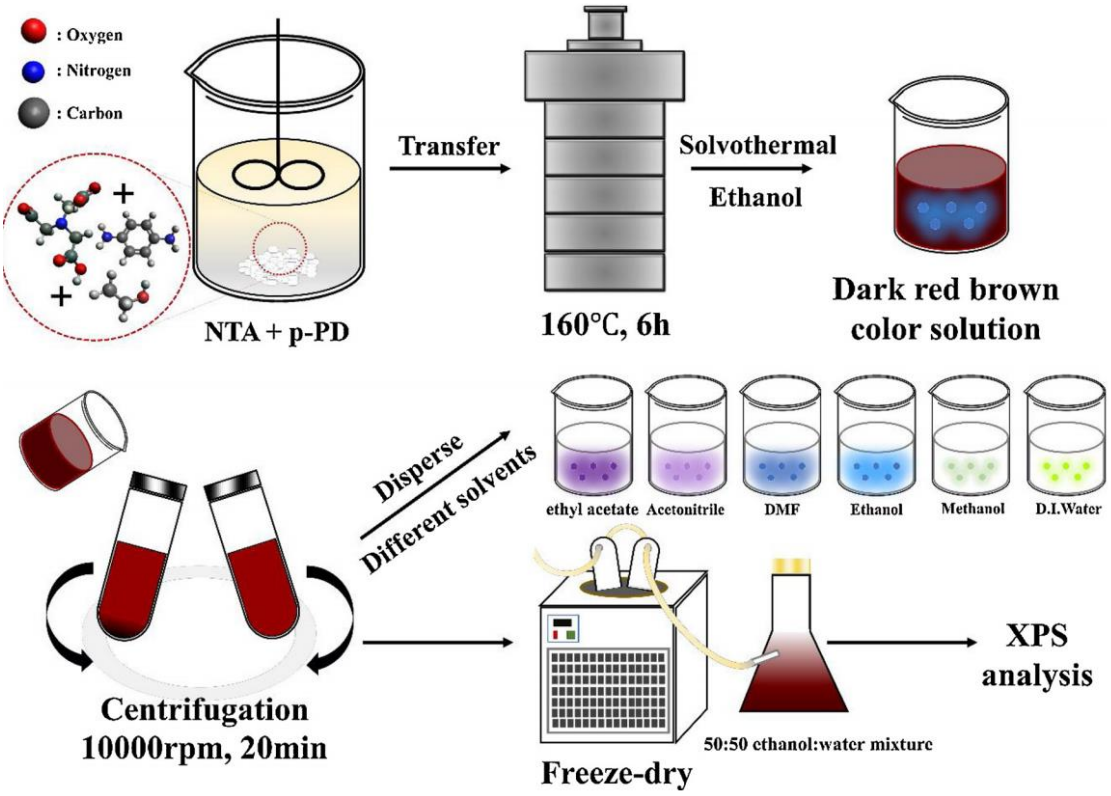

Fig 2.1. Schematic diagram of CDs synthesis.

2.3. Results and Discussion

2.3.1. Characterization of CDs

The morphology and structural parameters, and the size of CDs were investigated by TEM and XRD. As shown in Fig. 2.2a, CDs were spherical and of uniform size distribution in the range of 1.0 to 2.6 nm (1.84 ± 0.14 nm). The high-resolution TEM image in Fig. 2.2b reveals a lattice spacing of 0.21 nm, which corresponds to the (100) in-plane lattice of graphene [10–13,21]. A broad peak at around 21.2 ° shown in XRD patterns (Fig. 2.3) corresponds to the (002) plane of graphitic carbon [21–23]. When o-PD and m-PD were used instead of p-PD, no CDs are obtained, as shown in Fig. 2.4, perhaps because of the differences in pKa values, reaction electron-donating properties, and reactivity of o-PD and m-PD from those of p-PD [24,25]. In addition, during the synthesis process, the intermolecular amide linkage between amine and carboxylic acid groups can be limited by the steric hindrance around the reaction sites [26]. Relatively close positions of two amines in o-PD and m-PD can induce more steric hindrance, and the rigid aromatic ring itself of phenylenediamine can hinder the movement of polymer chains, which may limit the polymerization between o-PD or m-PD and NTA.

FT-IR was used to investigate the surface functional groups of CDs, as shown in Fig 2.5. The broad peak at 3422 cm^{-1} can be attributed to O-H stretching vibrations. The absorption peaks originating from amide and ester groups can be observed around 1300-1720 cm^{-1}. The strong peak at 1740 cm^{-1} can be assigned to C=O stretching vibration from the ester group, which might be formed by the esterification reaction between carboxylic acid and the alcohol that was used as solvent. The Amide I, Amide II, and Amide III peaks are observed at 1642 cm^{-1}, 1518 cm^{-1}, and 1403 cm^{-1}, respectively [27–29]. The peak at 2982 cm^{-1} and at 1202 cm^{-1} can be assigned to C-H and C-O stretching vibrations, respectively.

XPS was used to establish the elemental composition of CDs. As shown in Fig. 2.6a, three peaks corresponding to C_{1s}(285 eV), N_{1s}(399 eV), and O_{1s}(532 eV) are observed, and the relative content of C, O, and N is calculated to be 62.12%, 27.32%, and 10.57%, respectively, which indicates a high amount of nitrogen atoms in the CDs. The peaks at 284.4, 285.2, and 288.4 eV shown in the high-resolution C_{1s} XPS spectra (Fig. 2.6b) are attributed to the carbons of C-C/C=C, C-N, and C=O, respectively, which also reveals the highly incorporated nitrogen atoms in CDs. High-resolution O_{1s} XPS spectra (Fig. 2.6c) show only the C=O oxygen peak at 531.4 eV that originates from ester groups. Interestingly, a large amount of graphitic N (401.3 eV) is observed in the high-resolution N_{1s} XPS spectra (Fig. 2.6d), perhaps because of the intermolecular dehydrolysis between the amide and carboxylic acid groups as well as the tertiary amine in NTA [30].

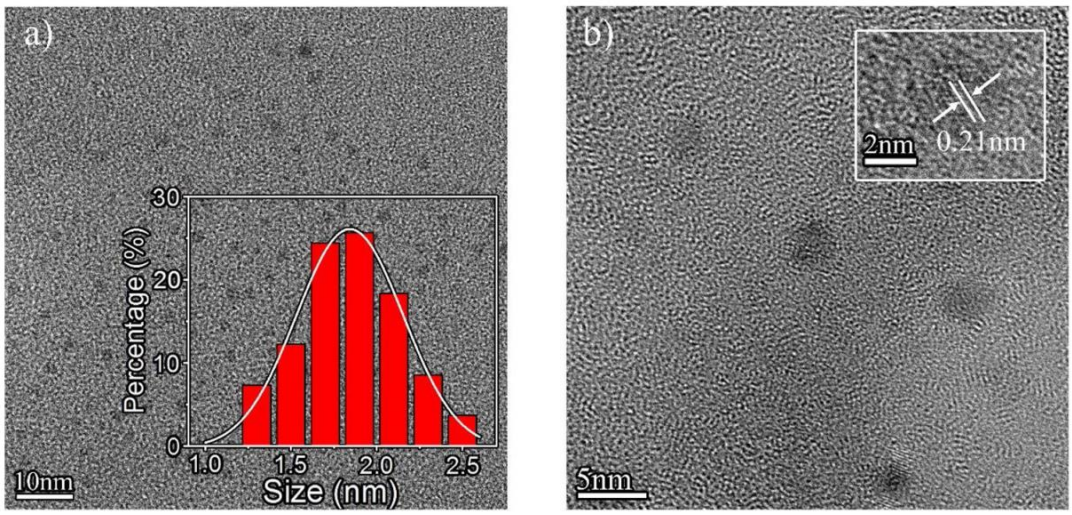

Fig 2.2. TEM images of CDs on a 10 nm and 5 nm scale. (a) Size distribution of CDs. (b) HR-TEM image and lattice spacing of CDs

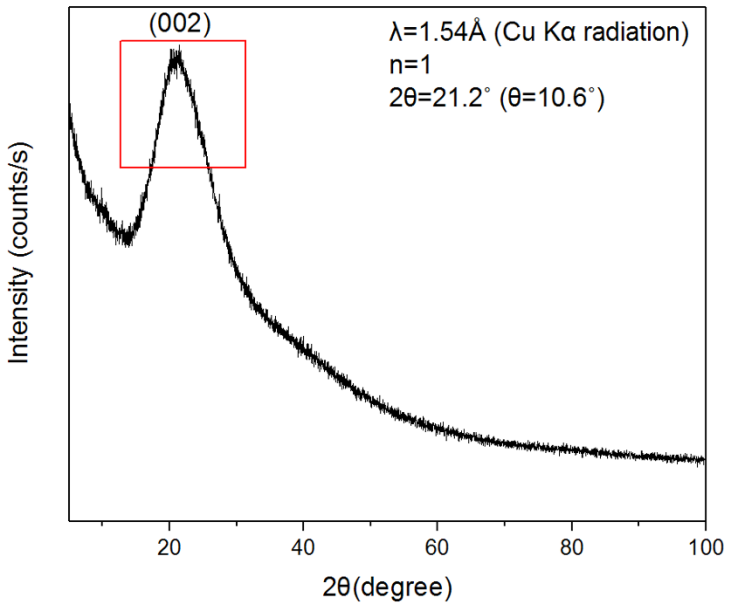

Fig 2.3. XRD pattern of CDs

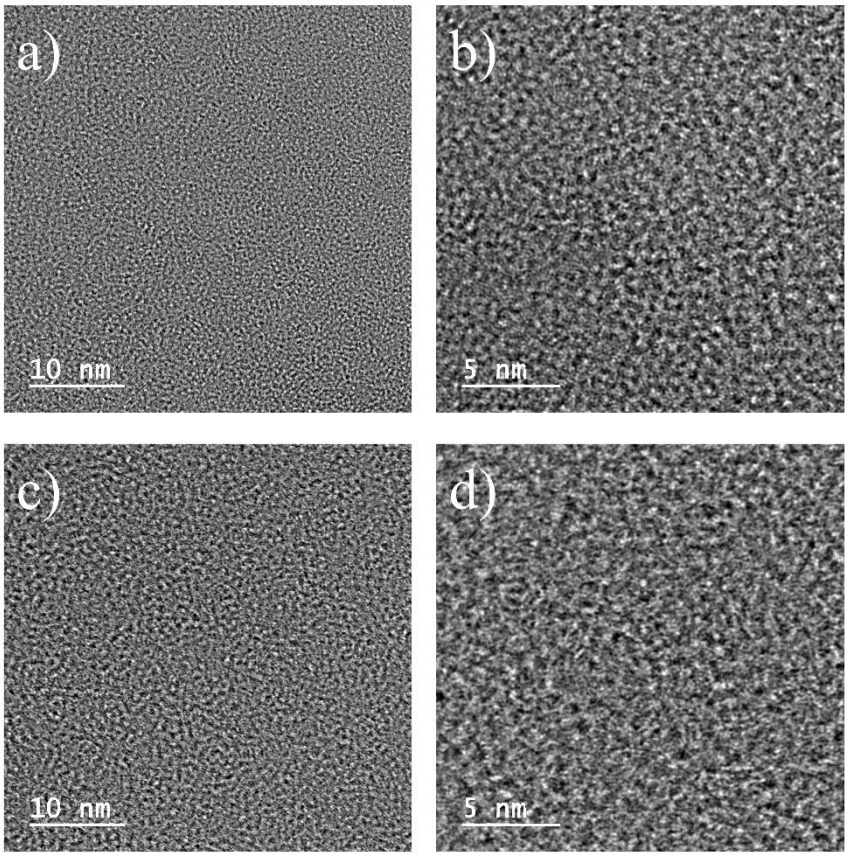

Fig 2.4. TEM image of CDs synthesized from ortho-phenylenediamine at (a) 10nm (b) 5nm TEM image of CDs synthesized from meta-phenylenediamine at (c) 10nm (d) 5nm

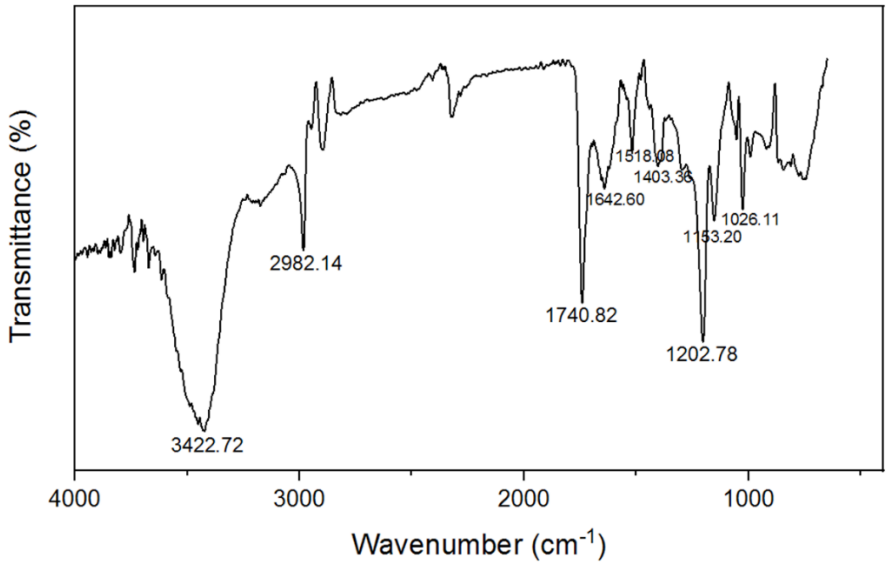

Fig 2.5. FT-IR spectra of CDs in ethanol

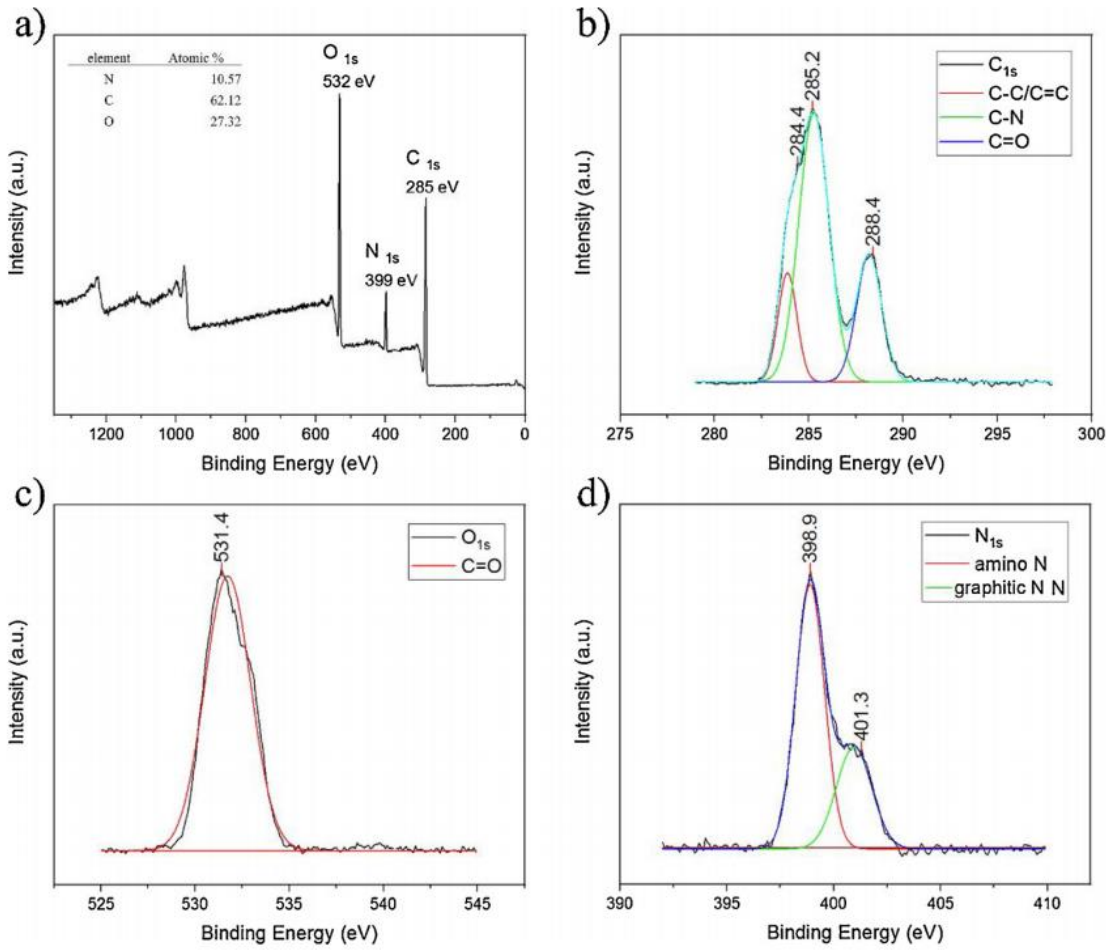

Fig 2.6. (a) XPS survey spectra, (b) high-resolution C_{1s} XPS spectra, (c) high-resolution O_{1s} XPS spectra, (d) high-resolution N_{1s} XPS spectra of CDs

2.3.2. Optical properties of CDs

UV-VIS absorption and PL were used to investigate the optical properties of CDs. The strong absorption of CDs at 290 nm shown in Fig. 2.7a results from the $\pi - \pi^*$ transition of the sp^2 C=C aromatic bond of the carbon core, which indicates successful formation of graphitic structures in the CDs. In addition, the broad absorption of CDs in the visible region also indicates the formation of sp^2 conjugated structures. The peak at 528 nm indicates that Mie scattering is caused by CDs in the presence of nanoparticles and conjugation structures [11,31–33]. The strong peak at 350 nm of p-PD can be attributed to the strong interaction between the amino group and the electron of the benzene ring [34]. After reaction with NTA, it disappears because of the incorporation of the nitrogen atom into the carbon core of CDs. The absence of a strong peak at 290 nm and different peak shapes in the PLE spectra (Fig 2.8) of various solvents indicate that most of the excitation energy is consumed as heat by means of non-radiation decay by the solvent-CDs interaction, because the carbon core region is so sensitive to the external media and easily interacts with quencher molecules [35]. As shown in Fig. 2.7c, the maximum absorption wavelength was almost the same regardless of solvents, which indicates that the band gap of CDs remains constant regardless of solvent properties. The slight difference in their shape could result from the slight structural change in the carbon core by the p-PD in CDs that exhibits different proton donor-acceptor interactions with various solvents [34].

The CDs generally show an excitation wavelength-dependent behavior in organic solvents because of the irregular size of CDs or various functional groups that can have different emissive traps [5]. However, PL originating from the surface state of CDs can be suppressed by the strong interaction between solvent molecules and CDs; instead, the interaction itself can

be act as a predominant source of PL. As shown in Figs. 2.7b and 2.9, the CDs fabricated in this study showed excitation wavelength-independent behavior in the organic solvents, which indicates there was a uniform surface state and low functional group content in the CDs [21]. If CDs are in the water, they can exhibit excitation wavelength-dependent behavior because of the conformational change induced by the swelling of CDs in the water and by the change of proton donor-acceptor properties in the carbon core.

Solvent polarity highly affects the PL emission wavelength of CDs. As shown in Fig. 2.7d and Table 2.1, as the solvent polarity increases, the PL emission shifts to a longer wavelength, the bandwidth is broadened and the quantum yield decreases. The red shift can be easily observed by the naked eye under UV illumination, as shown in the inset of Fig. 2.7d. The red shift of PL emission in a high polar solvent can be induced by edge N structures and a strong solvation effect. First, edge N structures, such as pyrrolic and pyridinic forms, can increase the charge-carrier density in a high polar solvent by attracting more charges by their easy interaction with the surrounding solvents [10,11]. Second, when the electron is excited from the ground state, it can be stabilized by changing the dipole direction of the surrounding solvent molecules. As solvent polarity increases, the energy required to change the dipole direction of the solvent molecules also increases because of the strong solvent dipole moment. As a result, excited electrons in a high polar solvent lose more energy than those in the low polar solvent, which results in a red shift of the PL emission. In addition, internal charge-transfer and conformational changes can be caused by the hydrogen bonds between the p-PD in CDs and polar protic solvents like water [12]. As shown in Fig. 2.10, a linear relationship between the wavelength of the emission peak and the solvent polarity parameter (E_N^T) is observed for all the solvent except for acetonitrile [36]. Because CDs act as proton donors in acetonitrile, a blue

shift occurs instead of a red shift in fluorescence spectra [34]. The emission band broadening is also observed in the high polar solvent, perhaps because of the longer nonradiative relaxation process [37].

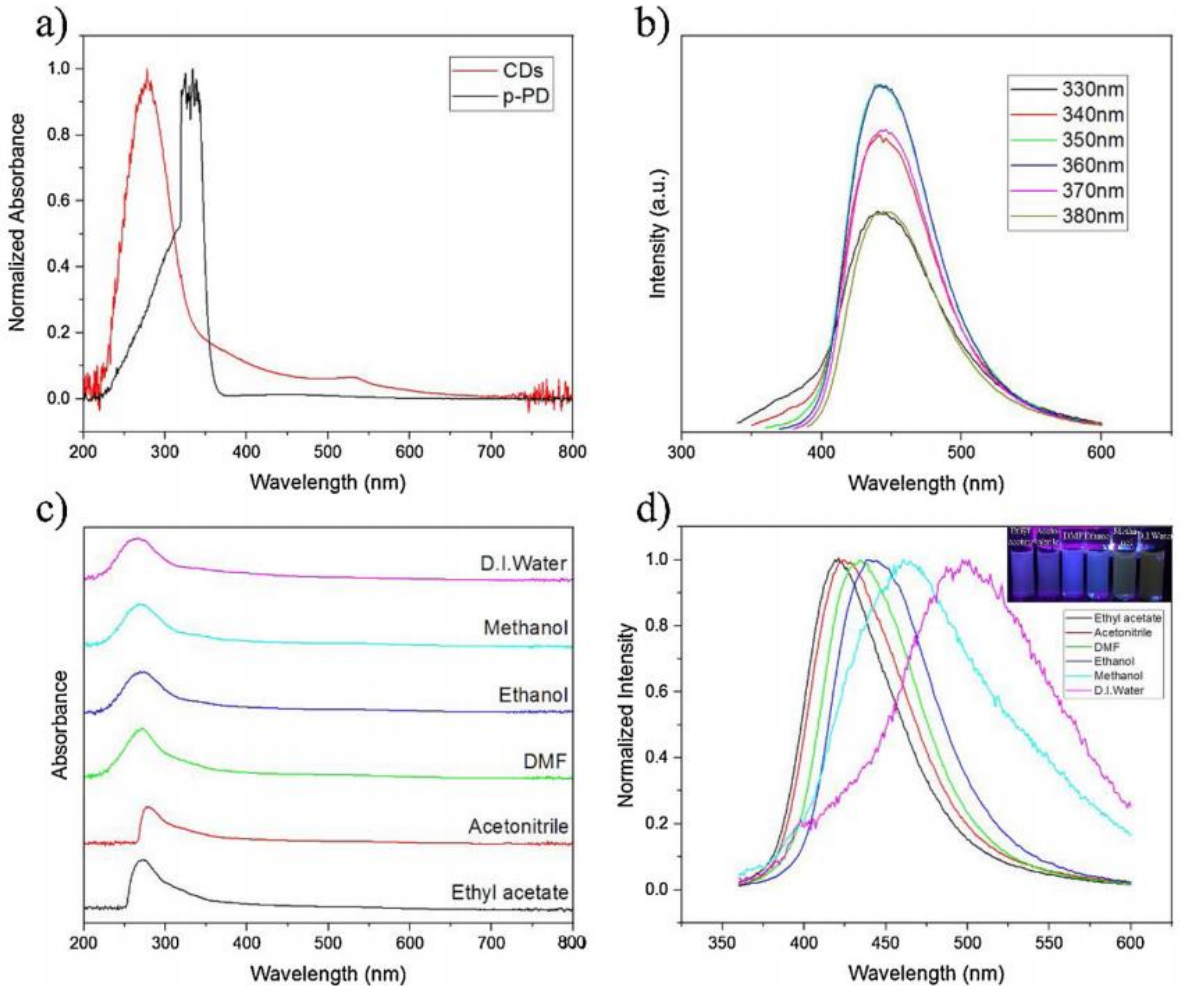

Fig 2.7. (a) UV–vis absorbance spectra of CDs. (b) Fluorescence spectra for CDs in ethanol at different excitation wavelengths. (c) UV–vis absorbance spectra for CDs in different solvents. (d) Normalized fluorescence spectra of CDs and photographs of CDs under UV illumination in different solvents

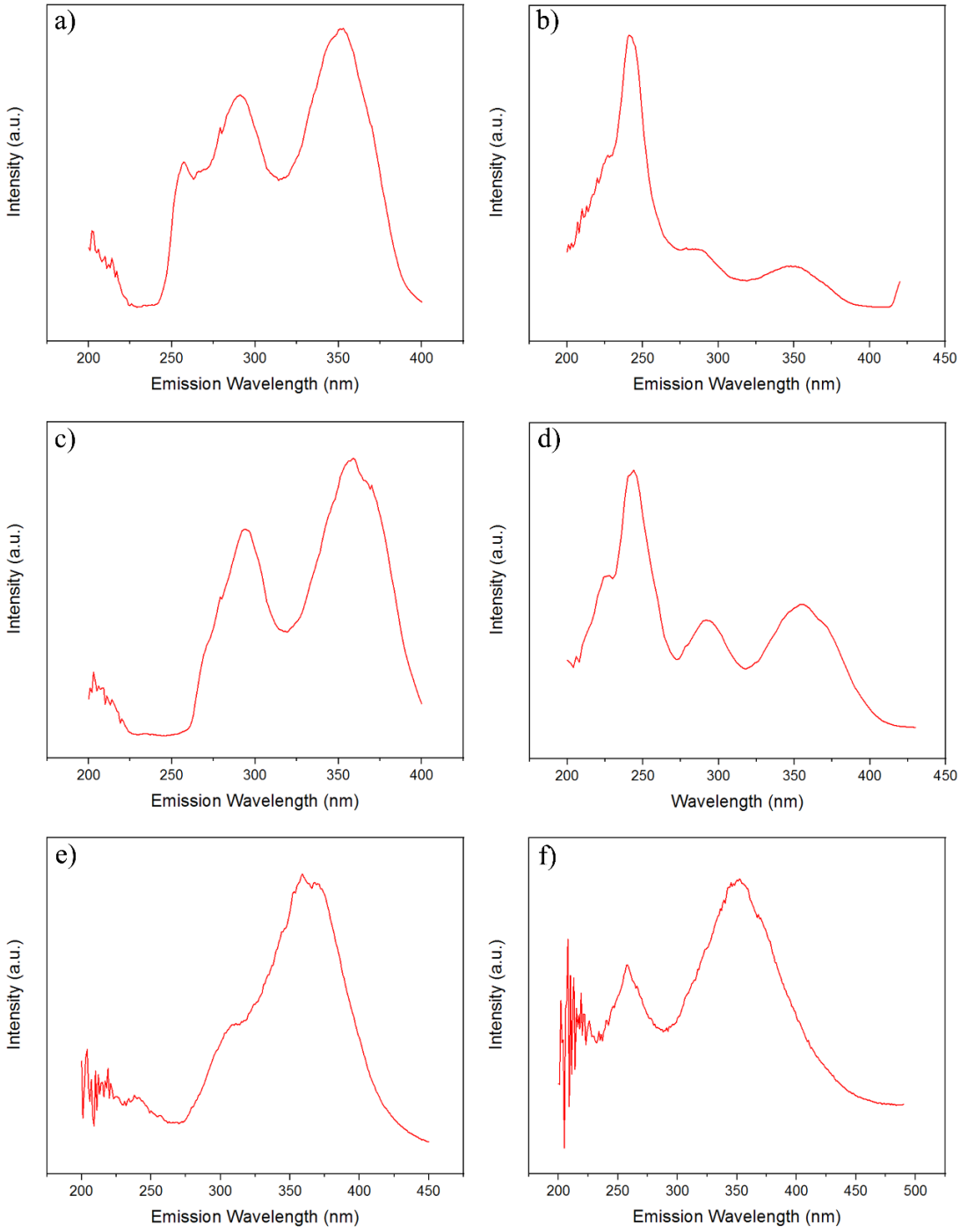

Fig 2.8. Photoluminescence excitation (PLE) spectra at respective emission wavelength of CDs in different solvents (a) ethyl acetate (b) acetonitrile (c) DMF (d) ethanol (e) methanol (f) D.I.water

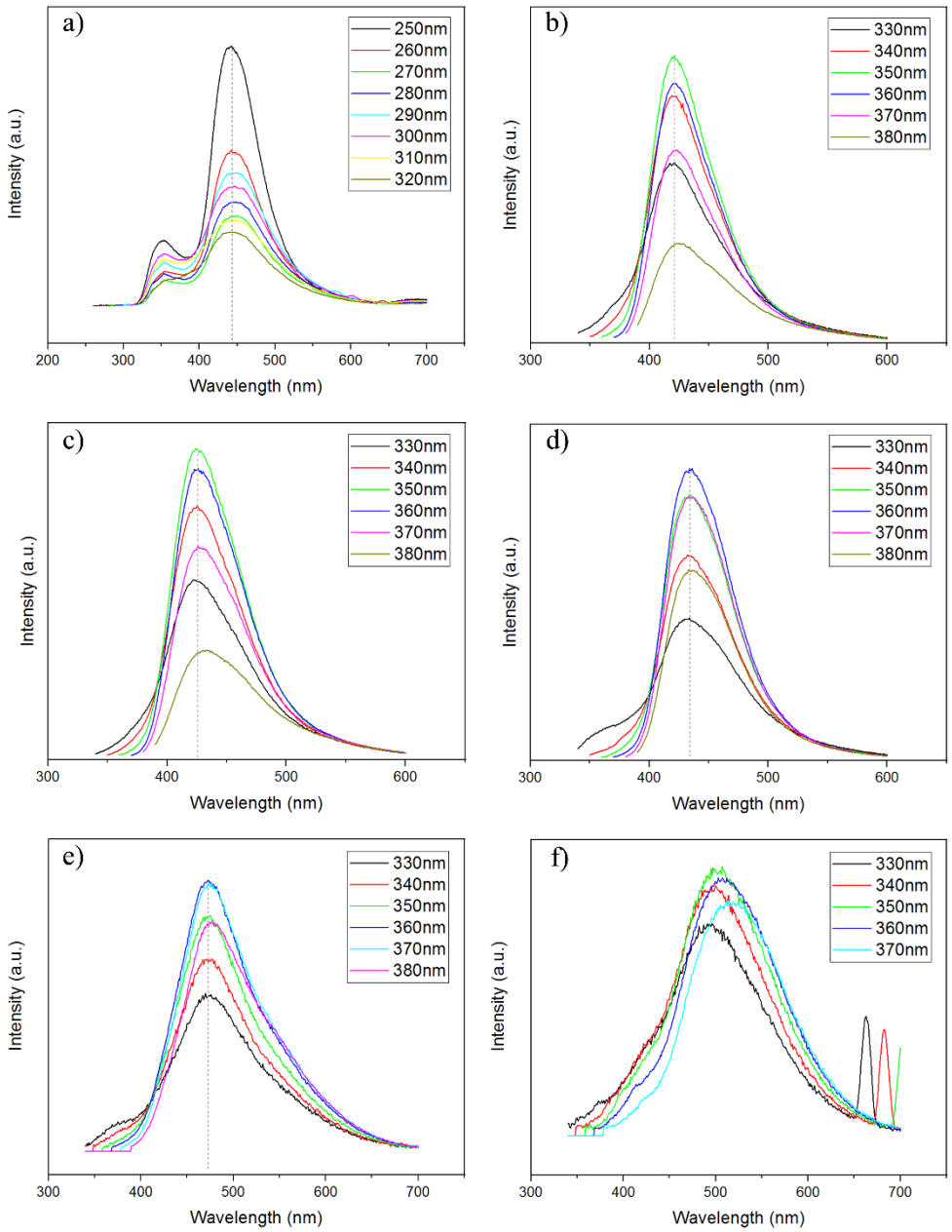

Fig 2.9. FL spectra of CDs at different wavelength in different solvents including (a) ethanol (b) ethyl acetate (c) acetonitrile (d) DMF (e) methanol (f) D.I.water

Table 2.1. Quantum yield (QY) of CDs in different solvents

Solvent	ethyl acetate	acetonitrile	DMF	ethanol	methanol	water
Emission peak (nm)	416	424	434	440	461	498
FWHM (nm)	61	66	66	70	104	98
QY	8.85	8.48	8.54	7.89	1.13	1.03

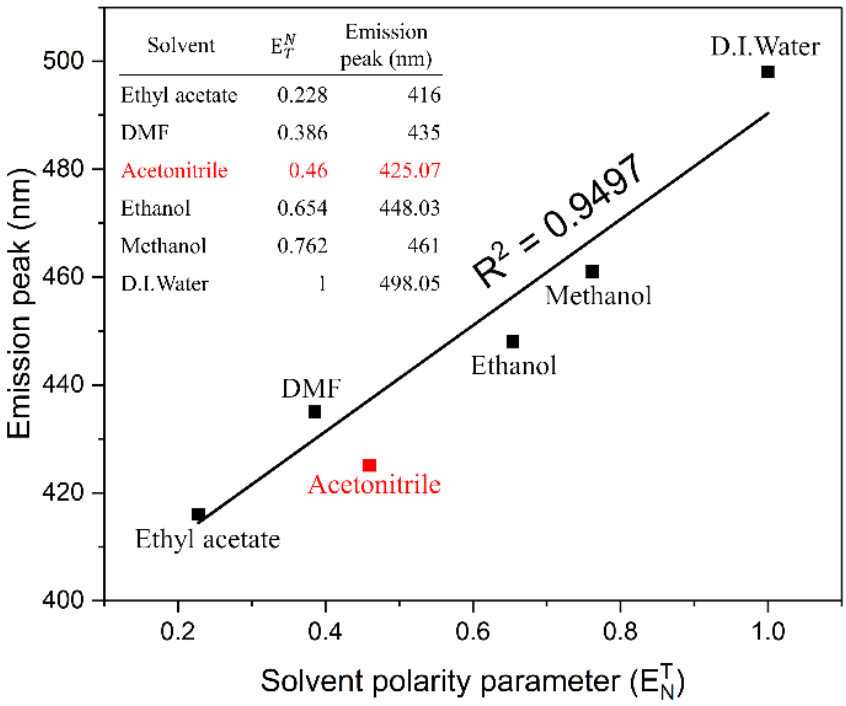

Fig 2.10. Linear relationship between Emission peak (nm) and solvent polarity parameter (E_T^N) except acetonitrile

2.3.3. Detection of water content in organic solvents

As shown in Figs. 2.11 and 2.12, as water content in ethanol increases, the position of the PL emission shifts to red and its intensity decreases. Two linear regions of 0 to 40% and 40 to 100% water content are observed with good linearity, which can be explained by the solvation properties in the binary mixture. Solvation factor (η) can be calculated from $E_{T(m)}$ vs. X_w [37]. $E_{T(m)}$ is the molar electronic transition energy (kcal/mol) and X_w is the molar fraction of a single component in a binary mixture; η = 1 corresponds to random solvation or non-specific solvation by a component of a binary solvent mixture, η > 1 mean that more polar components have a preference for solvation, and, on the other hand, η < 1 means that fewer polar components have a preference for solvation in the binary mixture. The following equation is used to calculate the solvation factor,

$$\eta = \frac{E_{T1(m)}}{E_{T2(m)}} \times \frac{X_{w2}}{X_{w1}}$$

Measured values are used for $E_{T(m)}$ in the literature [36].

As calculated in Table 2.2, η becomes below 1 between 30–40% of water content in ethanol. Water as a more polar component preferentially solvates CDs before reaching about 40%, and ethanol as a less polar component preferentially solvates CDs above 40% [13,37]. PL behaviors and solvation factors of other binary mixtures of water and various organic solvents are shown in Figs. 2.13 and 2.14, and in Tables 2.3 and 2.4, respectively. They exhibit behaviors similar to those of a water and ethanol binary mixture.

The detection limit can be calculated from sensitivity, which is the slope of the calibration curve of the linear regression line and standard deviation of the emission peak. The following

equation is typically used to calculate the detection limit as a signal-to-noise ratio (S/N ratio) is 3. S_a is the standard deviation of response and b is the sensitivity of the calibration curve [38].

$$\text{LOD (Limit Of Detection)} = \frac{3S_a}{b}$$

As shown in Table 2.5, the LOD of water detection in ethanol is as low as 1.67%, which indicates that the CDs fabricated in this study can be used to detect the water content in the ethanol industry.

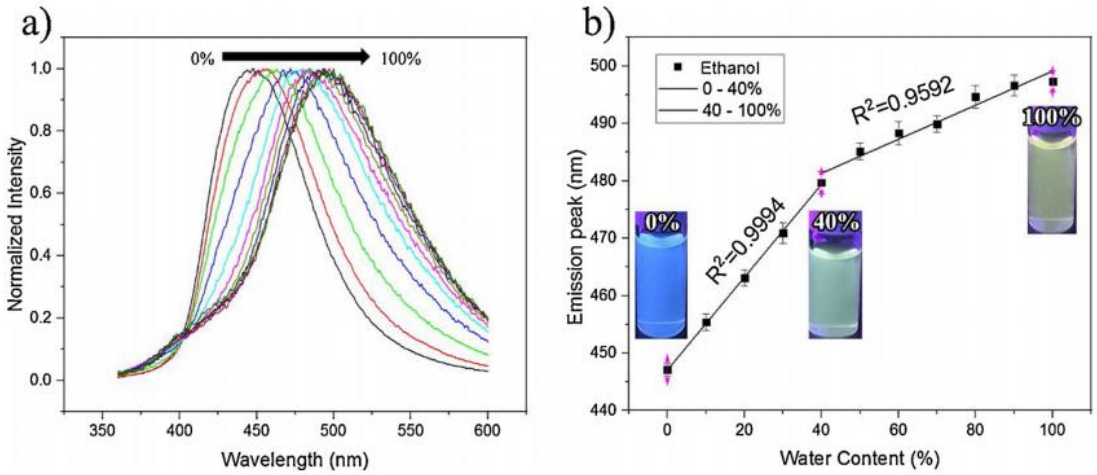

Fig 2.11. (a) Normalized fluorescence spectra of CDs at different water contents. (b) Relationship of emission wavelength peak versus water content. (c) Photographs of CDs with different water contents under UV illumination

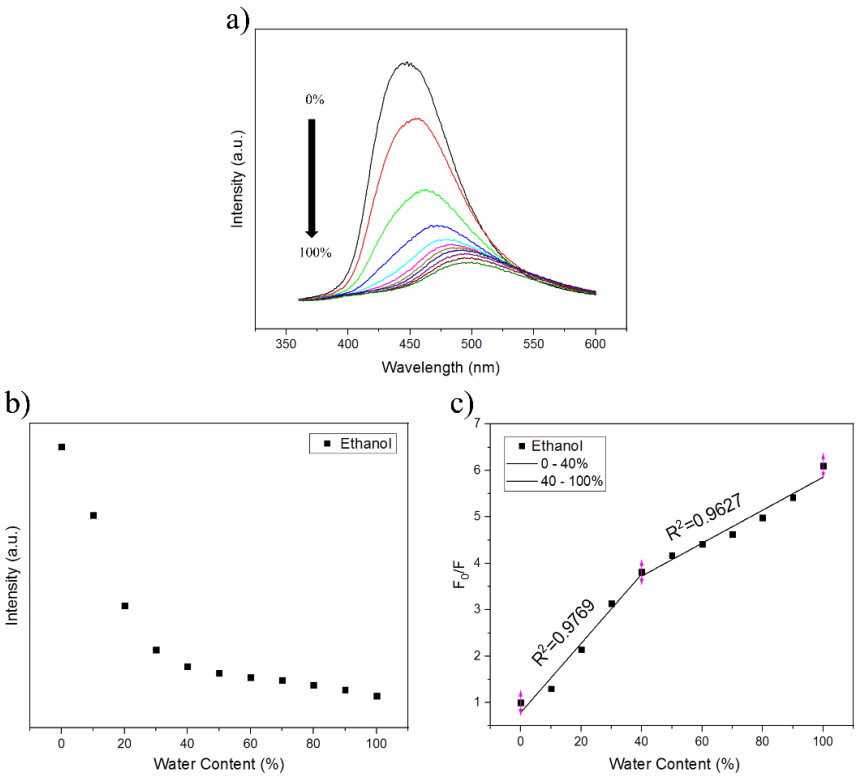

Fig 2.12. Detection of water in ethanol (a) FL spectra of CDs at different water contents (b) Graph of FL intensity versus water contents (c) Linear relationship of FL intensity ratio versus water contents

Table 2.2. Calculation of solvation factor in different volumetric ratios of water-ethanol mixture

Volumetric Ratio (v/v %)	$E_{T(m)}$ (kcal/mol)	molar fraction Ethanol	Water	Solvation factor (η)
0		1	0	∞
10		0.735059	0.264941	4.242248
20		0.552188	0.447812	1.885444
30		0.418367	0.581633	**1.09984**
40		0.316195	0.683805	**0.70704**
50	51.9	0.235632	0.764368	0.471361
60		0.170478	0.829522	0.314241
70		0.116698	0.883302	0.202012
80		0.071553	0.928447	0.11784
90		0.033118	0.966882	0.052373
100		0	1	0

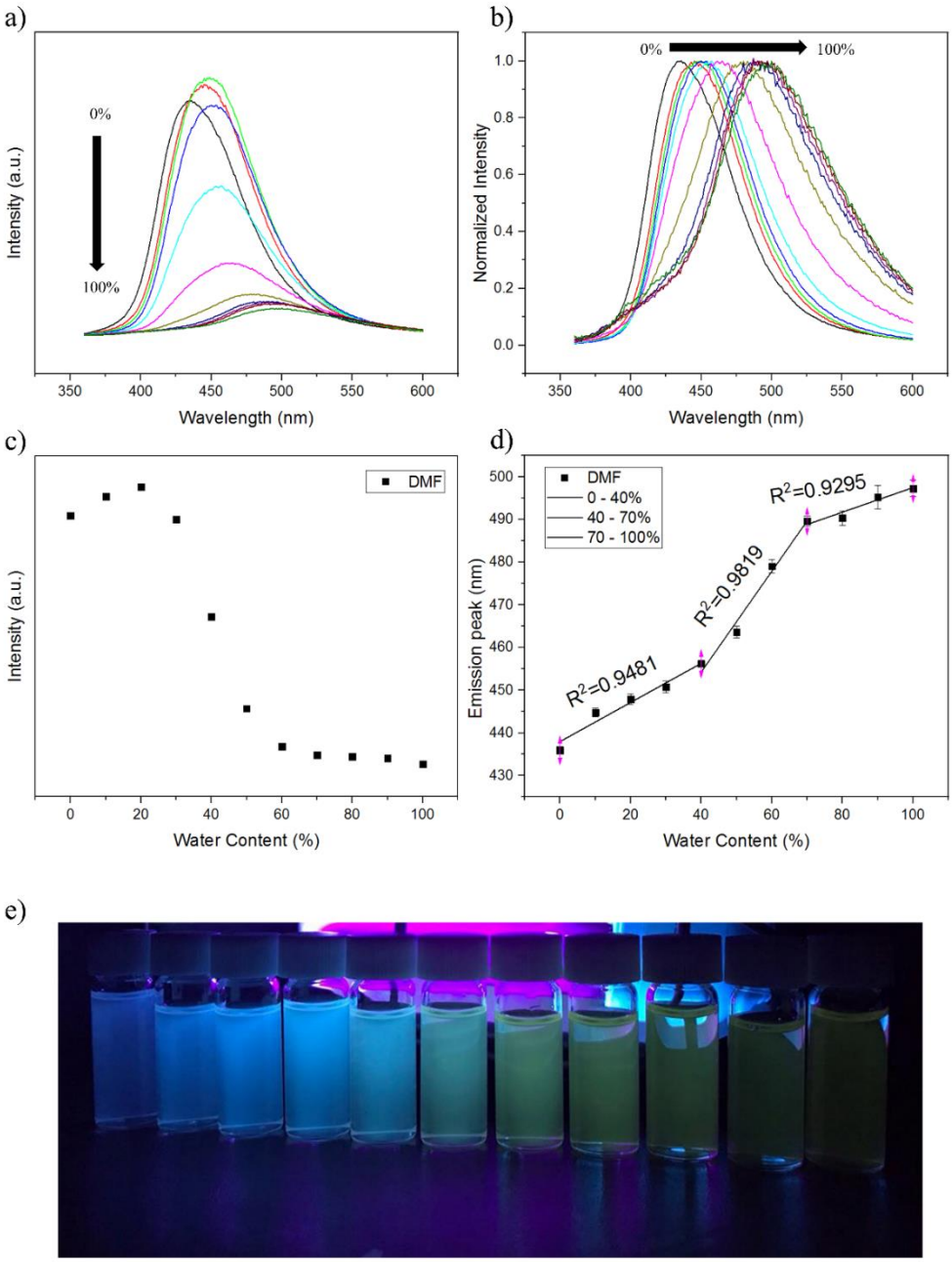

Fig 2.13. Detection of water in DMF (a) FL spectra of CDs at different water contents (b) Normalized FL spectra of CDs for different water contents (c) Graph of FL intensity versus water contents (d) Linear relationship of emission peak versus water contents (e) Photograph of CDs at different water contents under UV illumination

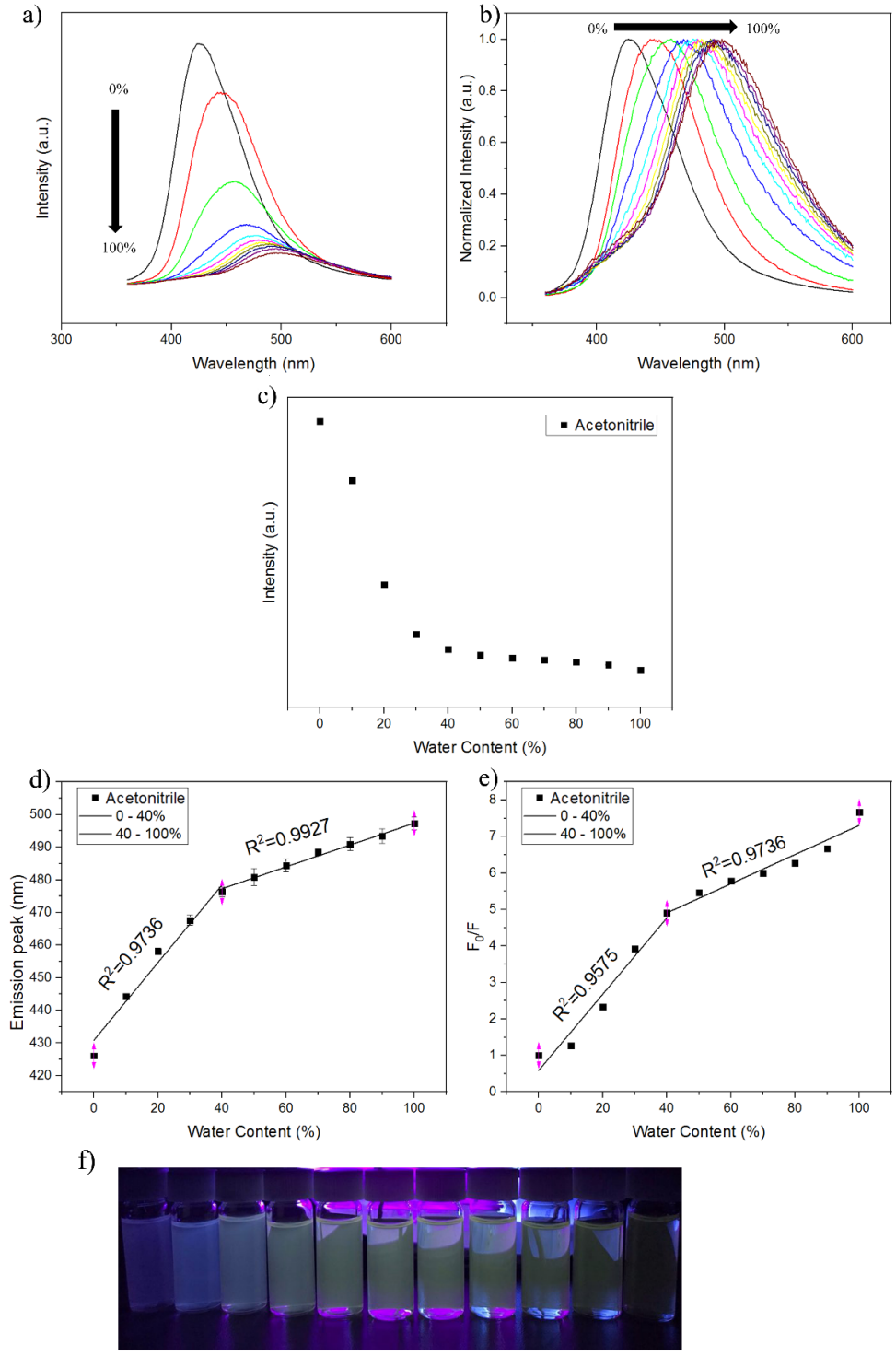

Fig 2.14. Detection of water in acetonitrile (a) FL spectra of CDs at different water contents (b) Normalized FL spectra of CDs in different water contents (c) Graph of FL intensity versus water contents (d) Linear relationship of emission peak versus water contents (e) Linear relationship of FL intensity ratio versus water contents (f) Photograph of CDs at different water contents under UV illumination

Table 2.3. Calculation of solvation factor in different volumetric ratio of water-DMF mixture

Volumetric Ratio(v/v%)	$E_{T(m)}$(kcal/mol)	molar fraction		Solvation factor (η)
		DMF	water	
0		1	0	∞
10		0.676619	0.323381	5.42053
20		0.481844	0.518156	2.409124
30		0.351683	0.648317	**1.40532**
40		0.258557	0.741443	**0.90342**
50	43.2	0.188628	0.811372	0.602281
60		0.134189	0.865811	0.401521
70		0.090607	0.909393	0.25812
80		0.054928	0.945072	0.15057
90		0.025181	0.974819	0.06692
100		0	1	0

Table 2.4. Calculation of solvation factor in different volumetric ratio of water-acetonitrile mixture

Volumetric Ratio(v/v%)	$E_{T(m)}$(kcal/mol)	molar fraction		Solvation factor (η)
		acetonitrile	water	
0		1	0	∞
10		0.756209	0.243791	6.743208
20		0.579587	0.420413	2.996981
30		0.445735	0.554265	1.748239
40		0.340795	0.659205	**1.12387**
50	45.6	0.256314	0.743686	**0.74925**
60		0.186839	0.813161	0.499497
70		0.128699	0.871301	0.321105
80		0.079328	0.920672	0.187311
90		0.036882	0.963118	0.083249
100		0	1	0

Table 2.5. Detection limit of colorimetric sensor for water

Solvent	R^2 (0 – 40% region)	LOD (%)
Ethanol	0.9994	1.666854
DMF	0.9481	12.3388
Acetonitrile	0.9736	8.920523

2.3.4. Quenching mechanism in presence of water

As shown in Figs. 2.12, 2.13 and 2.14, water content can be measured by the PL intensity change, especially at low water content. Water molecules can induce PL quenching by the destruction of the electronic state of CDs in organic solvents in three ways. First, when water is added to the organic solvents, the CDs starts to aggregate because of the low dispersion of CDs in water, which results in PL quenching because of the excessive resonance-energy transfer and $\pi-\pi^*$ interaction [10,13]. Second, the strong interaction between high polar solvents with p-PD in CDs can increase the rates of non-radiative decay [34]. Finally, water induced swelling can cause PL quenching, because swelling and shrinking are typical phenomena in graphene-like nanomaterials [39,40] because of the conformational change of CD molecules. In addition, water molecules, which partially exist as hydronium ions in multi-layers of CDs, have a role of as an electron-withdrawing compound [39,41], which can cause PL quenching. The water-induced structural change of CDs can be observed in the FT-IR spectra. As shown in Fig. 2.15, O-H stretching shifts from 3422 cm^{-1} to 3509 and 3540 cm^{-1} as the water content increases. In addition, the peak intensities at 1642 cm^{-1} and 1740 cm^{-1} originate from ester and amide bonding changes.

2.3.5. The paper-based humidity sensing strip

The paper-based sensing strip has several advantages, such as cost effectiveness, easy handling, and large production capability [17,42–44]. In this study, a paper-based sensing strip was fabricated simply by immersing a paper filter into the solution of CDs and air drying it. As shown in Fig. 2.16, as relative humidity level increases, gradual PL fading is observed, which can also be recognized by the naked eye.

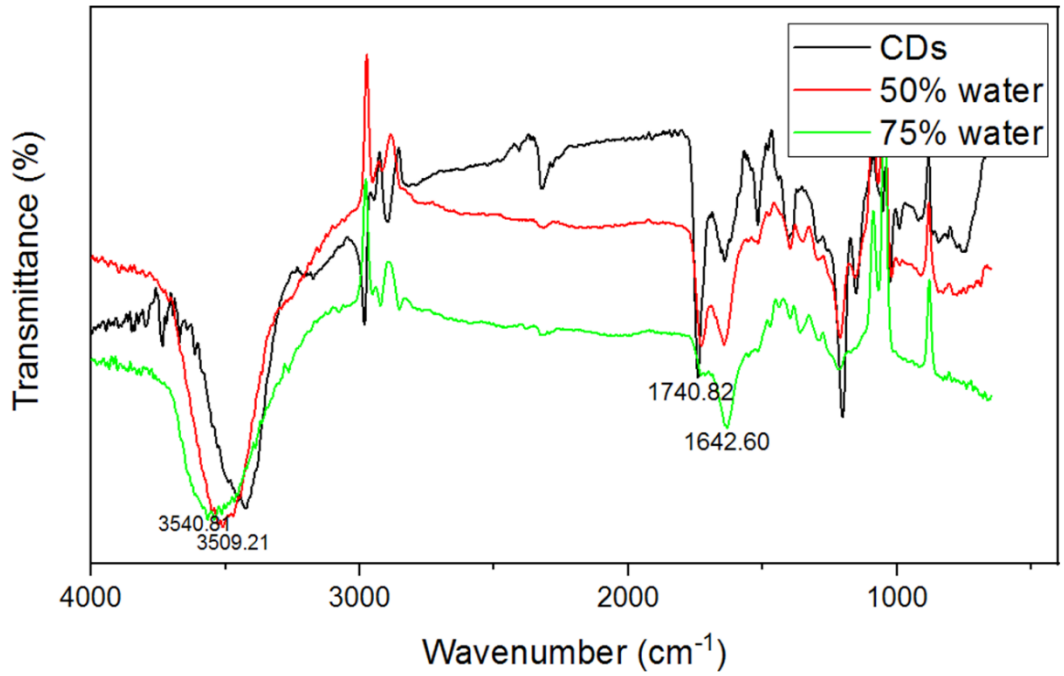

Fig 2.15. FT-IR spectra of CDs in the presence of water

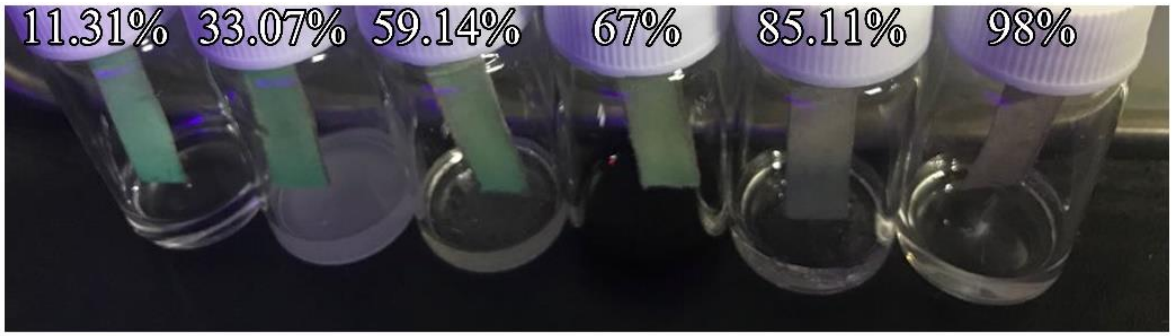

Fig 2.16. Photograph of paper sensor strips at different relative humidity (RH) level under UV illumination

2.4. Conclusions

Carbon dots (CDs) are successfully synthesized from NTA as a novel precursor and p-PD as aromatic amine precursor, but no CDs are obtained from other isomers of phenylenediamine, because of the differences in reactivity and steric hindrance about the reaction sites. The CDs fabricated in this study exhibit strong solvent-dependent optical properties. As the solvent polarity increases, the PL emission wavelength shifts to longer wavelengths and the bandwidth is broadened, perhaps because of the abundant edge N structures and strong solvation effect. When CDs are used to detect water content in organic solvents, they exhibit excellent linearity and a low detection limit, especially in ethanol. Using water-induced PL quenching behavior, a paper-based humidity sensing strip was also successfully demonstrated.

References

[1] S.N. Baker, G.A. Baker, Luminescent Carbon Nanodots: Emergent Nanolights, Angew. Chem. Int. Ed. 49 (2010) 6726-6744.

[2] S.Y. Lim, W. Shen, Z. Gao, Carbon quantum dots and their applications, Chem. Soc. Rev. 44 (2015) 362-381.

[3] Y. Wang, A. Hu, Carbon quantum dots: synthesis, properties and applications, J. Mater. Chem. C 2 (2014) 6921-6939.

[4] X.T. Zheng, A. Ananthanarayanan, K.Q. Luo, P. Chen, Glowing graphene quantum dots and carbon dots: Properties, syntheses, and biological applications, Small 11(2015) 1620–1636.

[5] S. Zhu, Y. Song, X. Zhao, J. Shao, J. Zhang, B. Yang, The photoluminescence mechanism in carbon dots (graphene quantum dots, carbon nanodots, and polymer dots): current state and future perspective, Nano Res. 8 (2015) 355–381.

[6] D. Gao, H. Zhao, X. Chen, H. Fan, Recent advance in red-emissive carbon dots and their photoluminescent mechanisms, Mater. Today 9 (2018) 103-113.

[7] M. Shamsipur, A. Barati, S. Karami, Long-wavelength, multicolor, and white-light emitting carbon-based dots: Achievements made, challenges remaining, and applications, Carbon 124 (2017) 429-472.

[8] Z.L. Wu, Z.X. Liu, Y.H. Yuan, Carbon dots: Materials, synthesis, properties and approaches to long-wavelength and multicolor emission, J Mater Chem B. 5 (2017) 3794–3809.

[9] K. Jiang, S. Sun, L. Zhang, Y. Lu, A. Wu, C. Cai, H. Lin, Red, green, and blue luminescence by carbon dots: Full-color emission tuning and multicolor cellular imaging, Angew. Chem. Int. Ed. 54 (2015) 5360-5363.

[10] H. Wang, C. Sun, X. Chen, Y. Zhang, V.L. Colvin, Q. Rice, J. Seo, S. Feng, S. Wang, W.W. Yu, Excitation wavelength independent visible color emission of carbon dots, Nanoscale 9

(2017) 1909–1915.

[11] S. Lin, C. Lin, M. He, R. Yuan, Y. Zhang, Y. Zhou, W. Xiang, X. Liang, Solvatochromism of bright carbon dots with tunable long-wavelength emission from green to red and their application as solid-state materials for warm WLEDs, RSC Adv. 7 (2017) 41552–41560.

[12] T. Zhang, J. Zhu, Y. Zhai, H. Wang, X. Bai, B. Dong, H. Wang, H. Song, A novel mechanism for red emission carbon dots: Hydrogen bond dominated molecular states emission, Nanoscale. 9 (2017) 13042–13051.

[13] D. Chao, W. Lyu, Y. Liu, L. Zhou, Q. Zhang, R. Deng, H. Zhang, Solvent-dependent carbon dots and their applications in the detection of water in organic solvents, J Mater Chem C 6 (2018) 7527–7532.

[14] H.S. Jung, P. Verwilst, W.Y. Kim, J.S. Kim, Fluorescent and colorimetric sensors for the detection of humidity or water content, Chem. Soc. Rev. 45 (2016) 1242–1256.

[15] Y. Guo, W. Zhao, Nanomaterials for luminescent detection of water and humidity, Analyst 144 (2019) 388-395.

[16] X. Wang, D. Wang, Y. Guo, C. Yang, A. Iqbal, W. Liu, W. Qin, D. Yan, H. Guo, Imidazole derivative-functionalized carbon dots: Using as a fluorescent probe for detecting water and imaging of live cells, Dalton Trans. 44 (2015) 5547-5554.

[17] C. Ye, Y. Qin, P. Huang, A. Chen, F.Y. Wu, Facile synthesis of carbon nanodots with surface state-modulated fluorescence for highly sensitive and real-time detection of water in organic solvents, Anal. Chim. Acta. 1034 (2018) 144–152.

[18] J. Wei, H. Li, Y. Yuan, C. Sun, D. Hao, G. Zheng, R. Wang, A sensitive fluorescent sensor for the detection of trace water in organic solvents based on carbon quantum dots with yellow fluorescence, RSC Adv. 8 (2018) 37028–37034.

[19] L. Greenspan, Humidity Fixed Points of Binary Saturated Aqueous Solutions, J. Res. Natl. Bur. Stand. 81A (1977) 89-96.

[20] L.B. Rockland, Saturated salt solutions for static control of relative humidity between 5° and 40 °C, Analytical Chemistry 38 (1960) 1375-1376.

[21] Y. Zhang, R. Yuan, M. He, G. Hu, J. Jiang, T. Xu, L. Zhou, W. Chen, W. Xiang, X. Liang, Multicolour nitrogen-doped carbon dots: Tunable photoluminescence and sandwich fluorescent glass-based light-emitting diodes, Nanoscale 9 (2017) 17849-17858.

[22] L. Li, G. Wu, G. Yang, J. Peng, J. Zhao, Jun-Jie Zhu, Focusing on luminescent graphene quantum dots: current status and future perspectives, Nanoscale 5 (2013) 4015-4039

[23] H. Peng, J. Travas-Sejdic, Simple Aqueous Solution Route to Luminescent Carbogenic Dots from Carbohydrates, Chem. Mater. 21 (2009) 5563-5565

[24] S. Dolai, S.K. Bhunia, R. Jelinek, Carbon-dot-aerogel sensor for aromatic volatile organic compounds, Sensors Actuators, B Chem. 241 (2017) 607–613.

[25] S. Dong, L. Chi, Z. Yang, P. He, Q. Wang, Y. Fang, Simultaneous determination of dihydroxybenzene and phenylenediamine positional isomers using capillary zone electrophoresis coupled with amperometric detection, J. Sep. Sci. 32 (2009) 3232-3238.

[26] Q.Q. Shi, Y.H. Li, Y. Xu, Y. Wang, X.B. Yin, X.W. He, Y.K. Zhang, High-yield and high-solubility nitrogen-doped carbon dots: formation, fluorescence mechanism and imaging application, RSC Adv. 4 (2014) 1563-1566.

[27] W.K. Surewicz, H.H. Mantsch, D. Chapman, Determination of Protein Secondary Structure by Fourier Transform Infrared Spectroscopy: A Critical Assessment, Biochemistry 32 (1993) 389–394.

[28] F. Mallamace, C. Corsaro, D. Mallamace, S. Vasi, C. Vasi, G. Dugo,The role of water in protein's behavior: The two dynamical crossovers studied by NMR and FTIR techniques,

Comput Struct Biotechnol J. 13 (2015) 33–37.

[29] D.K. Dang, C. Sundaram, Y.L.T. Ngo, W.M. Choi, J.S. Chung, E.J. Kim, S.H. Hur, Pyromellitic acid-derived highly fluorescent N-doped carbon dots for the sensitive and selective determination of 4-nitrophenol, Dyes and Pigments 165 (2019) 327-334.

[30] D. Qu, M. Zheng, L. Zhang, H. Zhao, Z. Xie, X. Jing, R.E. Haddad, H. Fan, Z. Sun, Formation mechanism and optimization of highly luminescent N-doped graphene quantum dots, Sci Rep. 4 (2014) 1-11.

[31] H. Auweter, H. Haberkorn, W. Heckmann, D. Horn, E. Lüddecke, J. Rieger, H. Weiss, Supramolecular Structure of Precipitated Nanosize b-Carotene Particles, Angew. Chem. Int. Ed. 38 (1999) 2188-2191

[32] L. Tian, D. Ghosh, W. Chen, S. Pradhan, X. Chang, S. Chen, Nanosized Carbon Particles From Natural Gas Soot, Chem. Mater. 21 (2009) 2803–2809

[33] S. Qu, X. Wang, Q. Lu, X. Liu, L. Wang, A Biocompatible Fluorescent Ink Based on Water-Soluble Luminescent Carbon Nanodots, Angew. Chem. Int. Ed. 51 (2012) 12215 –12218

[34] R. Manoharan, S.K. Dogra, Spectral Characteristics of Phenylenediamines and Their Various Protonated Species, Bull. Chem. Soc. Jpn. 60 (1987) 4409-4415

[35] A. Sharma, T. Gadly, S. Neogy, S.K. Ghosh, M. Kumbhakar, Molecular Origin and Self-Assembly of Fluorescent Carbon Nanodots in Polar Solvents,J. Phys. Chem. Lett. 8 (2017) 1044–1052.

[36] C. Reichardt, Solvatochromic Dyes as Solvent Polarity Indicators, 94 (1994) 2319–2358.

[37] A. Pramanik, S. Biswas, P. Kumbhakar, Solvatochromism in highly luminescent environmental friendly carbon quantum dots for sensing applications: Conversion of bio-waste into bio-asset, Spectrochim Acta - Part A Mol Biomol Spectrosc. 191 (2018) 498–512.

[38] A. Shrivastava, V. B Gupta, Methods for the determination of limit of detection and limit

of quantitation of the analytical methods, Review Article 2 (2011) 21–25.

[39] T. Alizadeh, M. Shokri, A new humidity sensor based upon graphene quantum dots prepared via carbonization of citric acid, Sensors Actuators, B Chem. 222 (2016) 728–734.

[40] T.S. Sreeprasad, A.A. Rodriguez, J. Colston, A. Graham, E. Shishkin, V. Pallem, V. Berry, Electron-tunneling modulation in percolating network of graphene quantum dots: fabrication, henomenological understanding, and humidity/pressure sensing applications, Nano Lett. 13 (2013) 1757–1763.

[41] P. Su, C. Chiou, Electrical and humidity-sensing properties of reduced graphene oxide thin film fabricated by layer-by-layer with covalent anchoring on flexible substrate, Sensors Actuators B Chem. 200 (2014) 9–18.

[42] Y. Kim, G. Jang, T.S. Lee, New Fluorescent Metal-Ion Detection Using a Paper-Based Sensor Strip Containing Tethered Rhodamine Carbon Nanodots, ACS Appl. Mater. Interfaces 7 (2015) 15649-15657.

[43] M. Zheng, Y. Li, Y. Zhang, Z. Xie, Solvatochromic fluorescent carbon dots as optic noses for sensing volatile organic compounds, RSC Adv. 6 (2016) 83501–83504.

[44] X. Tian, H. Peng, Y. Li, C. Yang, Z. Zhou, Y. Wang, Highly sensitive and selective paper sensor based on carbon quantum dots for visual detection of TNT residues in groundwater, Sensors Actuators, B Chem. 243 (2017) 1002–1009.

Chapter 3. Fabrication of dual emission carbon dots and its use in highly sensitive thioamide detection

3.1. Introduction

Many attempts have been made to develop effective sensing devices by using carbon allotrope families such as carbon nanotubes (CNT), graphene-like 2D materials, graphene quantum dot (GQD), carbon dot (CDs) for the industrial and biological applications [1–6]. Among them, CDs draw a great attention for the fluorescence sensor because of their high sensitivity, excellent selectivity, simplicity and rapid response, which are originated from their unique molecular system that physicochemical properties can be changed by the interaction with specific chemical species [7,8].

Generally, the synthesis of CDs can be classified into top-down [9–11] and bottom-up approaches [12–14]. Recently, bottom-up approaches have been widely studied because properties of CDs such as doping of heteroatoms and structures can be precisely controlled by the precursors and synthetic process [15–18]. Krysmann et al. synthesized CDs based on citric acid and ethanolamine through pyrolysis, which showed the presence of amide intermolecular reaction and formation of carbogenic cores by cross-linking reactions in the interchain of CDs [15]. Song et al. suggested the possible intermediate in synthesis process and formation of carbon core from assembly of fluorophore and crosslinking of polymer clusters [16]. Sarkar et al. presented the effect on optical properties of nitrogen doping in CDs through computational modeling based on time-dependent density functional theory (TD-DFT). They revealed that the graphitic nitrogen had an important role of long-wavelength emission [17]. Hola et al. clarified the role of graphitic nitrogen by the theoretical calculation and experimental result together. They showed that graphitic nitrogen created mid-gap states in original gaps, which

showed great effects on the photoluminescence properties of CDs [18].

Thioacetamide (TAA) is well-known as liver carcinogen to human. It can lead to necrosis and liver injury by inhibiting protein synthesis, RNA and DNA activity. Nonetheless, people can be exposed to it in various workplaces including leather, textile, and paper industries [19,20]. Even though the monitoring of TAA level is very important in view of health care, only limited studies have been reported so far. D. Cinghit¸a et al. reported the used a glass carbon (GC) electrode to detect TAA by the electro-catalytic system, especially by the anodic oxidation [21]. D. Saha et al. synthesize the ZnO quantum dot (QD) to detect the TAA via interaction between surface of QD and –NH and sulphur groups of TAA [22].

Herein, we report a very sensitive photoluminescence (PL) based TAA sensor. Photoluminescent CDs are successfully synthesized from EDTA (ethylenediaminetetraacetic acid) and L-tryptophan via hydrothermal synthesis which is one of the bottom-up approaches and has several advantages in view of freedom of precursor choice as well as easiness in the controlling of reaction conditions. In our knowledge, this is first time to show the thioacetamide sensor based on organic CDs, which is more advantageous than metal-based QDs in view of low toxicity of organic precursors [23]. The reaction conditions are systematically investigated to control the nitrogen and oxygen functionalities precisely, which resulted in high quantum yields (QYs). The CDs fabricated in this study exhibit excellent sensitivity and selectivity towards TAA with wide linear range and low detection limit, which can be due to photo-induced electron transfer (PET) between tryptophan structure of CDs and TAA. Especially, dual emission with different quenching characteristics can realize highly sensitive thioacetamide sensor with wide linear range and low detection limit. We have used fluorescence spectroscopy for the detection to achieve more sensitivity. The as-prepared probe

shows dual emission when excited at 240 nm. The dual emission peaks increased the accuracy of the assay method. In this way, the influence by external agents on the test results can also be avoided [24]. By using dual emission probe, we have achieved detection of TAA over two different ranges.

3.2. Experimental

3.2.1. Chemicals

Sodium hydroxide (NaOH), hydrochloric acid (HCl), thiourea, L-Cysteine, L-Glutathione (GSH) reduced, L-lysine, l-cysteine, sucrose and thioacetamide are purchased from Sigma-Aldrich Co. Ltd (USA). L-histidine is purchased from Acros Chemical Co. (USA). L-tryptophan, Ethylenediaminetetraacetic acid, glycine, lactose monohydrate and dextrose are purchased from Daejung Chemicals & Metals Co. Ltd. (Republic of Korea). Urea is purchased from Yakuri pure chemicals Co., Ltd. (Japan). All the reagents were used without further purification.

3.2.2. Characterization

The morphology and size of CDs were investigated by field emission transmission electron microscope (FE-TEM, JEL-2100F, JEOL, Japan). UV–Vis absorption spectra and fluorescence spectra were collected by Specord 210 Plus (Analytik Jena, Germany) and Cary Eclipse Fluorescence Spectrophotometer G9800AA (Agilent Technologies, USA), respectively. X-ray photoelectron spectroscopy (XPS, K-alpha, Thermo Fisher Scientific, USA) was used to determine element composition. Fourier-transform infrared spectroscopy (FT-IR, Nicolet iS5 FTIR Spectrometer, Thermo Fisher Scientific, USA) was used to investigate surface functional groups.

3.2.3. Synthesis of CDs

As illustrated in Fig 3.1, CDs were synthesized from EDTA and L-tryptophan via hydrothermal process. Firstly, EDTA (147 mg) and L-tryptophan (103 mg) were dissolved in 10 mL DI water while stirring for 30 min using magnetic bar. Before reaction, the pH value of

the solution was ~3. Then, the solution was transferred to Teflon-lined stainless-steel autoclave. It was placed into muffle furnace, heated to 160 ℃ and maintained for 6 h. After cooling down, resulting solution was kept at ambient condition for 1 day because the residual byproducts could be moved out very slowly. The solution was filtered using common filter paper to remove large brown powder-like byproduct and centrifuged at 10000 rpm for 10 min to remove the residues and impurities. For further purification, dialysis was performed [25]. The solution was then kept inside a dialysis bag (1000 Da) for 24 h and then the spectroscopic properties were measured. To investigate the formation mechanism and optimize the reaction conditions, several parameters including concentration of precursor, molar ratio of reactants, reaction temperature, and reaction time were varied.

Typically, when one parameter was changed within pre-determined range, other conditions are fixed. The ranges of the concentration of precursors, molar ratio of each precursor, reaction temperature, and reaction time were 50–500 mg, (9:1, 4:1, 3:2, 1:1, 2:3, 1:4, 1:9), 140–180 ℃, (4, 6, 8, 12 h), respectively.

3.2.4. Quantitative analysis of TAA

Firstly, 1.40 mL of CD solution (16 mg/mL) was diluted in D.I.water as the total amount of solution was set up 100 mL. Then, 3.6 mL of CD solution was mixed with the 0.4 ml of the target solutions which were prepared beforehand with pre-determined concentration of analytes. The concentration of various metal ions and organic molecules including urea, L-cysteine, L-glutathione, thiourea, and thioacetamide solution (1.0 M) was kept to 0.1 M. To determine the limit of detection (LOD) for TAA, fluorescence spectra were collected specific range, respectively. All measurement was done with 2.5 nm excitation slit.

3.2.5. Determination of quantum yield

The quantum yield of CDs fabricated in this study was determined by the comparison of the fluorescence spectra with those of the standard sample as described in the previous report [26]. Quinine bisulfate (0.1N H_2SO_4, ϕ=0.54) was selected by reference material for all range of the emissions. Fluorescence spectra was collected with 2.5 nm excitation slit bandwidth and 5 nm emission slit bandwidth. The following equation was used to determine the quantum yields.

$$\phi_x = \phi_s \frac{A_s}{A_x} \frac{F_x}{F_s} (\frac{n_x}{n_s})^2$$

The subscript of "χ" means the sample and "s" means the reference material. ϕ is quantum yield, A is absorbance at the excitation wavelength, F is the integrated emission area across the band and n is refractive index of solvents. The absorbance was kept below 0.1 and the measurement was done at room temperature.

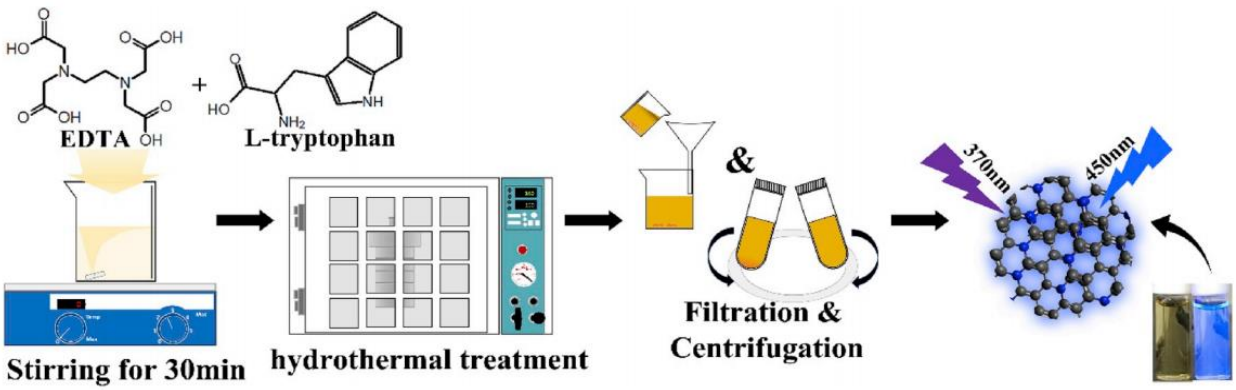

Fig 3.1. Schematic diagram of CDs synthesis

3.3. Results and Discussion

3.3.1. Optimization of reaction conditions

To obtain the high quantum yield CDs, the effects of four major factors including concentration of precursors, molar ratio of precursors, reaction temperature, reaction time during the hydrothermal synthesis on the photoluminescence properties were systematically investigated. All results are summarized in Fig. 3.2, and Tables 3.1 and 3.2.

Firstly, as the concentration of precursor are increased, maximum absorbance wavelength that is originated from the π-π* transition is red shifted as shown in Fig. 3.2a and 3.3, which indicates the increase of sp^2 cluster of carbon core by the enhanced reaction rate [27,28]. The highly red-shifted π-π* transition at very low concentration can be due to increased possibility of intermolecular condensation as well as consumption of abundant surface groups because polymeric chain growth easily terminated after almost precursors were consumed, which suggests that continuous flow reactor that can maintain the constant concentration of reactants may be more ideal to obtain uniform CDs at large industrial scale than batch-type reactor.

Secondly, as the molar ratio of EDTA increases, the QY of CDs initially increases and almost constant saturates over 1:1 ratio (Fig. 3.2b and Table 3.1), which can be due to n-π* transition contributed by abundant non-bonding lone pairs of electrons in the large amounts carboxylic acid groups in EDTA [29]. In addition, the increase in the maximum absorbance wavelength and surface/core intensity ratio (Fig. 3.3b) also indicates that disordered amorphous sp^3 structure and surface groups increase as the EDTA ratio increases [30].

Thirdly, the formation mechanism of CDs is explained by step-by step condensation, carbonization, and polymerization. High temperature and long reaction time can give fast

reaction and large clusters [7,15,16], however, such conditions can deteriorate the reactants or products at the same time. Fig. 3.2c clearly shows that as the reaction temperature increases, the absorption peak from sp^2 cluster of carbon core gradually blue-shifts, which can be due to the decomposition of EDTA [31], CD itself [32] and/or enhanced amide hydrolysis at high temperature acidic condition. The maximum QY of CDs in this study can be obtained at 160 ℃, 6 h with 1:1 EDTA : tryptophan ratio (Fig. 3.2d). All optical and instrumental analyses were conducted with the CDs fabricated in this condition.

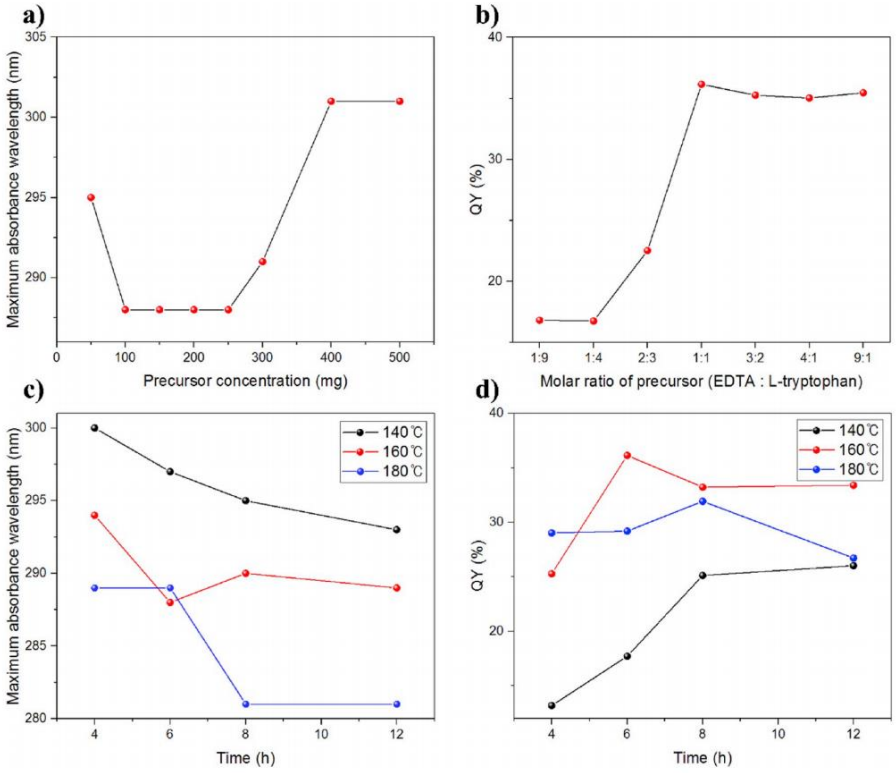

Fig 3.2. The change of maximum absorbance wavelength (a) at various concentration of precursor, (c) at various reaction time and temperature. Quantum yield (b) at various molar ratio of precursors (d) at various reaction time and temperature

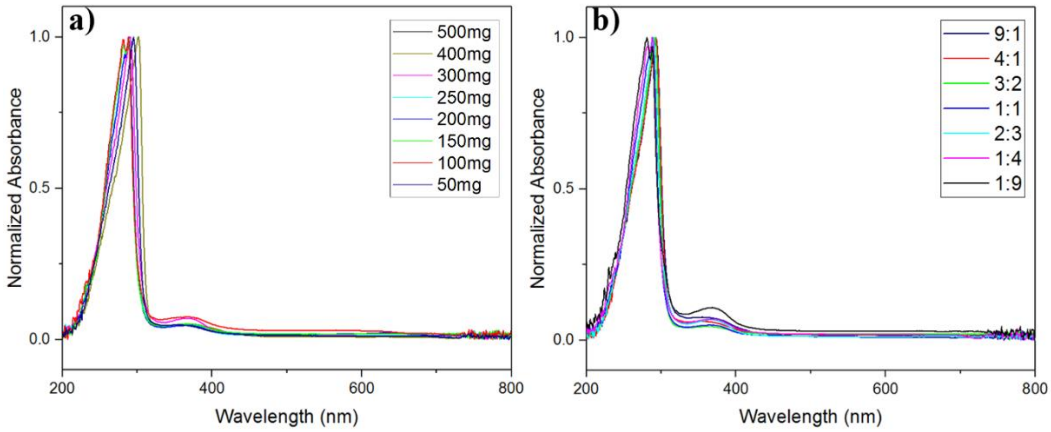

Fig 3.3. Normalized absorbance spectra at (a) different CD concentration (160℃, 6h, molar ratio of 1:1) and (b) various molar ratio of precursors (160℃, 6h, total molar concentration of 1 M)

Table 3.1. The effect of concentration and molar ratio of the precursors on the quantum yield

Reaction condition	Precursor concentration(mg)		FL spectra wavelength (nm)		UV-Vis Absorbance spectra		QY
	EDTA	Tryptophan	Excitation	maximum emission	Maximum wavelength(nm)	Core/surface ratio	
concentration (160℃, 6h, molar ratio 1:1)	29	21	360	453	295	0.04864	12.49
	59	41	370	453	288	0.07472	28.63
	88	62	370	452	288	0.05209	30.88
	118	82	370	452	288	0.04696	31.06
	147	103	370	455	288	0.05033	36.15
	176	124	370	451	291	0.06991	34.42
	235	165	370	453	301	0.05179	6.63
	294	206	370	443	301	0.05179	9.35
Molar ratio (160℃, 6h, total molar concentration 1 M)	29	184	360	454	293	0.07556	16.81
	58	163	360	453	293	0.06243	16.75
	117	122	360	452	292	0.04477	22.52
	147	103	370	455	288	0.05033	36.15
	175	82	370	452	290	0.05796	35.26
	234	41	370	453	288	0.06955	35.03
	263	20	370	453	281	0.1077	35.46

Table 3.2. The effect of reaction temperature and time on the quantum yield

Reaction condition (250mg, 1:1)		FL spectra wavelength (nm)		UV-Vis Absorbance spectra		QY (%)
Temp (℃)	Time (h)	Excitation	maximum emission	Maximum wavelength(nm)	Core/surface ratio	
140	4	370	457	300	0.06072	13.19
140	6	370	456	297	0.05426	17.72
140	8	370	456	295	0.05651	25.13
140	12	370	455	293	0.05326	26.03
160	4	370	453	294	0.05525	25.29
160	6	370	455	288	0.05033	36.15
160	8	370	453	290	0.05312	33.24
160	12	370	453	289	0.06519	33.42
180	4	360	452	289	0.08011	29.03
180	6	360	450	289	0.09673	29.21
180	8	360	450	281	0.09157	31.94
180	12	350	448	281	0.12285	26.74

3.3.2. Physicochemical property of CDs

The morphology and size of CDs were investigated by TEM. As shown in Fig. 3.4a, CDs are well-dispersed and possess clear crystalline structure with lattice spacing of 0.21 nm corresponding to (100) facet of graphitic structure [18,31]. The size distribution in the range of 4–16 nm is shown in Fig. 3.4b and the average size of CDs is calculated to be about 9.4 nm. As shown in Fig. 3.5, XRD patterns shows a broad peak at 22º, which is amorphous phase because of turbostratic disorder and a lot of functional groups on edges of CDs [33–35] The formation of relatively large CDs can be the effect of indole positioned at side chain of amino acid [36,37]. In addition, at acidic condition the aromatic structure of indole enhances π-π* stacking interactions, which can form rigid structure during the formation of CDs [38].

FT-IR was used to determine the functional groups of CDs and shown in Fig. 3.6. The strong peak at 3406 cm^{-1} can be assigned to N–H stretching vibrations of amide, indole, and primary and secondary amine groups. The reduced intensity of this peak shows the change of nitrogen containing structures. In addition, the C—O stretching vibration peak of amide shown at 1666 cm^{-1} disappears after 6 h hydrothermal reaction at 160 ℃, which indicates that the amide nitrogen atoms are converted to pyrrolic, pyridinic, graphitic form in sp^2 cluster [39,40]. The peaks shown at 1456, 1591, 3046 cm^{-1} can be attributed to C=C stretching vibrations of the aromatic structures. The increase in the intensity of the broad peak at 1615 cm^{-1} can be due to the increased sp^2 conjugated system as the elaborated reaction conditions. The peaks of CDs treated at 140 ℃ for 4 h including 1412 cm^{-1} (O–C=O stretching), 1357 cm^{-1} (C–N stretching), 1232 cm^{-1} (CH_2 bending), 1101 cm^{-1} (C–O stretching), 1008 cm^{-1}, 920 cm^{-1}, 850 cm^{-1} (aromatic mode), 746 cm^{-1} (O–C–=O bending) are all slightly shifted those at 160 ℃, 6 h, which also indicates that there are some subtle changes in chemical environment due to further

carbonization [38,41,42].

XPS was used to investigate chemical structure and the elemental composition of CDs in detail. As shown in Fig. 3.7, the binding energies of C_{1s} (286 eV), N_{1s} (402 eV), and O_{1s} (532 eV) in the CDs fabricated at 140 ℃ for 4 h are slightly down shifted to 285 (C_{1s}), 400 (N_{1s}), and 531 eV (O_{1s}) in the CDs fabricated at 160 ℃ for 6 h. This indicates more increased formation of nitrogen to carbon bonds such as pyrrolic and pyrrolidone as well as higher sp^2 to sp^3 bond ratio of carbon core at higher and longer hydrothermal treatment [39,40,43,45].

As shown in Fig. 3.8a and 3.8b, C_{1s} XPS spectra can be typically deconvoluted into three main peaks of C–=C peak (~284 eV), C–C/C–N/C–O (~286 eV), and C=O/O–C=O (~290.0 eV) [36–39,42,44]. It is obvious that O–C=O peak decreases and C=C peak increases at 160 ℃ for 6 h thermal treatment, which also indicates that more sp^2 carbon cores are formed after further carbonization [16,31]. In addition, the absence of carboxyl group and the presence of small amount of carbonyl group (278.8 eV) in the CDs fabricated at 160 ℃ for 6 h indicate the formation of amide bonds during the hydrothermal treatment.

The deconvoluted O_{1s} XPS spectrum shown in Fig. 3.8c exhibits quinone C=O (~530 eV) [45,46], carbonyl (~531 eV) [45,47], and carboxylic –OH (~533 eV) peaks [44,48]. After further carbonization (Fig. 3.8d), carboxylic –OH related peak disappears, which also can be the evidence of consumption of carboxylic acid during the formation of CDs.

N_{1s} XPS spectrum can be typically deconvoluted into 5 subpeaks including pyridinic N (398.1–399.3 eV), amino N (399-399.3 eV), pyrrolic N (399.8–401.2 eV), protonated or graphitic N (401.1–402.7 eV) and oxidized or N (403–405 eV) [49–52]. The small peak at 403.7 eV shown in Fig. 3.8e indicates the existence of the oxidized N, which is because tryptophan can be oxidized due to the protonation of carboxylic acid above 140 ℃ [43]. The

decreased intensity of oxidized N and increase of pyridinic N at higher and longer hydrothermal treatment indicates the formation of more sp^2 networks in the CD cores [39,53].

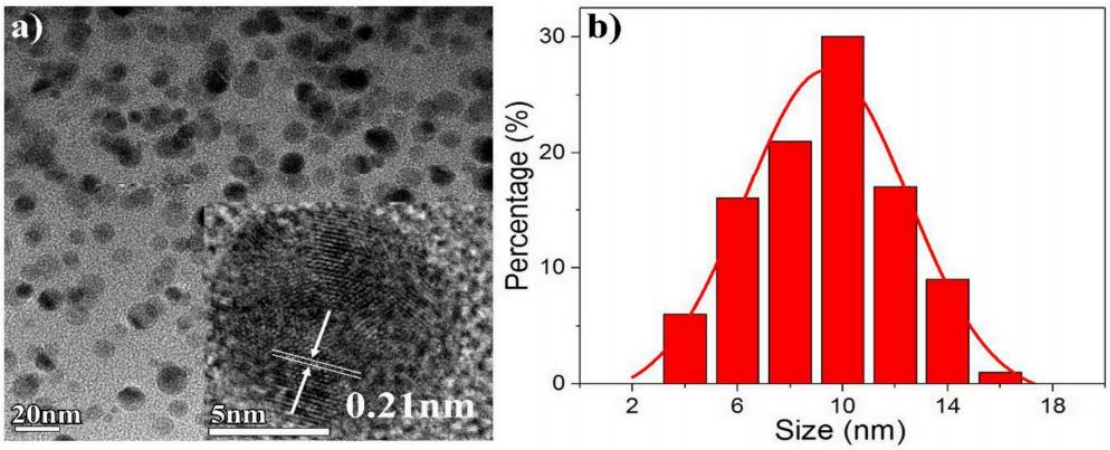

Fig 3.4. (a) TEM images of CDs (inset shows HR-TEM images of CDs. (b) Size distribution of CDs

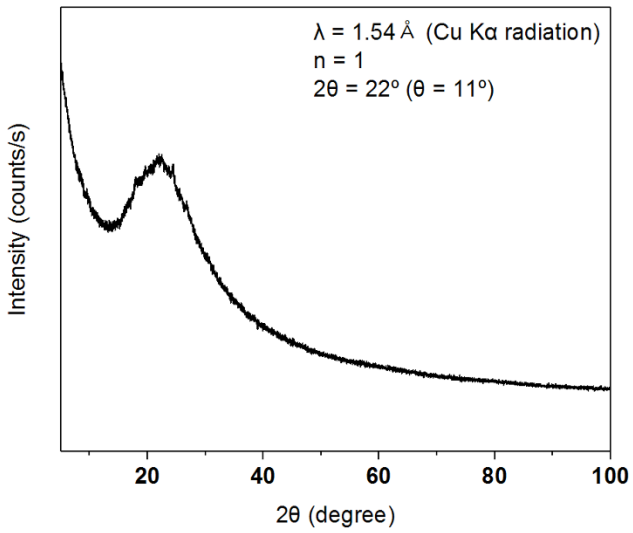

Fig 3.5. XRD spectra of CDs fabricated at 160℃ for 6h

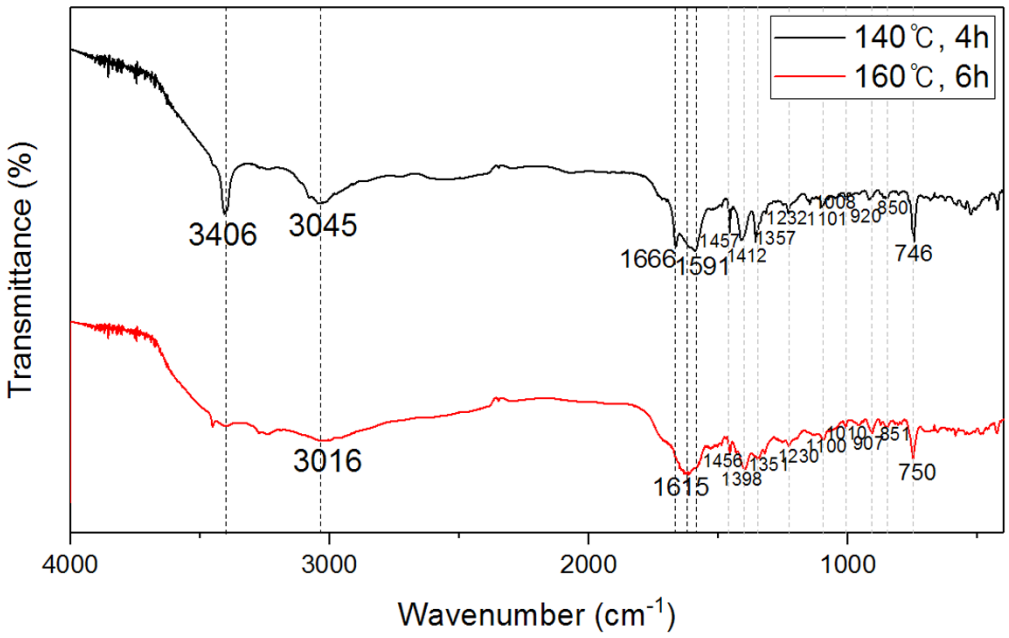

Fig 3.6 FT-IR spectra of CDs fabricated at (a) 140℃ for 4h and (b) 160℃ for 6h. The total molar concentration was 1 M and molar ratio of precursors was 1:1

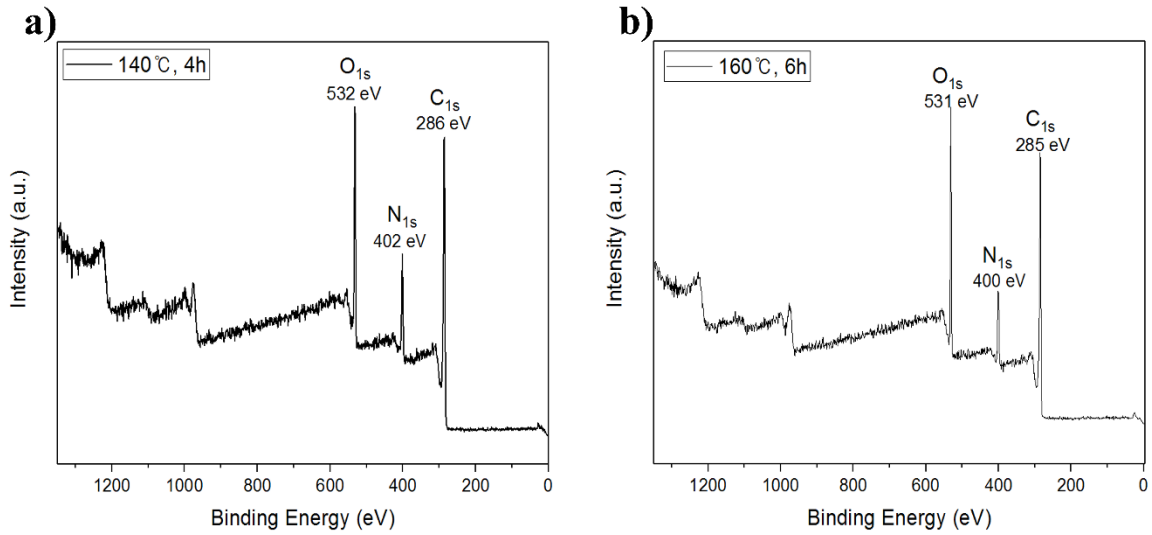

Fig 3.7. XPS spectra of CDs fabricated at (a) 140℃ for 4h and (b) 160℃ for 6h. The total molar concentration was 1 M and molar ratio of precursors was 1:1

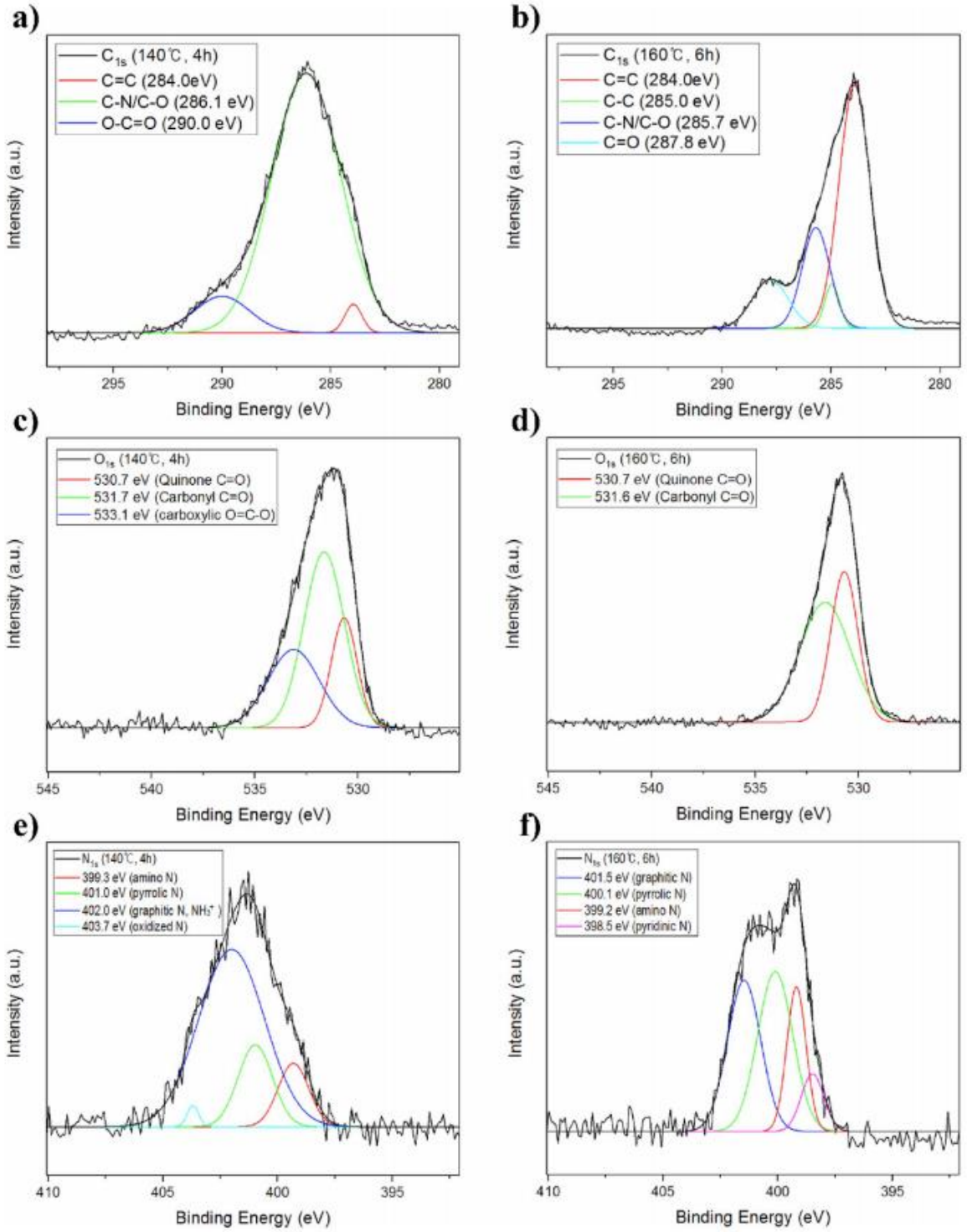

Fig 3.8. High-resolution XPS spectra of (a, b) C_{1s}, (c, d) O_{1s}, and (e, f) N_{1s}. CDs were fabricated at 140℃ for 4 h (total molar concentration 1 M, molar ratio 1:1) for (a, c, e) and at 160℃ for 6 h (total molar concentration 1 M, molar ratio 1:1) for (b, d, f)

3.3.3. Optical properties of CDs

To investigate the optical properties of CDs, fluorescence measurement was conducted. As shown in Fig. 3.9a, CDs exhibit dual emission bands centered at 360 nm and 450 nm in case of high energy excitation and single emission band centered at 450 nm in case of low energy excitation. The dual emission may be originated from tryptophanyl cores and functional groups at the surface. From the characterization part it is observed that there are different functional groups at the surface including –OH and –C=O etc. This passivated surface may be the reason for the emission along with the carbonized core.

Tryptophan itself is a fluorophore and shows emission band at 360 nm when it is excited with high energy (Fig. 3.10a). However, when the tryptophan molecules are physically mixed with CDs, they only quench the PL intensity of 450 nm emission (Fig. 3.9b), with the increase of n-π transition from functional groups [45,55] (Figs. 3.11c–d). Moreover, the physically mixed tryptophan does not show any effects on the TAA sensing. This means that not the residual tryptophan molecules, but the tryptophan structures formed via condensation reaction in the CDs may cause the emission at 360 nm [16,56]. The different PLE spectra between pure tryptophan (Fig. 3.10b) and CDs (Fig. 3.11) also reveals that luminescence center of tryptophan and tryptophanyl domain in the CDs are totally different. It is interesting to note that 360 nm emission disappears at high CD concentration (Fig. 3.11a), which can be due to the aggregation-induced quenching especially at tryptophanyl cores in the CDs.

Another emission band at 450 nm can be attributed to the defects, or nitrogen and oxygen related functional groups, which exhibits an excitation-wavelength independent behavior. Generally, CDs exhibit excitation-wavelength dependent behavior because of the abundant surface traps, edge states, and broad size distribution that can cause different emission

wavelength [54]. The uniform carbon cores and edge structures may cause uniform fluorescence radiative processes [36], which resulted in the excitation-wavelength independent PL emission of CDs fabricated in this study. As shown in Fig. 3.12, fluorescence quenching in the basic condition can be obviously observed, which can be due to the deprotonation of the nitrogen species [57,58]. The TAA sensing was carried out at pH 4 to ensure high photoluminescence intensity.

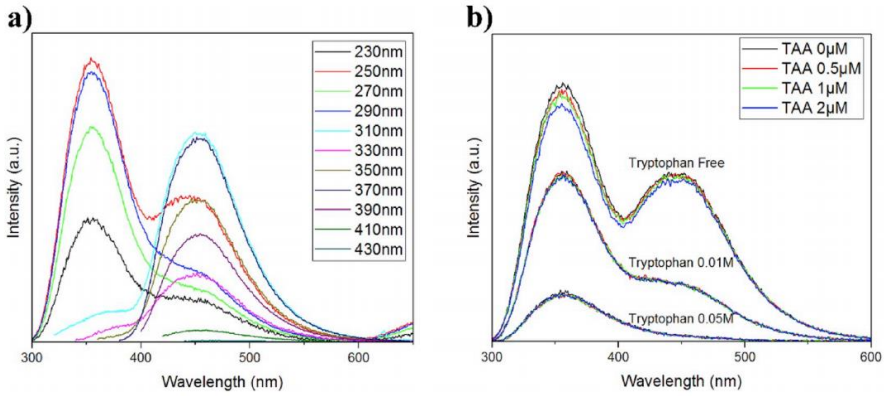

Fig 3.9. PL spectra of CDs (a) at different excitation wavelength, (b) at various tryptophan concentrations

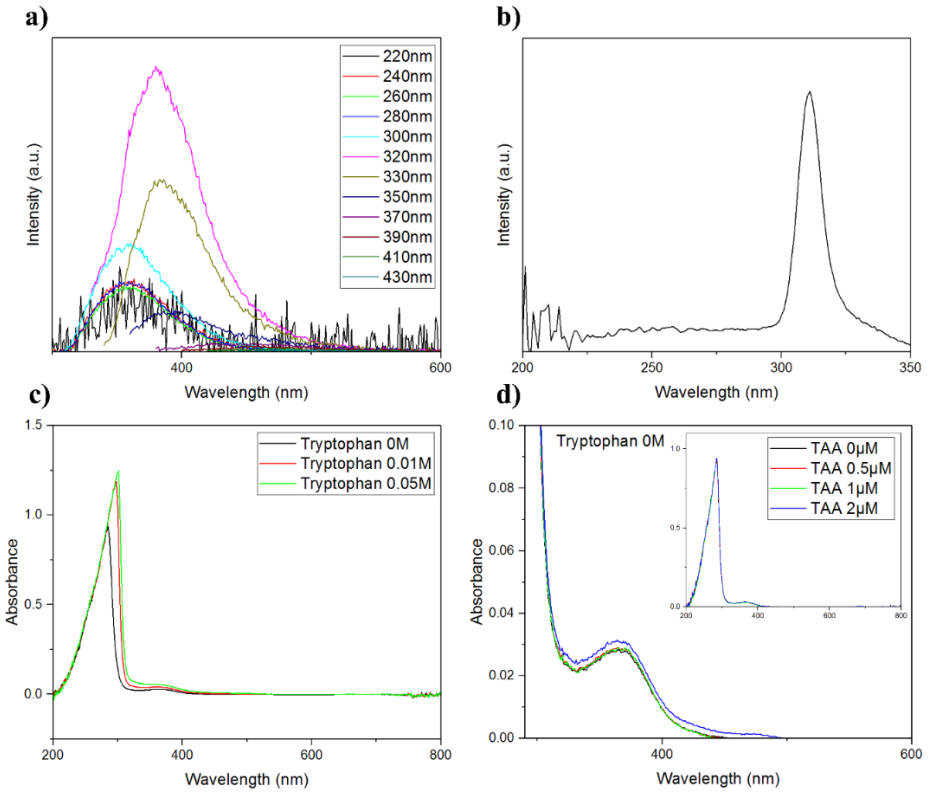

Fig 3.10. (a) PL spectra of pure tryptophan at various excitation wavelength. (b) Photoluminescence excitation spectrum of tryptophan (c) Absorbance spectra of CDs with pre-determined concentration of tryptophan (0, 0.01, 0.05M) (d) Absorbance spectra with TAA (0, 0.5, 1, 2μM)

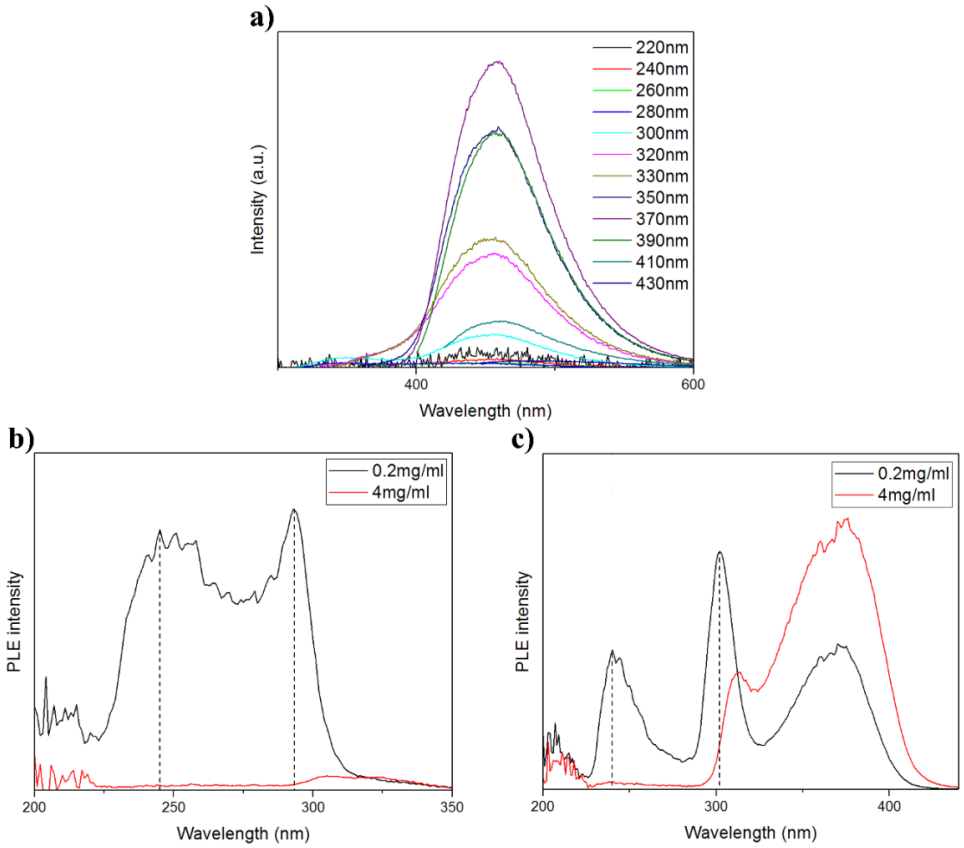

Fig 3.11. (a) PL spectra of CDs at high concentration (4mg/ml). Photoluminescence excitation spectra of CDs at different concentration excited (b) at 360nm and (c) at 450nm

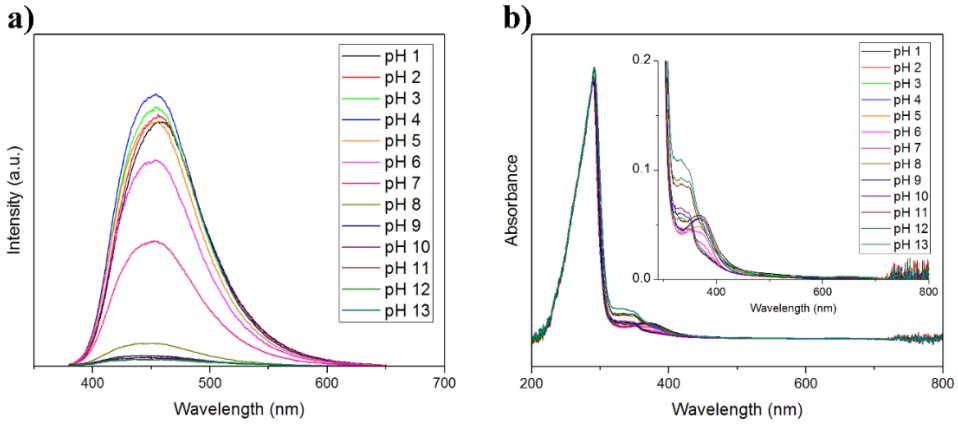

Fig 3.12. (a) PL spectra and (b) PL intensity of CDs at different pH. The excitation wavelength was 370 nm

3.3.4. Quantitative analysis of TAA in the aqueous solution

To optimize CD-based TAA sensing, the effect of concentration of CDs was systematically investigated in view of PL intensity and quenching efficiency (Fig. 3.13). As shown in Fig. 3.13a, as the concentration of CDs increases, PL intensities of both emission bands decreases at high energy excitation. However, PL intensity of 450 nm at low energy excitation initially increases as the CD concentration increases but decreases at too high CD centration as shown in Fig. 3.14a, which means that tryptophanyl cores aggregate at lower CD concentration that of defects or functional group originated emission sites.

The quenching efficiencies for both emission bands show same trend that more quenching can be obtained at lower CD concentration (Fig. 3.13b and Fig. 3.14b), which can be due to the more interaction between TAA and CDs than that between CDs themselves at lower CD concentration.

It is interesting to note that the sensitivity, low detection limit, and linear detection range depend on the excitation and emission wavelength, which means that each emission band can be used to obtain different sensing properties in TAA sensing. As shown in Fig. 3.13c–d, Fig. 3.14c-d, and Table 3.3, the high sensitivity and very low detection limit can be obtained when TAA induced quenching is monitored with the 360 nm emission band at 240 nm excitation. On the other hand, very wide linear range especially to very high TAA concentration can be achieved by using 450 nm emission band at 370 nm excitation. As compared in Table 3.4, a very low detection limit of 0.0703 μM (S/N = 3) and an extremely wide linear range of 0–10000 μM of CDs fabricated in this study are much better TAA sensing properties than those obtained from voltammetry or amperometry approaches. To determine TAA sensing properties, Stern-Volmer plot was used as shown in Fig. 3.14c-d. CD-TAA sensing system at both emission

band has good linearity (R^2 = 0.9995, 0.99855), which indicated that kinetics of fluorescence quenching is based on dynamic quenching. As shown in Fig. 3.15, fluorescence decay analysis revealed the decrease in lifetime in presence of TAA.

To study the quenching mechanism in detail, oxoamide compound such as urea and thioamide compound such as thiourea were tested further. As shown in Fig. 3.16, only thioamide compounds such as TAA and thiourea can cause PL quenching at both emission bands. Sulphur containing compounds can act as a good hole acceptor due to the presence of a lone pair of electrons on the nitrogen and sulphur atoms. It has been reported that oxoamide/thioamide induced quenching of fluorophores can occur through a dynamic photoinduced electron transfer mechanism [59–63] but the sensitivity and stability of charge transfer complex differ according to the electron donor ability of analytes [59, 60]. A lower oxidation potential (1.21 eV) of thioamide than that of oxoamide (3.25 eV) may result in the significant PL quenching of the CDs fabricated in this study [62,63].

To investigate selectivity of CDs, the interference study of biomolecule such as glucose, sucrose, lactose, some amino acids was done as shown in Fig. 3.17. There is slight interference of all given biomolecules at 360 nm emission band. However, strong quenching occurred from histidine and lysine, which interfered remarkably in TAA sensing system at 450 nm emission band. This interference can be removed by tuning the excitation wavelength. To apply on real sample assay, TAA sensing performances was shown in Table 3.5.

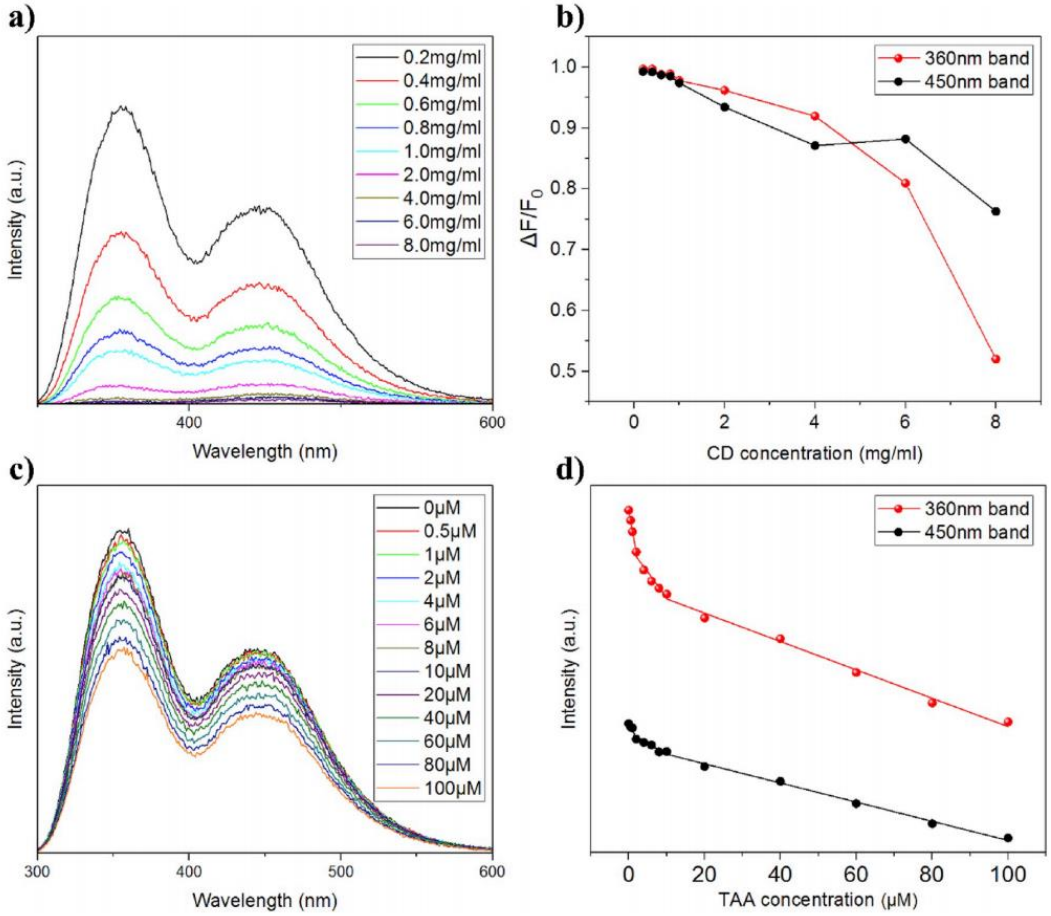

Fig 3.13. (a) PL spectra and (b) quenching efficiency at various CD concentrations. (c) PL spectra and (d) PL intensity at various TAA concentrations. The excitation wavelength was 240 nm

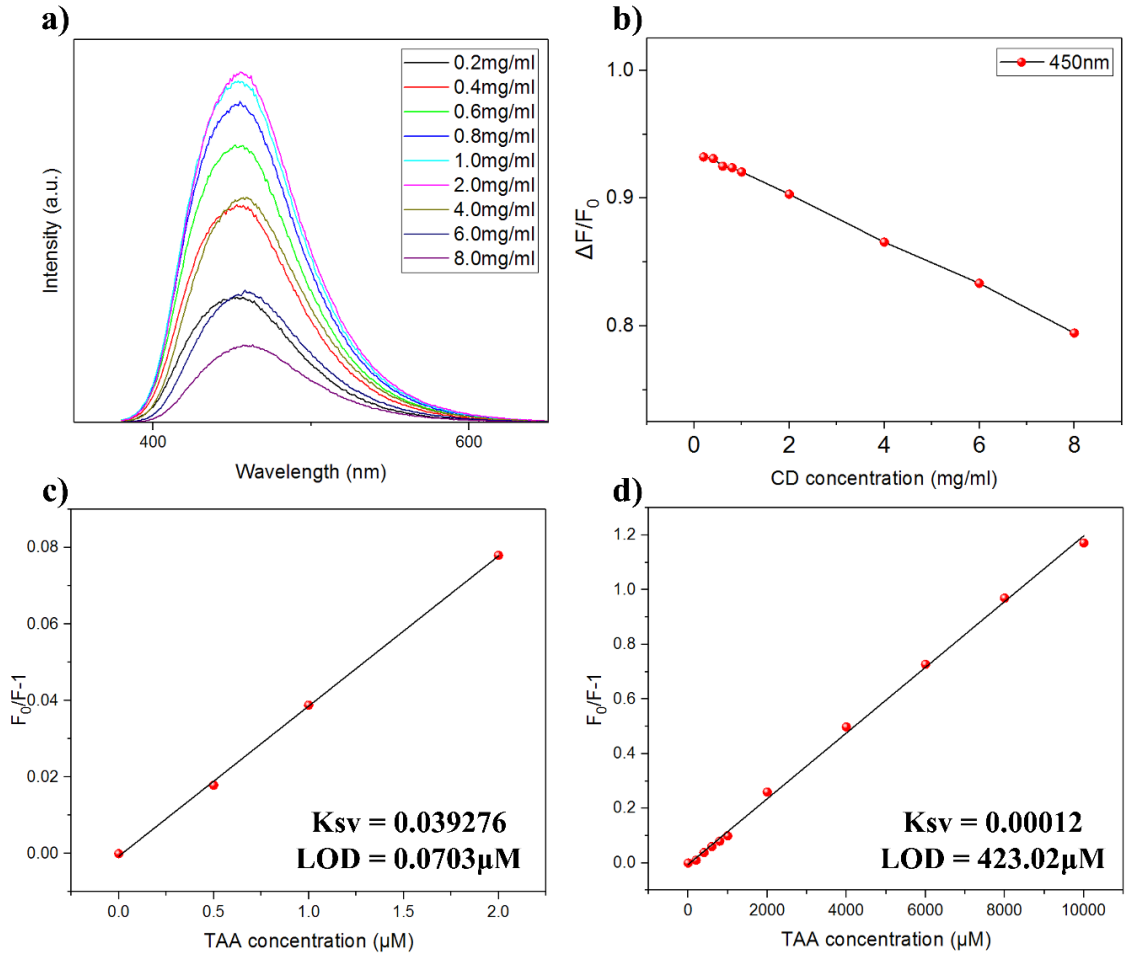

Fig 3.14. (a) PL spectra and (b) quenching efficiency of emission band at various CD concentration. The excitation wavelength was 370nm. Stern-Volmer plot of (c) 360 nm (excited at 240 nm) and (d) 450nm emission (excited at 370 nm) according to the TAA concentration

Table 3.3. TAA sensing properties at different excitation and emission wavelengths

Emission wavelength (Excitation wavelength)	Linear range (μM)	R^2 (0 – 40% region)	LOD (μM)
360nm (240nm)	0 – 2	0.9995	**0.01417**
450nm (370nm)	**0 – 10000**	0.9911	59.20

Table 3.4. Comparison of the sensing performances of CDs fabricated in this study with those of previous results

Analytical Method	Linear range (μM)	R^2	LOD (μM)	reference
Voltammetry	5–60	0.998	0.84	[64]
Amperometry	-	-	3	[65]
Fluorimetry	0 – 2	0.9995	0.0703	Present work
Fluorimetry	0 - 10000	0.99855	423.02	Present work

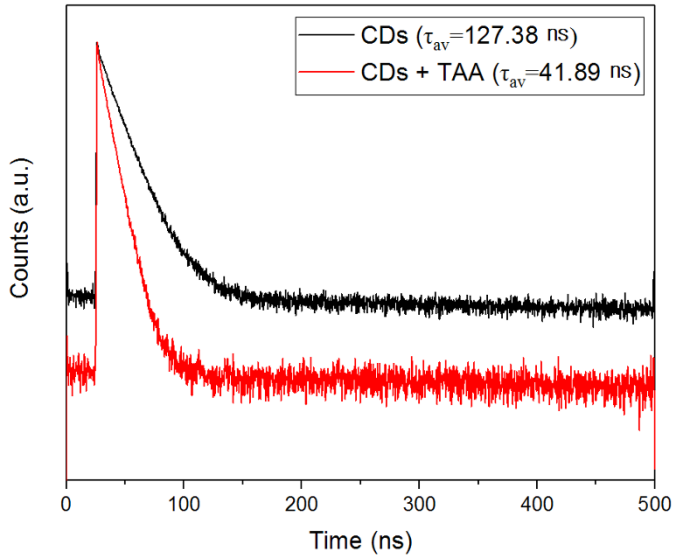

Fig 3.15. Fluorescence decay profile of CD and CD with TAA (10mM)

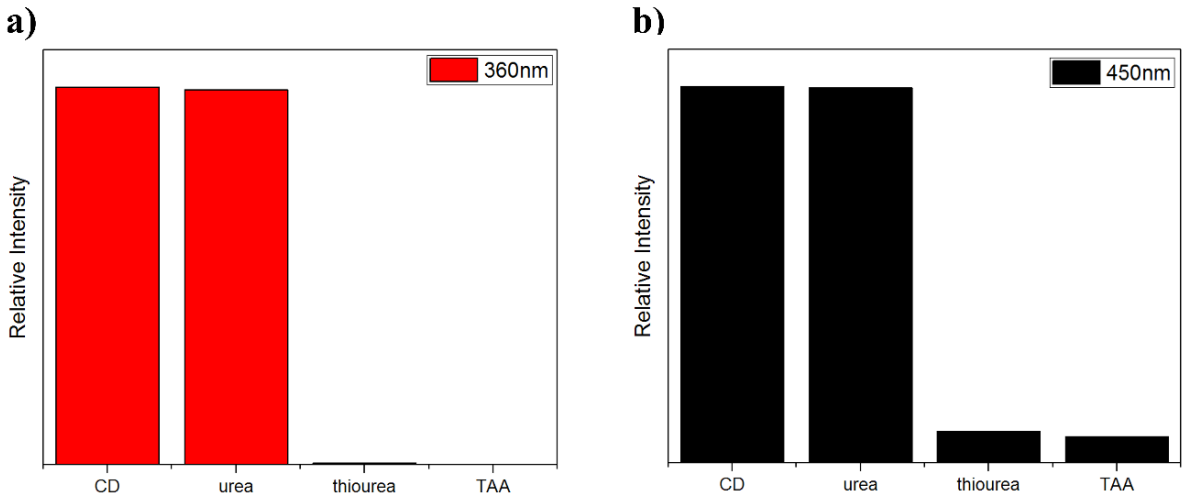

Fig 3.16. Relative intensity of CDs in presence of various molecules (0.1M). (a) 360 nm emission band at 240nm excitation wavelength. (b) 450 nm emission band at 370nm excitation wavelength

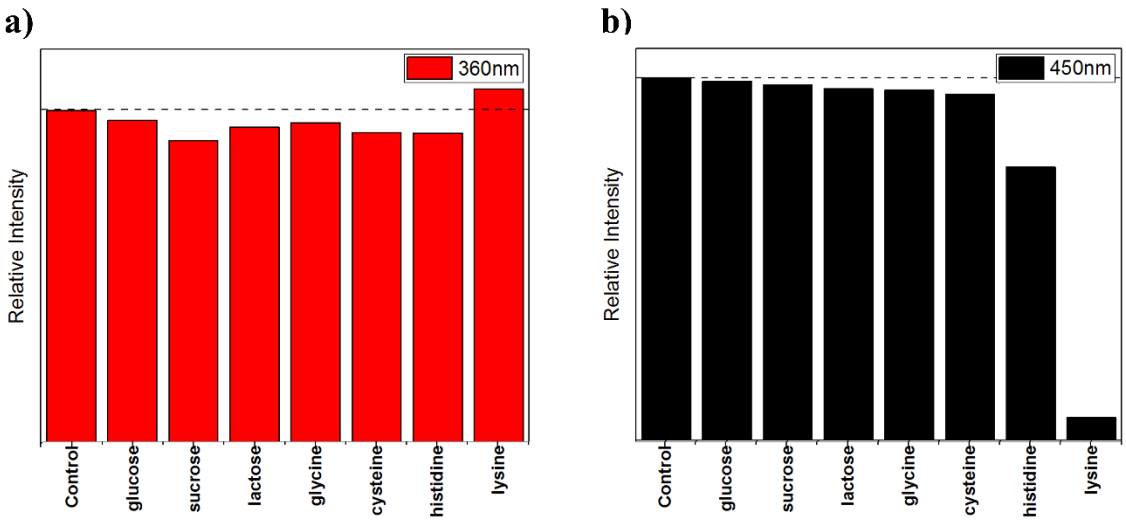

Fig 3.17. Relative intensity of CDs-TAA system in presence of biomolecule (1mM) for interference study (a) 360 nm emission band at 240nm excitation wavelength (b) 450nm emission band at 370nm excitation wavelength

Table 3.5. Sensing performances of CDs in river water for real sample assay

Real sample	Concentration of TAA (μM)	Recovery of TAA (μM)	Recovery of TAA (%)
River water	2000	1487.237±6	74.36
	4000	3627.961±5	90.70
	6000	5197.76±2	86.63

3.4. Conclusions

Highly fluorescent CDs were successfully synthesized from EDTA and L-tryptophan as novel precursors. The quantum yield was optimized by adjusting the reaction conditions including reaction temperature, time, molar ratio of precursors, and concentration of CDs. The PL emission of as-synthesized CDs could be controlled by changing the excitation wavelength. The as-synthesized CDs possess unique dual emission bands that might be originated from tryptophanyl cores and functional groups. TAA, a well-known liver carcinogen, which can be released easily from leather, textile, and paper industries, has been detected via the quenching of the fluorescence of the as-synthesized CDs. As both the emissive peaks show quenching in the presence of TAA, the sensing range has been tuned by changing the excitation wavelength. The generation of thioamide functional groups during the interaction between the as-synthesized CDs and TAA, may cause the quenching. A low detection limit of 70 nM and wide linear range of 0–10 mM has been achieved for the prescribed method. This study has a possible application on monitoring the protein dynamics or protease assay using thioamide-CDs FRET pair as a probe.

References

[1] D. Jariwala, V.K. Sangwan, L.J. Lauhon. T.J. Marks, M.C. Hersam. Carbon nanomaterials for electronics, optoelectronics, photovoltaics, and sensing, Chem. Soc. Rev. 42 (2013) 2824-2460.

[2] C.B. Jacobs, M.J. Peairs, B.J. Venton. Review: Carbon nanotube based electrochemical sensors for biomolecules, Anal. Chim. Acta 662 (2010) 105–127.

[3] P. Bollella, G. Fusco, C. Tortolini, G. Sanzo, G. Favero, L. Gorton, R. Antiochia. Beyond graphene: Electrochemical sensors and biosensors for biomarkers detection, Biosens Bioelectron 89 (2017) 152-166.

[4] M. Pumera, A. Ambrosi, A. Bonanni, E.L.K. Chng, H.L. Poh. Graphene for electrochemical sensing and biosensing, Trends Anal. Chem 29 (2010) 954-965.

[5] S.Y. Lim, W. Shen, Z. Gao. Carbon quantum dots and their applications, Chem. Soc. Rev. 44 (2015) 362-381.

[6] Y. Wang, A. Hu. Carbon quantum dots: synthesis, properties and applications, J. Mater. Chem. C 2 (2014) 6921-6939.

[7] S. Zhu, Q. Meng, L. Wang, J. Zhang, Y. Song, H. Jin, K. Zhang, H. Sun, H. Wang, B. Yang. Highly Photoluminescent Carbon Dots for Multicolor Patterning, Sensors, and Bioimaging, Angew. Chem. 125 (2013) 4045-4049.

[8] Y.L.T Ngo, W.M. Choi, J.S. Chung, S.H. Hur. Highly biocompatible phenylboronic acid-functionalized graphitic carbon nitride quantum dots for the selective glucose sensor, Sensors Actuators, B Chem. 282 (2019) 36-44.

[9] Y. Sun, B. Zhou, Y. Lin, W. Wang, K.A.S. Fernando, P. Pathak, M.J. Meziani, B.A. Harruff, X. Wang, H. Wang, P.G. Luo, H. Yang, M.E. Kose, B. Chen, L.M. Veca, S. Xie, S. Carolina. Quantum-Sized Carbon Dots for Bright and Colorful Photoluminescence, J. Am. Chem. Soc. 128 (2006) 7756–7757.

[10] L. Zheng, Y. Chi, Y. Dong, J. Lin, B. Wang. Electrochemiluminescence of Water-Soluble Carbon Nanocrystals Released Electrochemically from Graphite, J. Am. Chem. Soc. 131 (2009) 4564-4565.

[11] Q.L. Zhao, Z.L. Zhang, B.H. Huang, J. Peng, M. Zhang, D.W Pang. Facile preparation of low cytotoxicity fluorescent carbon nanocrystals by electrooxidation of graphite, Chem. Commun. 2008 5116–5118.

[12] H. Liu, T. Ye, C. Mao. Fluorescent carbon nanoparticles derived from candle soot, Angew. Chem. 46 (2007) 6473-6475.

[13] R. Liu, D. Wu, S. Liu, K. Koynov, W. Knoll, Q. Li. An Aqueous Route to Multicolor Photoluminescent Carbon Dots Using Silica Spheres as Carriers, Angew. Chem. 48 (2009) 4598–4601.

[14] H. Zhu, X. Wang, Y. Li, Z. Wang, X. Yang. Microwave synthesis of fluorescent carbon nanoparticles with electrochemiluminescence properties, Chem. Commun. (2009) 5118-5120.

[15] M.J. Krysmann, A. Kelarakis, P. Dallas, E.P. Giannelis. Formation Mechanism of Carbogenic Nanoparticles with Dual Photoluminescence Emission, J. Am. Chem. Soc. 134 (2012) 747-750.

[16] Y. Song, S. Zhu, S. Zhang, Y. Fu, L. Wang, X. Zhao, B. Yang. Investigation from chemical structure to photoluminescent mechanism: A type of carbon dots from the pyrolysis of citric

acid and an amine, J Mater Chem C. 3 (2015) 5976-5984.

[17] S. Sarkar, M. Sudolska, M. Dubecky, C.J. Reckmeier, A.L. Rogach, R. Zboril, M. Otyepka. Graphitic Nitrogen Doping in Carbon Dots Causes Red-Shifted Absorption, J Phys Chem C. 120 (2016) 1303-1308.

[18] K. Hola, M. Sudolska, S. Kalytchuk, D. Nachtigallova, A.L. Rogach, M. Otyepka, R. Zboril, Graphitic Nitrogen Triggers Red Fluorescence in Carbon Dots, ACS Nano 11 (2017) 12402–12410.

[19] T. Akhtar, N. Sheikh. An overview of thioacetamide-induced hepatotoxicity, Toxin Rev. 32 (2013) 43-46.

[20] U.S. Department of Health and Human Services Public Health Service National Toxicology Program, Report on Carcinogens (12th ed.) Substance Profiles; 2011 p. 403-404.

[21] D. Cinghiţă, C. Radovan, D. Dascălu. Anodic Voltammetry of Thioacetamide and its Amperometric Determination in Aqueous Media, Sensors 8 (2018) 4560-4581.

[22] D. Saha, D.P.S. Negi. Spectroscopic investigations on the interaction of thioacetamide with ZnO quantum dots and application for its fluorescence sensing, Spectrochim. Acta A 189 (2018) 516–521.

[23] A. Valizadeh, H. Mikaeili, M. Samiei, S.M. Farkhani, N. Zarghami, M. kouhi, A. Akbarzadeh, S. Davaran. Quantum dots: synthesis, bioapplications, and toxicity, Nanoscale Research Letters 7 (2012) 1-14.

[24] J. Wang, H. Zhang, R. Guan, Dual-Emission Fluorescent Microspheres for the Detection of Biothiols and Hg^{2+}. Materials 11 (2018) 2232.

[25] T. Zhang, F.Zhao, L. Li, B. Qi, D. Zhu, J. Lü, C. Lü, Tricolor White-Light-Emitting Carbon Dots with Multiple-Cores@Shell Structure for WLED Application. *ACS Appl. Mater. Interfaces* 10 (2018) 19796-19805.

[26] D.F. Eaton. Reference materials for fluorescence measurement, Pure Appl Chem. 60 (1988) 1107–1114.

[27] S. Yan, S. Yang, L. He, C. Ye, X. Song, F. Liao. Quantum size effect of poly(o-phenylenediamine) quantum dots: From controllable fabrication to tunable photoluminescence properties, Synth. Met. 198 (2014) 142-149.

[28] T. Ogi, K. Aishima, F.A. Permatasari, F. Iskandar, E. Tanabec, K. Okuyama., Kinetics of nitrogen-doped carbon dot formation via hydrothermal synthesis, New J. Chem. 40 (2016) 5555-5561.

[29] Y. Park, J. Yoo, B. Lim, W. Kwon, S.-W. Rhee. Improving the functionality of carbon nanodots: doping and surface functionalization, J. Mater. Chem. A 4 (2016) 11582-11603.

[30] S. Bhattacharyya, F. Ehrat, P. Urban, R. Teves, R. Wyrwich, M. Doblinger, J. Feldmann, A.S. Urban, J.K. Stolarczyk. Effect of nitrogen atom positioning on the trade-off between emissive and photocatalytic properties of carbon dots, Nat. Commun. 8 (2017) 1-9.

[31] Q.Q. Shi, Y.H. Li, Y. Xu, Y. Wang, X.B. Yin, X.W. He, Y.K. Zhang. High-yield and high-solubility nitrogen-doped carbon dots: formation, fluorescence mechanism and imaging application, RSC Adv. 4 (2014) 1563-1566.

[32] Z. Bagheri, H. Ehtesabi, M. Rahmandoust, M.M. Ahadian, Z. Hallaji, F. Eskandari, E. Jokar. New Insight into the Concept of Carbonization Degree in Synthesis of Carbon Dots to Achieve Facile Smartphone Based Sensing Platform, Sci Rep. 7 (2017) 1-11.

[33] H. Peng, J. Travas-Sejdic, Simple Aqueous Solution Route to Luminescent Carbogenic Dots from Carbohydrates, Chem. Mater. 21 (2009) 5563-5565

[34] S. Chena, C. Xub, Y. Yub, J. Wang, Multichannel fluorescent sensor array for discrimination of thiols using carbon dot–metal ion pairs, Sensors and Actuators B 266 (2018) 553-560

[35] Q. Fang, Y. Dong, Y. Chen, C. Lu, Y. Chi, H. Yang, T. Yu, Luminescence origin of carbon based dots obtained from citric acid and amino group-containing molecules, Carbon 118 (2017) 319-326

[36] W. Wei, C. Xu, L. Wu, J. Wang, J. Ren, X. Qu. Non-Enzymatic-Browning-Reaction: A Versatile Route for Production of Nitrogen-Doped Carbon Dots with Tunable Multicolor Luminescent Display, Sci Rep. 4 (2014) 1-7.

[37] H.V. Xu, X.T. Zheng, Y. Zhao, Y.N. Tan. Uncovering the Design Principle of Amino Acid-Derived Photoluminescent Biodots with Tailor-Made Structure−Properties and Applications for Cellular Bioimaging, ACS Appl. Mater. Interfaces 10 (2018) 19881-19888.

[38] S. Lu, X. Zhao, S. Zhu, Y. Song, Bai Yang. Novel cookie-with-chocolate carbon dots displaying extremely acidophilic high luminescence, Nanoscale 6 (2014) 13939-13944.

[39] Z. Moua, X. Chen, Y. Dua, X. Wanga, P. Yanga, S. Wang. Forming mechanism of nitrogen doped graphene prepared by thermal solid-state reaction of graphite oxide and urea, Appl Surf Sci. 258 (2011) 1704-1710.

[40] D. Qu, M. Zheng, L. Zhang, H. Zhao, Z. Xie, X. Jing, R.E. Haddad, H. Fan, Z. Sun. Formation mechanism and optimization of highly luminescent N-doped graphene quantum dots, Sci Rep. 4 (2014) 1-11.

[41] G. da S. Mello, A. de P. Cardoso, E.W.R.S. Oliveira, A.B. Siqueira. Tryptophan: A proposal of the mechanism of thermal decomposition, J. Therm. Anal. Calorim. 122 (2015) 1395-1401.

[42] L. Li, L. Li, C. Wang, K. Liu, R. Zhu, H. Qiang. Y. Lin. Synthesis of nitrogen-doped and amino acid-functionalized graphene quantum dots from glycine, and their application to the fluorometric determination of ferric ion, Microchim. Acta 182 (2015) 763-770.

[43] A. Snis, S.F. Matar, O. Plashkevych, H. Ågren. Core ionization energies of carbon-nitrogen molecules and solids, J. Chem. Phys.111 (1999) 9678-9686.

[44] J.S. Stevens, A.C. de Luca, M. Pelendritis, G. Terenghi, S. Downesc, S.L.M. Schroeder. Quantitative analysis of complex amino acids and RGD peptides by X-ray photoelectron spectroscopy (XPS), Surf. Interface Anal. 45 (2013) 1238–1246.

[45] D. Qu, M. Zheng, J. Li, Z. Xie, Z. Sun. Tailoring color emissions from N-doped graphene quantum dots for bioimaging applications, Light Sci. Appl 4 (2015) 1-8.

[46] M. Mohandoss, S.S. Gupta, A. Nelleri, T. Pradeepc, S.M. Maliyekkal. Solar mediated reduction of graphene oxide, RSC Adv. 7 (2017) 957-963.

[47] X. Miao, D. Qu, D. Yang, B. Nie, Y. Zhao, H. Fan, Z. Sun. Synthesis of Carbon Dots with Multiple Color Emission by Controlled Graphitization and Surface Functionalization, Adv. Mater. 30 (2018) 1704740.

[48] Z. Yang, M. Xu, Y. Liu, F. He, F. Gao, Y. Su, H. Wei, Y. Zhang. Nitrogen-doped, carbon-rich, highly photoluminescent carbon dots from ammonium citrate, Nanoscale 6 (2014) 1890-1895.

[49] F.A. Permatasari, A.H. Aimon, F. Iskandar, T. Ogi, K. Okuyama. Role of C–N

Configurations in the Photoluminescence of Graphene Quantum Dots Synthesized by a Hydrothermal Route 6 (2016) 1-8.

[50] N. Graf, E. Yegen, T. Gross, A. Lippitz, W. Weigel, S. Krakert, A. Terfort, W.E.S. Unger. XPS and NEXAFS studies of aliphatic and aromatic amine species on functionalized surfaces, Surf. Sci 603 (2009) 2849–2860.

[51] W. Ding, Z. Wei, S. Chen, X. Qi, T. Yang, J. Hu, D. Wang, L.J. Wan, S.F. Alvi, L. Li. Space-Confinement-Induced Synthesis of Pyridinic- and Pyrrolic- Nitrogen-Doped Graphene for the Catalysis of Oxygen Reduction, Angew. Chem. 125 (2013) 11971-11975.

[52] N. Hellgren, R.T. Haasch, S. Schmidt, L. Hultman, I. Petrov. Interpretation of X-ray photoelectron spectra of carbon-nitride thin films: New insights from in situ XPS, Carbon 108 (2016) 242-252.

[53] Y. Yamada, J. Kim, S. Matsuo, S. Sato. Nitrogen-containing graphene analyzed by X-ray photoelectron spectroscopy, carbon 70 (2014) 59-74.

[54] Z. Gan, H. Xub, Y. Hao. Mechanism for excitation-dependent photoluminescence from graphene quantum dots and other graphene oxide derivates: consensus, debates and challenges, Nanoscale 8 (2016) 7794-7807.

[55] N. Dhenadhayalan, K. Lin, R. Suresh, P. Ramamurthy, Unravelling the Multiple Emissive States in Citric-Acid-Derived Carbon Dots, J. Phys. Chem. C 120 (2016)1252−1261.

[56] W. Wang, B. Wang, H. Embrechts, C. Damm, A. Cadranel, V. Strauss, M. Distaso, V. Hinterberger, D. M. Guldi, W. Peukert. Shedding light on the effective fluorophore structure of high fluorescence quantum yield carbon nanodots, RSC Adv. 7 (2017) 24771-24780.

[57] A. White. Effect of pH on Fluorescence of Tyrosine, Tryptophan and Related Compounds, Biochem J. 71 (1959) 217-220.

[58] Y. Jiaoa, X. Gonga, H. Hana, Y. Gaoa, W. Lua, Y. Liua, M. Xiana, S. Shuanga, C. Dong. Facile synthesis of orange fluorescence carbon dots with excitation independent emission for pH sensing and cellular imaging, Anal. Chim. Acta 1042 (2018) 125-132.

[59] P.M. Froehllch, K. Nelson. Fluorescence Quenching of Indoles by Amides, J. Phys. Chem. A 82 (1978) 2401-2403.

[60] Y. Chen, B. Liu, H.-T Yu, M.D. Barkley. The Peptide Bond Quenches Indole Fluorescence, J. Am. Chem. Soc. 118 (1996) 9271-9278.

[61] Y. Chen, M.D. Barkley. Toward Understanding Tryptophan Fluorescence in Proteins, Biochemistry 37 (1998) 9976-9982.

[62] J.M. Goldberg, R.F. Wissner, A.M. Klein, E.J. Petersson. Thioamide quenching of intrinsic protein fluorescence, Chem. Commun. 48 (2012) 1550-1552.

[63] J.M. Goldberg, L.C. Speight, M.W. Fegley, E.J. Petersson. Minimalist Probes for Studying Protein Dynamics: Thioamide Quenching of Selectively Excitable Fluorescent Amino Acids, J. Am. Chem. Soc. 134 (2012) 6088-6091.

[64] D. Cinghiță, C. Radovan, D. Dascălu, Anodic voltammetry of thioacetamide and its amperometric determination in aqueous media, Sensors 8 (2008) 4560–4581.

[65] A. Asghari, O. Ghaderi, M. Rajabi, M. Ameri, A. Amoozadeh, Mechanistic and electrochemical investigation of catechol oxidation in the presence of thioacetamide:

application for voltammetric determination of thioacetamide in aqueous media, Prog. React. Kinet. Mech. 40 (2015) 95–103

Chapter 4. Uncovering the actual inner-filter effect between highly efficient carbon dots and nitroaromatics

4.1. Introduction

Nitroaromatics are used widely as intermediates in the dye, pharmaceutical, pesticide, and explosives industries. On the other hand, these compounds are hazardous to humans and wildlife because of their toxicity, carcinogenicity, and mutagenicity [1]. In addition, their widespread use has resulted in serious environmental contamination in air, soil, and water. Nitrophenols have negative effects on health, such as skin irritation, blood disorders, and even death [2]. For example, 2,4-dinitrophenol (DNP) causes increased basal metabolic rates, a feeling of warmth, sweating, weight loss, and increased heart rate, breathing rate, and body temperature [3]. Nitroaniline also induces hypoactivity, convulsions, prostration, salivation, piloerection, shallow respiration, and a loss of muscle coordination [4].

Recently, fluorescence-based sensing of nitroaromatics has been attempted widely because of its high sensitivity, excellent accuracy, rapid response, and simple operation process. Soni et al. reported a fluorescent sensor for mono-, di-, and tri-nitrophenols operated in the micromolar range using graphene quantum dots (GQDs) [5]. Tian et al. fabricated a paper-based sensor for trinitrotoluene in the nanomolecular range using carbon dots (CDs) and CDs-polyvinyl alcohol composites [6]. Yuan et al. demonstrated a fluorescent probe for p-nitroaniline sensing in both aqueous and ethanol solutions using CDs [7].

Fluorescent CDs are promising candidates for fluorescence probes because of their non-toxicity, photostability, and excellent luminescent properties [8–11]. Their properties can be controlled easily by precursor design [12], surface passivation [13], and optimization of the reaction conditions [14]. To obtain the desirable sensing properties, understanding the detection

mechanism and designing their chemical structures is crucial. Many researchers have suggested photo-induced electron transfer (PET), Förster resonance energy transfer (FRET), and inner-filter effect (IFE) [15–17], as a major detection mechanism. In particular, Inner filter effect (IFE) was widely applied on the fields of chemical sensing [18–21]. Cayuela et al. fabricated Inner-filter effect based sensor for detection of silver nanoparticles, whose aggregation shows high absorption in visible range [19]. Sai et al. used CDs for determining acetone via inner filter effect because of spectral overlap in range of 240–320 nm [20]. Fan et al. fabricated inner-filter effect based fluorescent probe for detecting 2,4,6-trinitrophenol [21]. Although there are a lot of interest of IFE based probe, but it is not clearly explained or misunderstood between other mechanisms.

This study investigated the detection mechanism of CDs towards various nitroaromatics, including 2-nitroaniline (2-NA), 3-nitrophenol (3-NP), 2,4-dinitrophenol (DNP), and 4-nitrophenol (4-NP). The IFE and FRET mechanisms in sensing can be confused because both are based on spectral overlap between the emission band of the energy donor and the absorption of the acceptor. The IFE and FRET models were compared and discussed through mathematical models, including Lakowicz [22] and the Parkers and Barnes correction [23]. The CDs used in this study were synthesized from citric acid and uric acid as novel precursors after optimizing the reaction conditions, which exhibited the excellent linearity and low detection limits towards nitroaromatics. As shown in Table S2, previous studies used the functional group induced specific interaction between CDs and each analyte, which resulted in limited sensing of nitroaromatics. In contrast, the CDs fabricated in this study can detect a range of nitroaromatics by the IFE.

4.2. Experimental

4.2.1. Chemicals

Sodium hydroxide (NaOH), uric acid, ortho-phenylenediamine (o-PD), meta-phenylenediamine (m-PD) and para-phenylenediamine (p-PD) are purchased from Sigma-Aldrich Co. Ltd (USA). Citric acid and 2-NA are purchased from Daejung Chemicals & Metals Co. Ltd. (Republic of Korea). DNP was purchased from Yakuri Pure Chemicals Co., Ltd. (Japan). 4-NP was purchased from Alfa Aesar Co. Inc (USA). 3-NP was purchased from Tokyo Chemical Co., Ltd (Japan). Aniline was purchased from Junsei Chemical Co., Ltd. (Japan). All the reagents were used without further purification.

4.2.2. Characterization

The morphology and size distribution of CDs were investigated by field emission transmission electron microscope (FE-TEM, JEL-2100F, JEOL, Japan). UV-Vis absorption spectra and fluorescence spectra were collected by Specord 210 Plus (Analytik Jena, Germany) and Cary Eclipse Fluorescence Spectrophotometer G9800AA (Agilent Technologies, USA), respectively. Time-correlated single-photon counting (TCSPC) was performed by FS5 spectrophotometer (Edinburgh Instruments, EPL-375 ps pulsed diode laser the light source). X-ray photoelectron spectroscopy (XPS, K-alpha, Thermo Fisher Scientific, USA) was performed to investigate element composition. Fourier-transform infrared spectroscopy (FT-IR, Nicolet iS5 FTIR Spectrometer, Thermo Fisher Scientific, USA) was performed to investigate functional groups. Zeta potential was measured by Zetasizer Nano ZSP (Malvern Panalytical, UK).

4.2.3. Synthesis of CDs

As illustrated in Fig 4.1, CDs were synthesized from citric acid (105 mg) and uric acid (168 mg) via a hydrothermal process. First, a pre-determined NaOH solution (0, 0.2, 0.4, 0.6, 0.8, and 1.0 M) was prepared. Uric acid and citric acid were then dissolved in 10 mL of the above solutions with stirring for 10 min using a magnetic bar. To achieve a homogeneous dispersion, the solution was sonicated for 1 h. After the solution was transferred to a Teflon-lined stainless-steel autoclave, it was placed into a muffle furnace, heated to 160 °C, and maintained at that temperature for 6 h for CD formation. After cooling to room temperature, the resulting solution was mixed with 20 mL of ethanol and centrifuged at 5000 rpm for 10 min to remove the residues and organic byproducts. The sediment was collected and re-dispersed in 10 mL of D.I. water. To obtain the solid CDs, 2 mL of CD solution was freeze dried for one day at −46 °C. CDs synthesized by the 0.8 M NaOH solution was selected to examine the physicochemical properties and sensing performance after optimizing the optical properties and yields.

4.2.4. Detection of nitroaromatics

Two milliliters of a CD solution (34 mg/mL) was diluted in D.I. water, while the total volume of solution was kept to 40 mL. Subsequently, 3.6 mL of a CD solution was mixed with 0.4 mL of the target analyte solutions, which were prepared beforehand with a pre-determined amount of various analytes. The concentration of organic molecules, including aniline o-PD, m-PD, p-PD, 2-NA, 3-NP, DNP, and 4-NP was kept to 1 mM for the sensitivity test. To determine the limit of detection (LOD), fluorescence and UV–Vis absorption spectra were collected for a specific range (0–100 μM, and 0–1000 μM, respectively). All measurements were taken with a 2.5 nm excitation slit.

4.2.5. Determination of quantum yield

The quantum yields (QYs) of the CDs fabricated in this study were determined by comparing the fluorescence spectra at four absorbance values with those of a standard sample, quinine bisulfate (0.1 M H2SO4, ϕ = 0.54). The fluorescence spectra were collected with a 2.5 nm excitation slit bandwidth and 5 nm emission slit bandwidth. The following equation was used to determine the quantum yields.

$$\phi_x = \phi_s \frac{A_s}{A_x} \frac{F_x}{F_s} \left(\frac{n_x}{n_s}\right)^2$$

The subscript, "χ", means the sample and "s" means the reference material. ϕ, A, F, and n are the quantum yield, absorbance at the excitation wavelength, integrated emission area across the band, and refractive index of the solvents, respectively. The absorbance was kept at approximately 0.2–0.6, and the measurements were taken at room temperature.

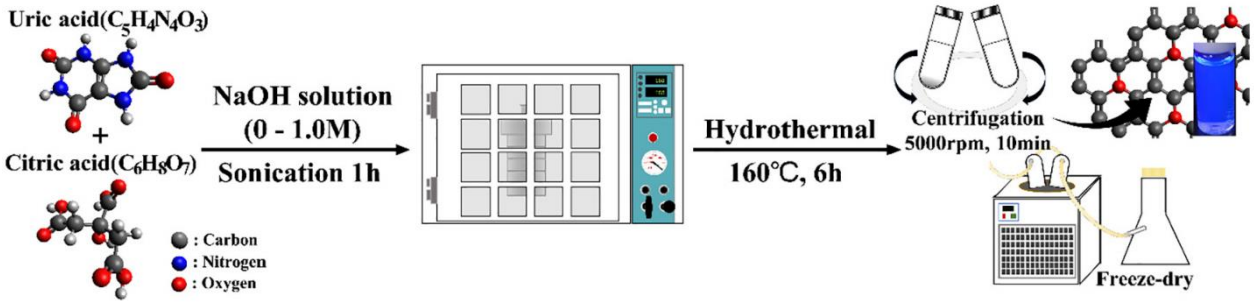

Fig 4.1. Schematic diagram of CDs synthesis

4.3. Results and Discussion

4.3.1. Effect of basicity in the CD formation

The effects of basicity on the yield and optical properties of CDs were investigated to optimize the reaction conditions. As shown in Fig. 4.2a and Table 4.1, both the quantum yield and yield increased remarkably under high basic conditions (NaOH 0.8–1.0 M). No CDs formed under low basic conditions (NaOH 0–0.2 M), indicating that a base catalyst is necessary for the carbonization process [14]. A red shift of the maximum absorbance wavelength was also observed (Fig. 4.3 and Table 4.1) under high basic conditions, which can be due to the increased sp2 cluster of the carbon core and reduced band gaps [24,25]. The constant maximum excitation and emission wavelengths, and the excitation-wavelength independent behavior shown in Figs. 4.2b and 4.4b suggest that the CDs possess uniform edge/surface states [26,27]. The CDs exhibited deep-blue luminescence near UV (Fig. S4.3a), which was attributed to the small amounts of doped nitrogen atoms that can cause long wavelength emission [28,29].

Table 4.1. The effect of basicity on the quantum yield and yield

NaOH concentration (M)	Maximum wavelength (nm)			QY (%)	Yield (%)	Yield (mg/2ml)	After freeze-dry
	Absorbance	PLE	PL				
0	255	337	425	-	-	-	
0.2	377	410	471	-	-	-	
0.4	261	335	402	8.91	11.55	10	
0.6	292	334	398	10.84	34.11	35	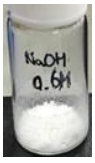
0.8	304	338	397	29.15	56.50	67	
1.0	304	336	396	27.43	57.95	78	

Data notes:

Yield was calculated by dividing by sum of all amounts of solid reactants including NaOH. After freeze-dry, luminescence materials synthesized in low basic condition (NaOH 0 and 0.2 M) could not be collected as a powder form, which indicate that stable CDs was not formed.

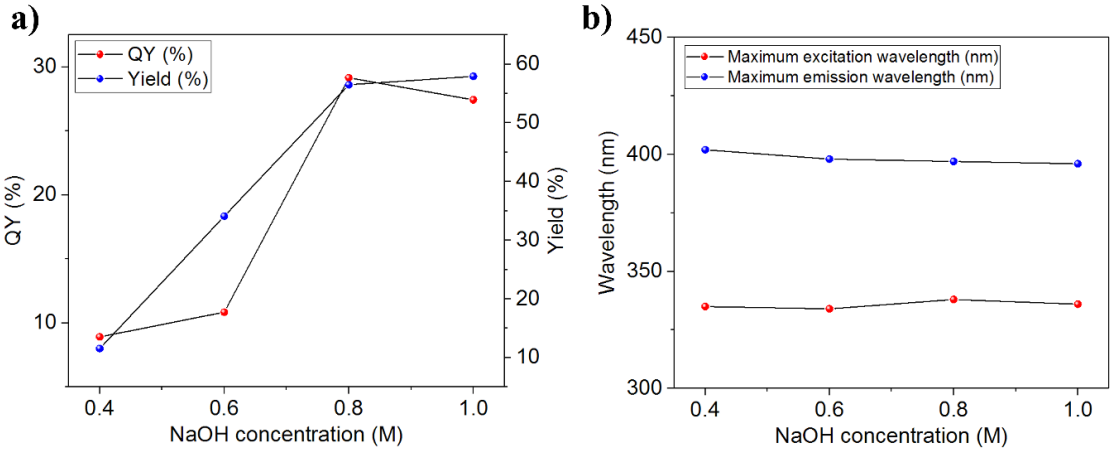

Fig 4.2. Changes in (a) Quantum yield and yield. (b) Maximum excitation and emission wavelengths at various NaOH concentrations

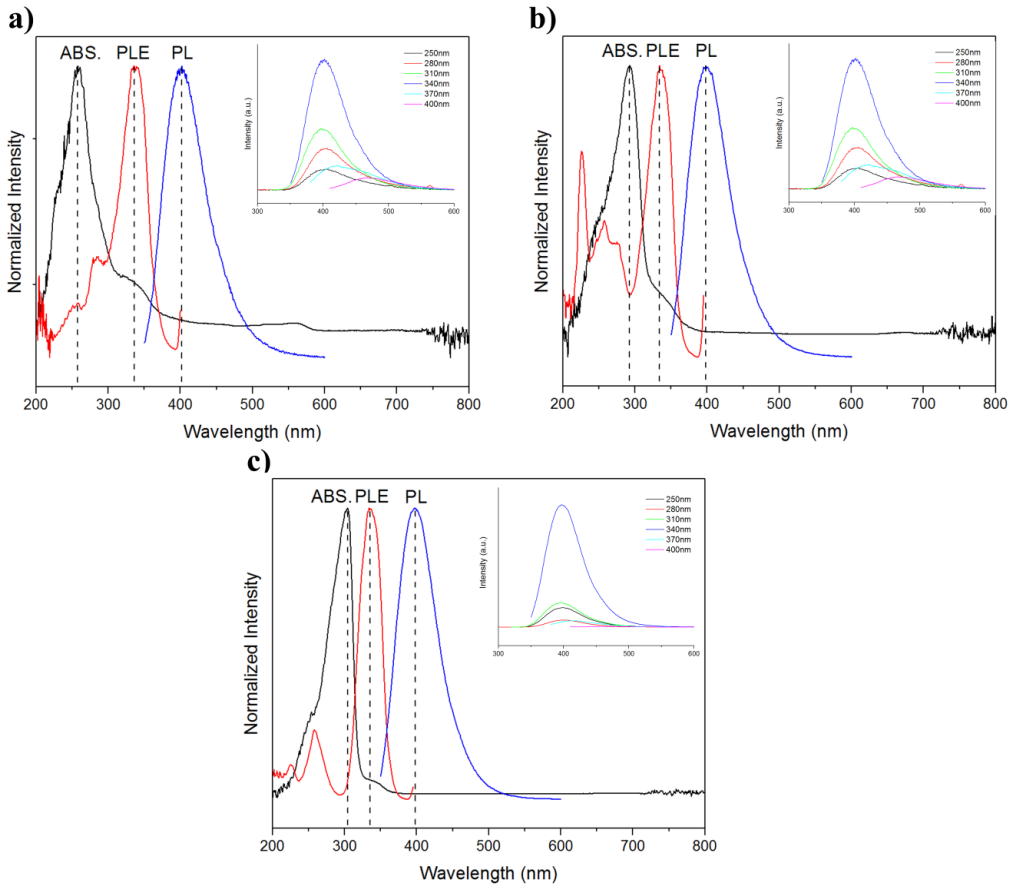

Fig 4.3. Normalized absorbance, PLE and PL spectra of CDs synthesized in (a) 0.4 M (d) 0.6 M (c) 1.0M of NaOH (inset shows PL spectra at different excitation wavelengths)

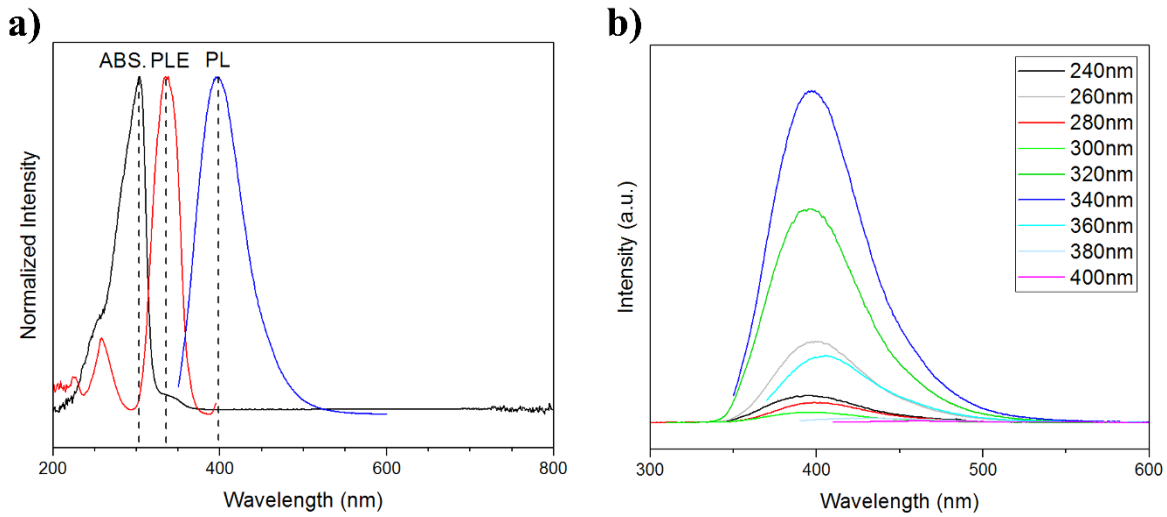

Fig 4.4. Normalized Absorbance, PLE, and PL spectra of CDs. (b) PL spectra of CDs at various excitation wavelengths

4.3.2. Characterization of as-synthesized CDs

The morphology and the size distribution of CDs were investigated by transmission electron microscopy (TEM). As shown in Fig. 4.5, the CDs exhibited a spherical morphology with an average size of 2.32 nm. The broad size distribution resulted in a broad fluorescence emission band due to the quantum size effect [24]. The high resolution-TEM images in the inset in Fig. 4.5a suggest that CDs possess the (100) plane of a graphitic structure, corresponding a lattice spacing of 0.213 nm [28,30]. XRD spectra (Fig. 4.6) show a broad peak near 20°, corresponded with (002) plane [31]. And, the sharp peaks near 30–40° are due to presence of sodium [32].

XPS was performed to investigate the elemental composition and chemical structure of CDs. As shown in Fig. 4.7, strong peaks were observed at 1071 (Na_{1s}), 531 (O_{1s}), and 289 eV (C_{1s}). The strong Na_{1s} peak indicates the formation of a salt by an acid-base reaction between the carboxylic acid groups of CDs and NaOH under high basic conditions [33]. The deconvoluted O_{1s} spectrum revealed quinone C=O at 530.7 eV, which indicates the presence of oxygen-related functional groups on the CDs [34]. The C_{1s} spectra could be deconvoluted into three peaks centered at 284.8, 287.5, and 289.0 eV, which were assigned to carbon-carbon (C-C/C=C), carbonyl (C=O), and carboxyl/carboxylate groups (C=O-O) [34,35].

Surface functional groups were analyzed by Fourier transform infrared (FT-IR) spectroscopy, as shown in Fig. 4.8. A broad absorption band centered at 3390 cm−1 was ascribed to O-H stretching vibrations. Two broad absorbances at 1593 and 1455 cm−1 were assigned to C=C aromatic stretching vibrations and carboxylate symmetric and asymmetric vibrations, respectively [35,36]. The measured zeta potential was −23.0 mV, which also indicates that large amounts of oxygen-related functional groups are present in the as-synthesized CDs [37].

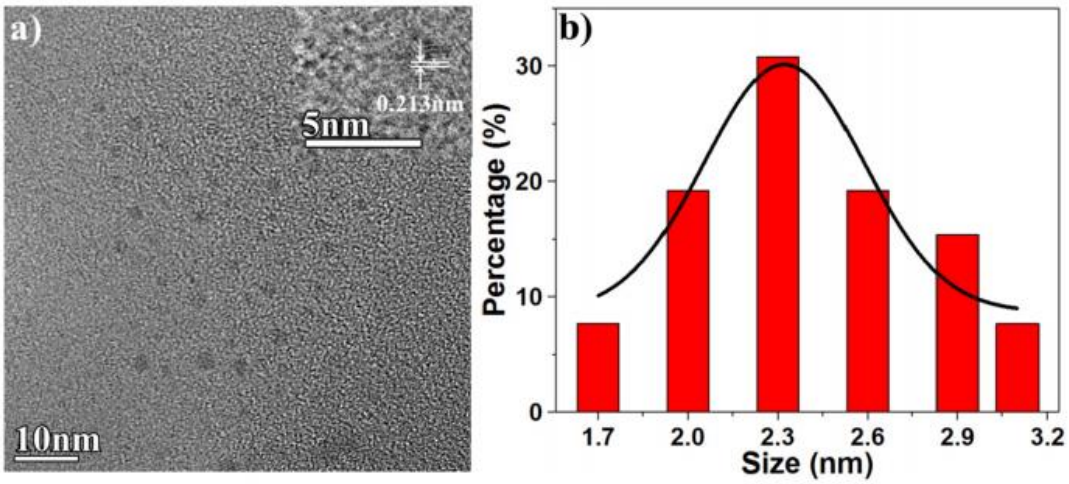

Fig 4.5. (a) TEM images of CDs (inset shows HR-TEM images of CDs). (b) Size distribution of CDs

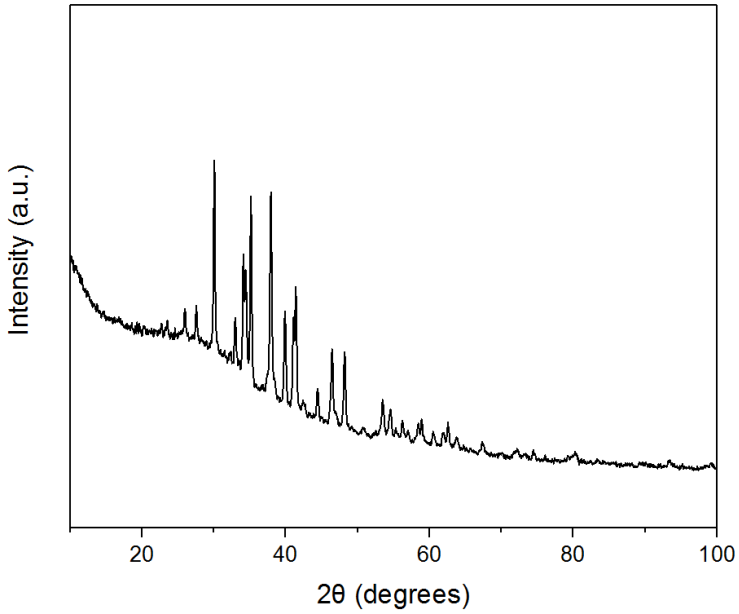

Fig 4.6. XRD spectra of CDs

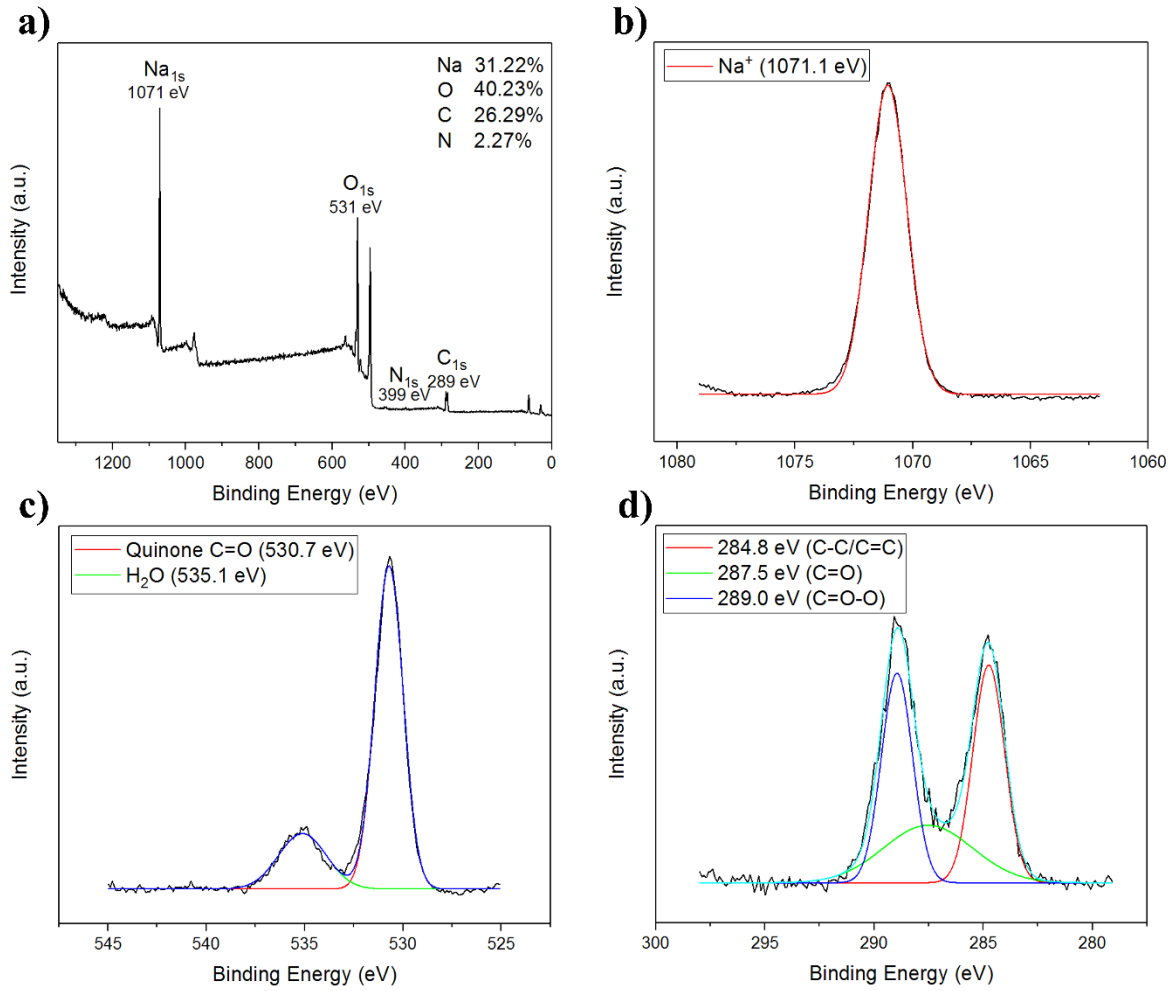

Fig 4.7. (a) XPS spectra of CDs. High resolution XPS spectra of CDs oft (b) Na_{1s} (c) O_{1s}, and (d) C_{1s}

Data notes:

XPS spectra shows a peak near 499 eV observed in presence of Na, due to X-ray source [50], as shown in Fig S4.1a. The peak at 535.1 eV shown in O_{1s} spectra (Fig S4.1c) was attributed to the O-H bond (water) or XPS signal [51-52]. N_{1s} spectra could not be deconvoluted because of very week intensity and less contents in CDs.

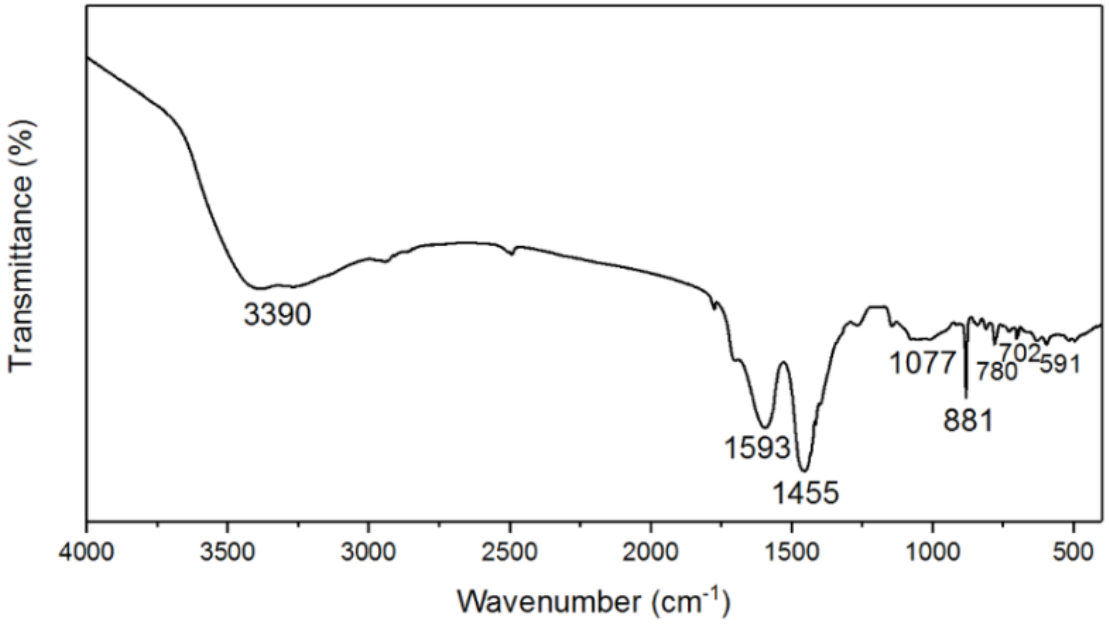

Fig 4.8. FT-IR spectrum of as-synthesized CDs

4.3.3. Detection of nitroaromatics

The sensing performances of the nitroaromatics, including 4-NP, DNP, 3-NP, and 2-NA were investigated using a fluorometric method as shown in Figs. 4.9 and 4.10–4.12. Table 4.2 lists all the sensing parameters. CDs have shown good linearity in a range of 0–20 and 0–200 μM for 4-NP and DNP, 3-NP and 2-NA, respectively. They possess high sensitivity (0.02967, 0.03414 μM^{-1}) for 4-NP and DNP compared to previous study as shown in Table 4.3. And, this is the first study to detect 3-NP and 2-NA and they also shown good Ksv value (0.00495, 0.00647 μM^{-1}), respectively. The fluorescence intensity of the CDs decreased sharply with increasing concentration of analytes. A Stern-Volmer plot was used to investigate the quenching behaviors (Fig. 4.9b). There was a significant positive deviation from linearity as the concentration of the analytes increased, suggesting that both dynamic and static quenching co-exist [22]. The ground state and sphere action model can explain this type of quenching behavior [22,38], but the Stern-Volmer quenching constant is not recovered fully in both models, as shown in Fig. 4.9c and Table 4.4. This indicates that the dynamic and static quenching model cannot explain the quenching behavior sufficiently. The recovery values were calculated using the following equation:

$$Recovery = \frac{K_{SV,ground}(or\ K_{SV,sphere})}{K_{SV}\ (for\ dymamic\ linear\ range)} \times 100\ (\%)$$

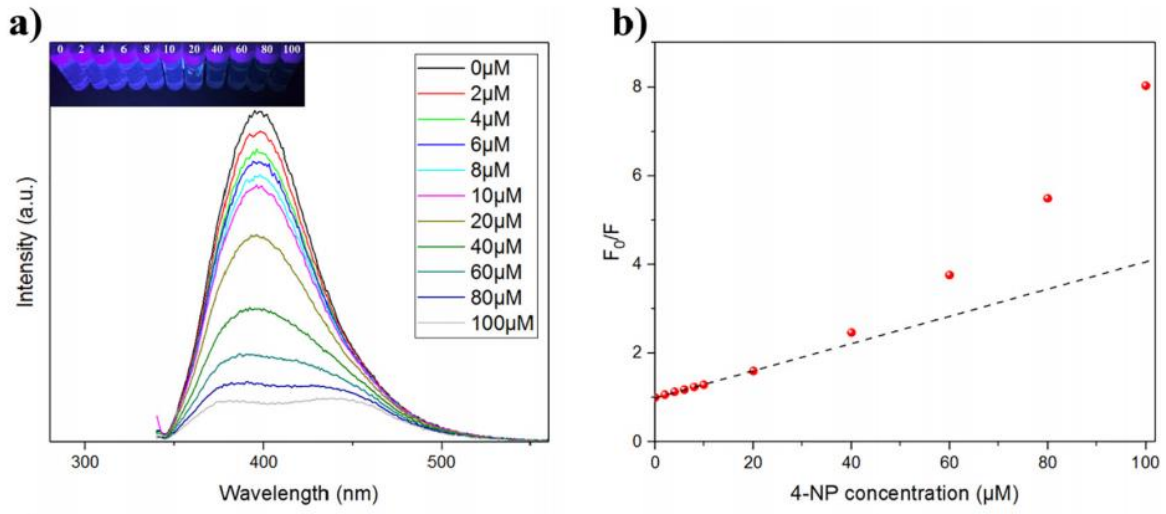

c)

	Ground-state complex			Sphere-action			Stern-Volmer
Analytes	R^2	$K_{sv,ground}$	**Recovery (%)**	R^2	$K_{sv,sphere}$	**Recovery (%)**	K_{sv}
4-NP	0.986193	0.01745	**58.81**	0.999929	0.01191	**40.14**	**0.02967**
DNP	0.980431	0.0212	**62.10**	0.999982	0.01267	**37.11**	**0.03414**
3-NP	0.976141	0.003054	**61.70**	0.999926	0.002225	**44.95**	**0.00495**
2-NA	0.978765	0.0038	**58.73**	0.999433	0.003881	**59.98**	**0.00647**

Fig 4.9. (a) PL spectra (inset shows photographs of CDs under UV illumination). (b) Stern-Volmer Plot of the PL intensity change at various 4-NP concentrations of 0–100 μM. (c) Parameters obtained from the quenching equations

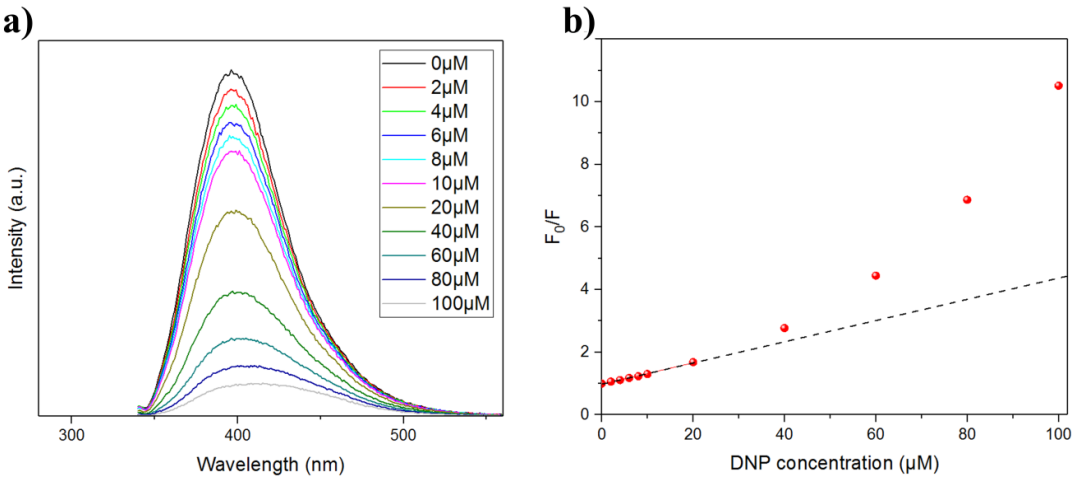

Fig 4.10. (a) PL spectra and (b) Stern-Volmer Plot at various DNP concentrations (0-100μM)

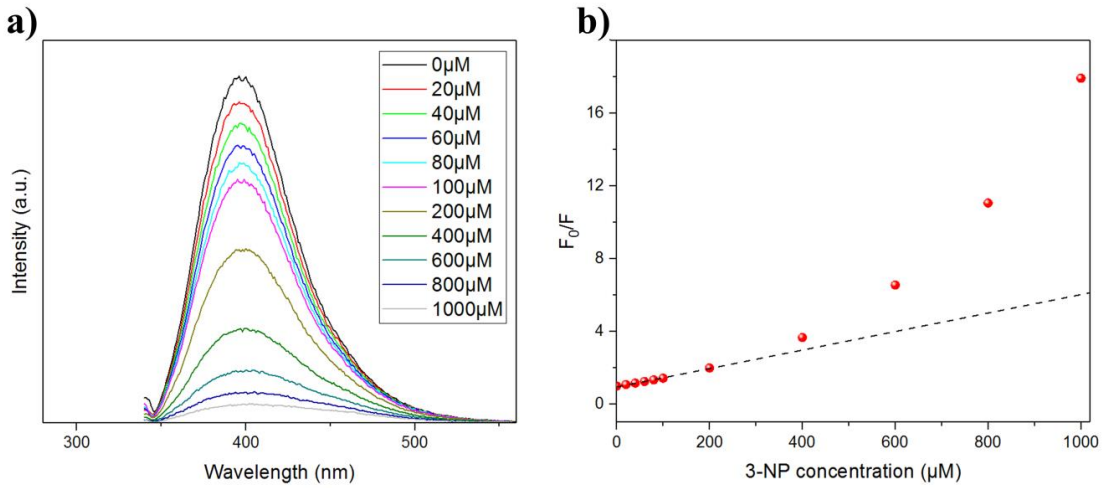

Fig 4.11. (a) PL spectra and (b) Stern-Volmer Plot at various 3-NP concentrations (0-1000μM)

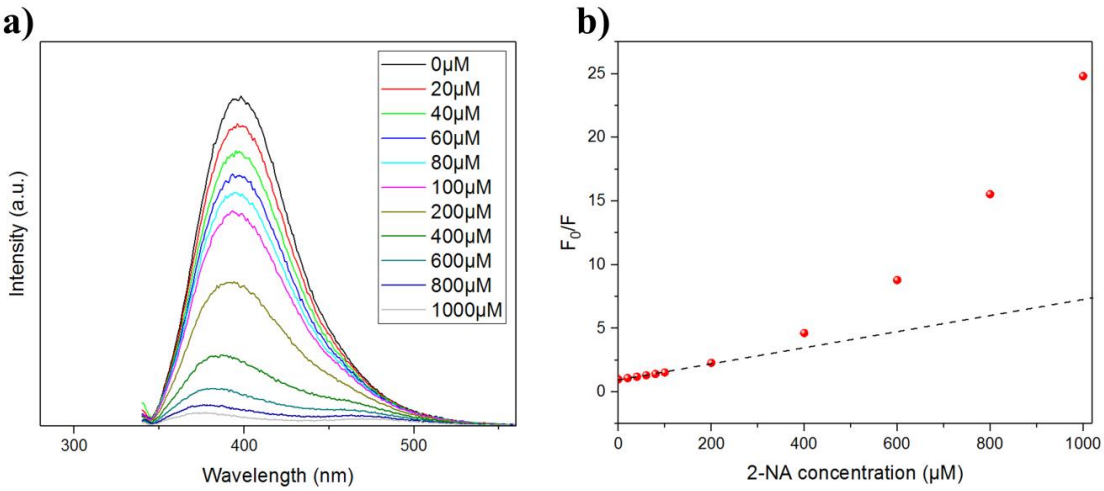

Fig 4.12. (a) PL spectra and (b) Stern-Volmer Plot at various 2-NA concentrations (0-1000μM)

Table 4.2. Fluorescence sensing parameters of nitroaromatics

Sensing methods (Sensing mechanism)	Analytes	**Linear dynamic range (μM)**	R^2	LOD (μM)	**K_{sv} (μM^{-1})**
Fluorometric (IFE)	4-NP	**0-20**	0.99906	0.669	**0.02967**
	DNP	**0-20**	0.99489	1.557	**0.03414**
	3-NP	**0-200**	0.9923	19.165	**0.00495**
	2-NA	**0-200**	0.98899	22.94	**0.00647**

Table 4.3. Comparison of nitroaromatic sensing performances

Analytes	Linear range (μM)	**K_{sv} (μM^{-1})**	ref	Analytes	Linear range (μM)	**K_{sv} (μM^{-1})**	ref
4-NP	0.2-50	**0.01605**	[39]	4-NP	0.1-39	**0.0309**	[43]
4-NP	0.8-150	**0.00395**	[40]	4-NP	0.02-33	**0.0218**	[44]
4-NP	0.5-60	**0.00961**	[41]	DNP	1.3-500	**0.0201**	[45]
4-NP	0.5-60	**0.01711**	[42]	DNP	0.3-210	-	[46]

Data notes:

All given fluorescent probe can detect 4-nitrophenol or 2,4-dinitrophenol **solely**. In this study, CDs show high sensitivity (**K_{sv}**) for **all nitroaromatics**.

Table 4.4. Parameter fitted by the static quenching model

	Ground-state complex			**Sphere-action**		
Analytes	R^2	K_{sv}	K_g	R^2	**K_{sv}**	V
4-NP	0.986193	**0.01745**	0.01745	0.999929	**0.01191**	0.01298
DNP	0.980431	**0.0212**	0.0212	0.999982	**0.01267**	0.01535
3-NP	0.976141	**0.003054**	0.003054	0.999926	**0.002225**	0.001717
2-NA	0.978765	**0.0038**	0.0038	0.999433	**0.003881**	0.001661

Data notes:

Ground-state complex model is estimated by:

$$F_0/F = (1 + K_g)(1 + K_{SV}[Q])$$

Sphere-action quenching model is estimated by:

$$F_0/F = (1 + K_{sv})e^{V[Q]}$$

F_0 is emission peak intensity of CDs without analytes and F is intensity with pre-determined concentration of analytes. K_g is the ground state association constant of complex. K_{sv} is the Stern-Volmer constant. [Q] is the quencher concentration (μM). V is an active volume element surrounding the excited fluorescent material [38].

Recovery value is calculated by:

$$Recovery = \frac{K_{SV,ground}(or\ K_{SV,sphere})}{K_{SV}\ (for\ dymamic\ linear\ range)} \times 100\ (\%)$$

4.3.4. Proving inner-filter effect (IFE)

To examine the rational quenching mechanism, the absorbance spectra of specific molecules were collected, and then their spectral overlap with the excitation and emission spectra of the CDs were investigated. As shown in Fig. 4.13a, a large amount of spectral overlap was observed between the PL and PLE of CDs and the absorbance of 4-NP, DNP, 3-NP, and 2-NA, which shows that both FRET (Förster resonance energy transfer) and secondary IFE (Inner-filter effect) can exist in this sensing system. FRET can occur in the presence of spectral overlap between the emission spectrum of the fluorescent probe and the absorption spectrum of the acceptor. IFE is involved with the absorption of the quencher overlapped with the excitation (primary inner-filter effect) or emission of the CDs (secondary inner-filter effect) [16,17]. For these reasons, the quenching mechanism can sometimes be confusing. Nevertheless, the obvious difference between them is that energy or electron transfer accompanies the decrease in lifetime. As shown in Fig. 4.13b and Table 4.5, the lifetime of the photon remains the same even after adding the analyte, which can exclude the FRET mechanism. In addition, the lack of a relationship between the energy transfer efficiency and spectral overlap in CDs-nitroaromatics system (Table 4.6) indicates non-FRET quenching.

To verify the IFE-induced quenching mechanism, the observed fluorescence intensity was corrected using the following mathematical models. The Parker and Barnes model is the first model containing a correction of IFE-induced deviation of the fluorescence parameter [23], which considers the geometry and fluorescence observation field [47].

$$F_{corr} = F_{obs} \times f_p \times f_s = F_{obs} \times \frac{2.303A_{ex}(x_2 - x_1)}{10^{-Aex \times x_1} - 10^{-A_{ex} \times x_2}} \times \frac{2.303A_{em}(y_2 - y_1)}{10^{-Aem \times y_1} - 10^{-A_{em} \times y_2}}$$

$$f_p = \frac{2.303A_{ex}(x_2 - x_1)}{10^{-Aex \times x_1} - 10^{-A_{ex} \times x_2}} \quad f_s = \frac{2.303A_{em}(y_2 - y_1)}{10^{-Aem \times y_1} - 10^{-A_{em} \times y_2}}$$

where f_p is the factor for primary IFE involved with excitation and f_s is the factor for secondary IFE from the absorption effect of emission light. The correction factor was calculated using the suggested geometry parameter in the case of a Cary Eclipse spectrophotometer. x_1, x_2, y_1, and y_2 are 0.207, 1.085, 0.258 and 0.727, respectively [48].

Lakowicz suggested a correction of the IFE-induced deviation of the fluorescence intensity using the following equation [22]:

$$F_{corr} = F_{obs} 10^{\frac{A_{ex}+A_{em}}{2}}$$

F_{corr} is the corrected fluorescence intensity. F_{obs} is the experimental fluorescence intensity. A_{ex} is the absorbance value at the excitation wavelength. A_{em} is the absorbance value at the emission wavelength. This can be used generally because it avoids considering the instrument geometry, which is not provided by the manufacturers.

As shown in Figs. 4.13c and 4.14 and summarized in Tables 4.7-4.11, the deviations from linearity converge almost to zero for all nitroaromatic analytes, regardless of the correction equations, which confirms that the quenching of CDs by the nitroaromatic analytes that occurred in this study was due mainly to the inner-filter effect.

The selectivity of nitroaromatics sensing can be achieved using this inner-filter effect. The spectral overlap between the CDs and the analytes is the essential condition for the inner-filter effect. As shown in Table 4.12 and Fig. 4.15a, aniline and m-, o- and p-phenylenediamine exhibit minimal spectral overlap with CDs, despite their similar chemical structures as nitroaromatics, which results in a very low quenching property (Fig. 4.15b). The selectivity depends on their spectral properties of the nitroaromatics compound. For precise recognition, the peaks at 400, 353, 390, 412nm, for 4-NP, DNP, 3-NP and 2-NA, respectively, can be

observed in the absorbance spectra as shown in Fig 4.16. Again, isobestic point methods proposed by El-Ghobashy et al. help to distinguish the nitroaromatic compound when present at the mixture and avoid interference from other absorbed compounds [49].

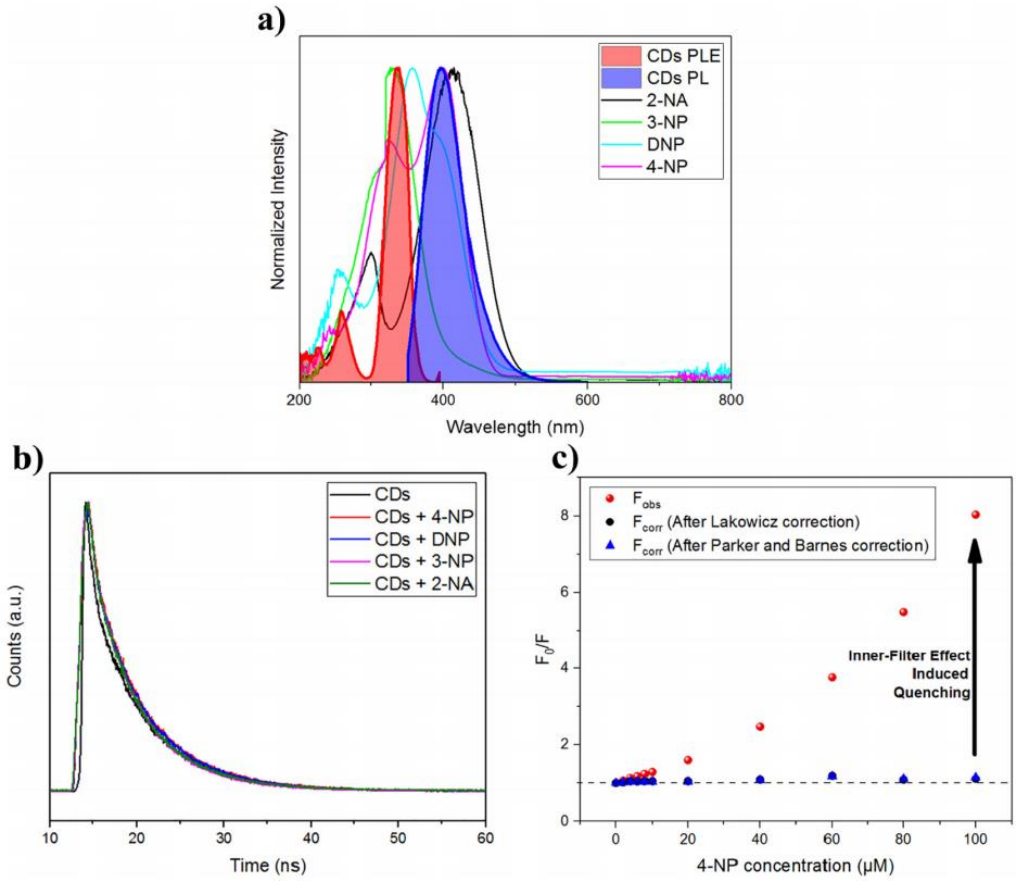

Fig 4.13. (a) Spectra overlap between PL, PLE of CDs, and the absorbance of various nitroaromatics (1000 μM). (b) Time-correlated single-photon counting (TCSPC) of CDs. (c) Inner filter effect (IFE)-corrected fluorescence intensity versus analyte concentration

Table 4.5. Time-correlated single-photon counting (TCSPC) parameters

Analytes	α_1	τ_1	α_2	τ_2	τ_{av}*	τ_0/τ**
CDs	6.57	1.1314	93.43	6.4326	6.3678	-
CDs + 4-NP	6.83	1.5917	93.17	6.3928	6.3067	1.0097
CDs + DNP	8.01	1.8066	91.99	6.4243	6.3139	1.0085
CDs + 3-NP	8.03	1.8102	91.97	5.8406	5.7344	1.1105
CDs + 2-NA	6.42	1.4397	93.58	5.8448	5.7716	1.1033

* τ_{av} is calculated using the following equation:

$$\tau_{av} = \frac{\alpha_1\tau_1^2 + \alpha_2\tau_2^2}{\alpha_1\tau_1 + \alpha_2\tau_2}$$

** τ_0: $\tau_{av}\ of\ CDs\ alone, \tau : \tau_{av}\ of\ (CDs + each\ analyte)$

Table 4.6. Spectral overlap of various nitroaromatics

Parameter	4-NP	DNP	3-NP	2-NA
J ($\times 10^{13}$,$M^{-1}cm^{-1}nm^4$)	33.19	22.34	1.607	4.802
E	0.009595	0.008464	0.09947	0.09363

Data notes:

J (spectral overlap) and **E (energy transfer efficiency)** are calculated by following equation [22]:

$$J = \frac{\int_0^\infty F_D(\lambda)\varepsilon_A(\lambda)\lambda^4 d\,\lambda}{\int_0^\infty F_D(\lambda) d\,\lambda} \quad E = 1 - \tau_o/\tau$$

$F_D(\lambda)$ is fluorescent CDs emission intensity at specific excitation wavlength and $\varepsilon_A(\lambda)$ is absorbance at excitation wavelength and λ is excitation wavelength. $\int_0^\infty F_D(\lambda) d\,\lambda$ is the overall area of fluorescence intensity and used for normalization.

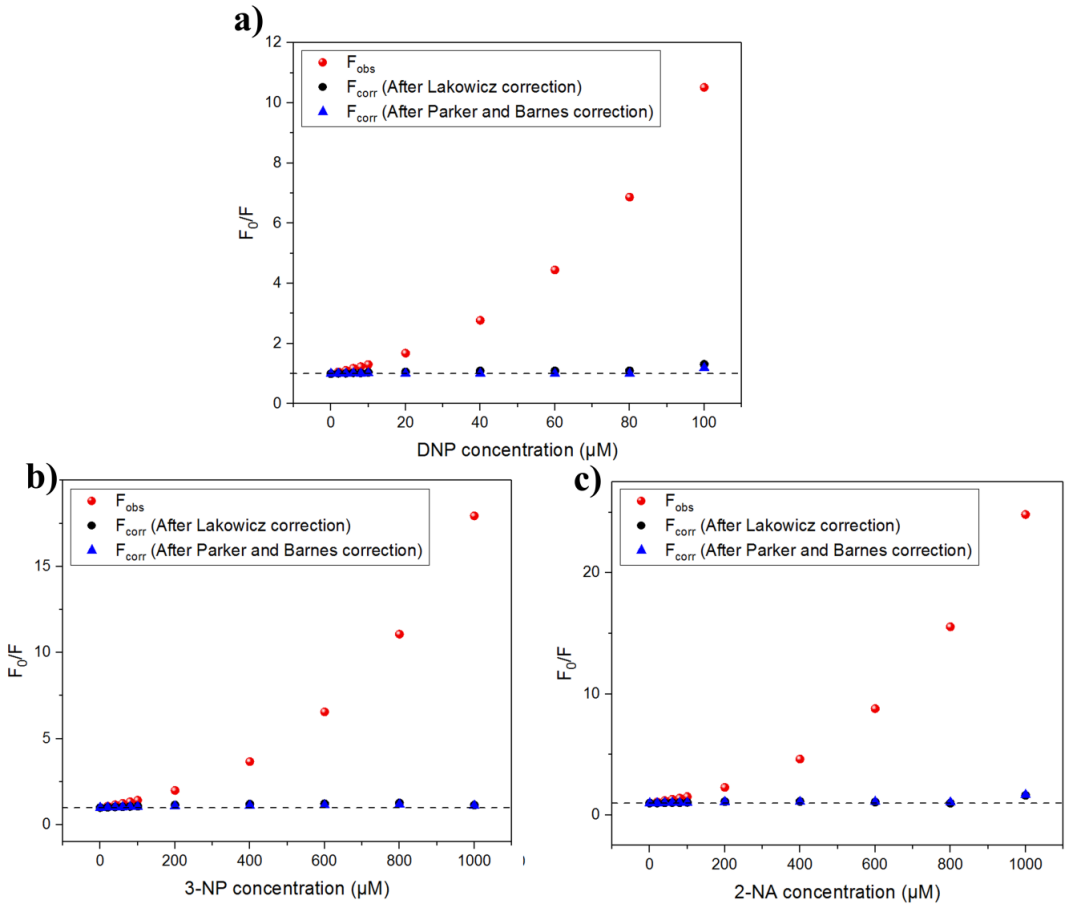

Fig 4.14. Inner filter effect (IFE) corrected fluorescence intensity versus various concentrations of (a) DNP, (b) 3-NP, and (c) 2-NA

Table 4.7. Parker and Barnes correction parameter (4-NP)

4-NP concentration (μM)	f_p	f_s	Correction Factor	F_{obs}	F_{corr}	$F_{obs,0}/F_{obs}$	$F_{corr,0}/F_{corr}$
0	1.172645	0.999	1.17	273.989	321	1	1
2	1.185513	1.03	1.23	257.128	315	1.066	1.02
4	1.190655	1.07	1.27	242.48	308	1.13	1.04
6	1.207658	1.10	1.33	232.216	310	1.18	1.04
8	1.219949	1.14	1.39	220.989	308	1.24	1.04
10	1.228485	1.18	1.45	212.559	309	1.29	1.04
20	1.291465	1.40	1.81	171.214	309	1.60	1.04
40	1.409696	1.89	2.67	111.135	296	2.47	1.08
60	1.544952	2.42	3.74	72.877	272	3.76	1.18
80	1.691417	3.42	5.79	49.902	289	5.49	1.11
100	1.845509	4.44	8.19	34.119	279	8.03	1.15

Table 4.8. Lakowicz correction parameter (4-NP)

4-NP concentration (μM)	A_{ex}	A_{em}	Correction Factor	F_{obs}	F_{corr}	$F_{obs,0}/F_{obs}$	$F_{corr,0}/F_{corr}$
0	0.10829	-0.00006	1.13	273.989	310	1	1
2	0.11582	0.02988	1.18	257.128	304	1.066	1.02
4	0.11881	0.05661	1.22	242.48	297	1.13	1.05
6	0.12862	0.08712	1.28	232.216	298	1.18	1.04
8	0.13564	0.11643	1.34	220.989	295	1.24	1.05
10	0.14048	0.14826	1.39	212.559	296	1.29	1.05
20	0.17535	0.29908	1.73	171.214	296	1.60	1.05
40	0.23715	0.57637	2.55	111.135	284	2.47	1.09
60	0.30278	0.80653	3.59	72.877	261	3.76	1.19
80	0.36870	1.13965	5.68	49.902	283	5.49	1.09
100	0.43317	1.39576	8.21	34.119	280	8.03	1.11

Table 4.9. Fluorescence correction of DNP by IFE mechanism

DNP concentration (μM)	A_{ex}	A_{em}	Correction Factor (Lakowicz)	Correction Factor (Parker and Barnes)	$F_{corr,0}/F_{corr}$ (Lakowicz)	$F_{corr,0}/F_{corr}$ (Parker and Barnes)	$F_{obs,0}/F_{obs}$
0	0.10988	0.00332	1.14	1.18	1	1	1
2	0.12932	0.02276	1.19	1.24	1.01	1.01	1.06
4	0.15059	0.04328	1.25	1.31	1.01	1.00	1.11
6	0.16786	0.0622	1.30	1.37	1.03	1.01	1.18
8	0.18854	0.08464	1.37	1.45	1.03	1.01	1.23
10	0.20777	0.10156	1.43	1.52	1.04	1.01	1.30
20	0.30948	0.20544	1.81	1.96	1.06	1.01	1.68
40	0.50836	0.41487	2.89	3.24	1.09	1.01	2.77
60	0.70734	0.62442	4.63	5.25	1.09	1.00	4.45
80	0.90169	0.80504	7.13	8.07	1.10	1.00	6.87
100	1.10802	0.81395	9.14	10.4	1.31	1.20	10.52

Table 4.10. Fluorescence correction of 3-NP by IFE mechanism

3-NP concentration (μM)	A_{ex}	A_{em}	Correction Factor (Lakowicz)	Correction Factor (Parker and Barnes)	$F_{corr,0}/F_{corr}$ (Lakowicz)	$F_{corr,0}/F_{corr}$ (Parker and Barnes)	$F_{obs,0}/F_{obs}$
0	0.09522	-0.00268	1.11	1.15	1	1	1
20	0.11676	0.03092	1.19	1.23	1.01	1.01	1.08
40	0.13485	0.05404	1.24	1.30	1.04	1.02	1.16
60	0.15693	0.08704	1.32	1.39	1.05	1.03	1.25
80	0.17472	0.11386	1.39	1.47	1.06	1.04	1.33
100	0.19404	0.14121	1.47	1.56	1.08	1.05	1.42
200	0.29034	0.28286	1.93	2.09	1.14	1.09	1.99
400	0.49037	0.57391	3.41	3.76	1.20	1.12	3.67
600	0.68831	0.86259	5.96	6.60	1.22	1.14	6.55
800	0.87658	1.10182	9.75	10.7	1.26	1.19	11.07
1000	1.07506	1.40902	17.5	18.4	1.14	1.12	17.93

Table 4.11. Fluorescence correction of 2-NA by IFE mechanism

2-NA concentration (μM)	A_{ex}	A_{em}	Correction Factor (Lakowicz)	Correction Factor (Parker and Barnes)	$F_{corr,0}/F_{corr}$ (Lakowicz)	$F_{corr,0}/F_{corr}$ (Parker and Barnes)	$F_{obs,0}/F_{obs}$
0	0.09372	-0.00528	1.11	1.14	1	1	1
20	0.10762	0.04744	1.20	1.24	1.01	1.01	1.09
40	0.12222	0.10041	1.29	1.34	1.03	1.02	1.20
60	0.13547	0.15402	1.40	1.45	1.04	1.03	1.31
80	0.14930	0.20162	1.50	1.56	1.04	1.03	1.41
100	0.16317	0.24939	1.61	1.68	1.06	1.04	1.53
200	0.22251	0.48974	2.27	2.38	1.12	1.10	2.29
400	0.37670	0.93131	4.51	4.72	1.14	1.12	4.63
600	0.50824	1.39577	8.95	9.05	1.09	1.11	8.79
800	0.64536	1.83668	17.4	16.7	0.988	1.06	15.54
1000	0.78241	1.66782	16.8	16.8	1.64	1.69	24.81

Table 4.12. Spectral overlap calculation between the excitation and emission spectra of the CDs and absorbance spectra of the nitroaromatics

Parameter*	4-NP	DNP	3-NP	2-NA	p-PD	o-PD	m-PD	aniline
J_{ex}	5750	7780	1560	619	290	98	68	53
J_{em}	12766	9057	643	1727	45	0.17	-2.60	-1.94
J′	18516	16837	2203	2346	335	97.8	65.4	51.4

Data Notes:

J_{ex} (spectral overlap from excitation spectra) and J_{em} (spectral overlap from excitation spectra) are defined as:

$$J' = J_{ex} + J_{em} = \frac{\int_0^\infty F_{ex}(\lambda)\varepsilon(\lambda)d\,\lambda}{\int_0^\infty F_{ex}(\lambda)d\,\lambda} + \frac{\int_0^\infty F_{em}(\lambda)\varepsilon(\lambda)d\,\lambda}{\int_0^\infty F_{em}(\lambda)d\,\lambda}$$

$$J_{ex} = \frac{\int_0^\infty F_{ex}(\lambda)\varepsilon(\lambda)d\,\lambda}{\int_0^\infty F_{ex}(\lambda)d\,\lambda} \quad J_{em} = \frac{\int_0^\infty F_{em}(\lambda)\varepsilon(\lambda)d\,\lambda}{\int_0^\infty F_{em}(\lambda)d\,\lambda}$$

$F_{ex}(\lambda)$ is the intensity of the fluorescence excitation spectra and $F_{em}(\lambda)$ is the intensity of the emission spectra. $\varepsilon(\lambda)$ is the absorbance at the excitation wavelength. $\int_0^\infty F_{ex}(\lambda)d\,\lambda$ and $\int_0^\infty F_{em}(\lambda)d\,\lambda$ are used for normalization.

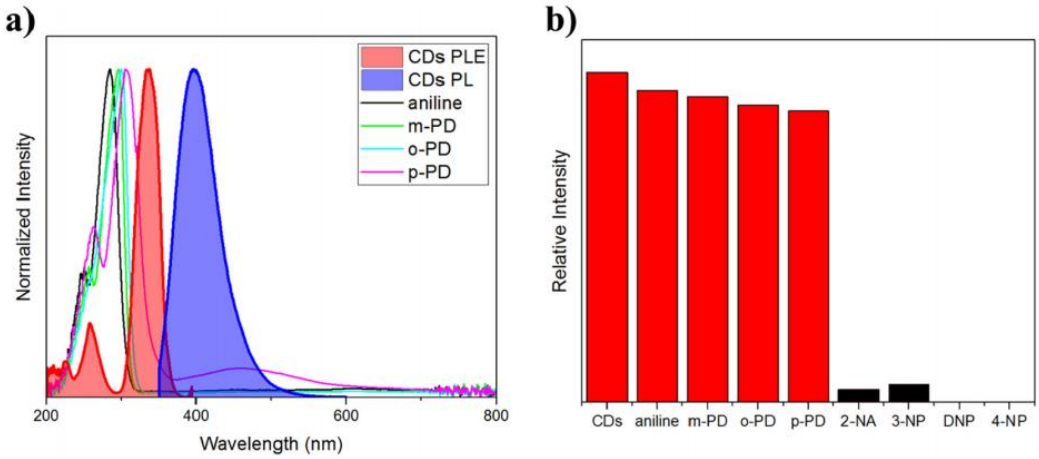

Fig 4.15. (a) Spectra overlap between PL, PLE of CDs, and the absorbance of phenylenediamine isomers (1000 μM). (b) Relative PL intensity change of CDs for various analytes (1000 μM)

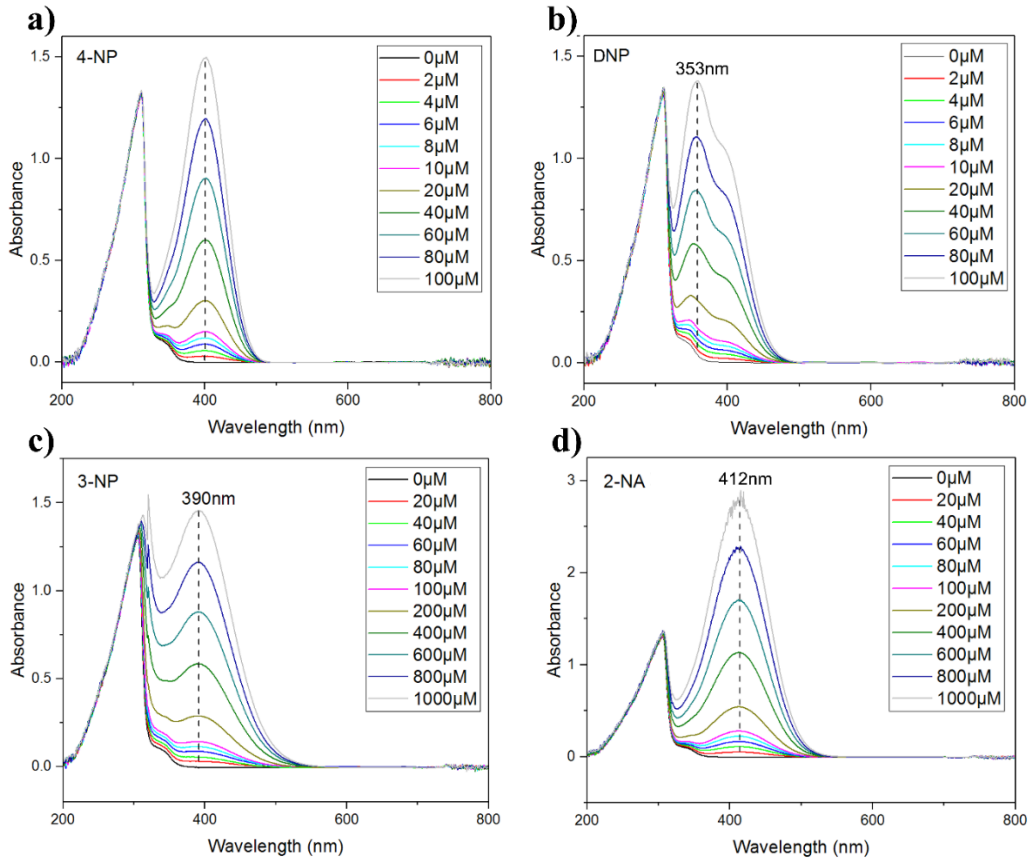

Fig 4.16. Absorbance spectra of CDs at various nitroaromatics concentration (0-100, 0-1000μM)

4.3.5. Conclusions

Highly luminescent CDs were fabricated using novel precursors of citric acid and uric acid by facile hydrothermal synthesis. The as-synthesized CDs could detect a range of nitroaromatics by the IFE mechanism. Mathematical correction and lifetime measurements showed that PL quenching occurred by the IFE instead of the FRET mechanism. In addition, spectral overlap between the CDs and analytes was the critical parameter rather than the specific interaction between the CDs and analyte during the quenching process, which resulted in excellent selectivity towards interfering molecules and a wide range of nitroaromatic detections.

References

[1] K.S. Ju, R.E. Parales, Nitroaromatic Compounds, from Synthesis to Biodegradation, Microbiol. Mol. Biol. Rev 74 (2010) 250-272.

[2] Agency for Toxic Substances and Disease Registry (ATSDR). Toxicological Profile for Dinitrophenols. Public Health Service, U.S. Department of Health and Human Services, Atlanta, GA. 1992.

[3] Agency for Toxic Substances and Disease Registry (ATSDR). Toxicological Profile for Dinitrophenols. Public Health Service, U.S. Department of Health and Human Services, Atlanta, GA. 2019.

[4] U.S. EPA. Provisional Peer-Reviewed Toxicity Values for Nitroaniline, 2-. U.S. Environmental Protection Agency, Washington, DC, EPA/690/R-09/036F, 2009.

[5] H. Soni, P. Padmaja, Liquid crystalline multilayer graphene quantum dots with hackelite structures: Characterisation and application for sensing nitrophenols, Sens. Actuator B-Chem. 268 (2018) 100–107.

[6] X. Tian, H. Peng, Y. Li, C. Yang, Z. Zhou, Y. Wang, Highly sensitive and selective paper sensor based on carbon quantum dots for visual detection of TNT residues in groundwater, Sens. Actuator B-Chem. 243 (2017) 1002–1009.

[7] H. Yuan, D. Li, Y. Liu, X. Xub, C. Xiong, Nitrogen-doped carbon dots from plant cytoplasm as selective and sensitive fluorescent probes for detecting p-nitroaniline in both aqueous and soil systems, Analyst 140 (2015) 1428-1431.

[8] S.Y. Lim, W. Shen, Z. Gao, Carbon quantum dots and their applications, Chem. Soc. Rev. 44 (2015) 362-381.

[9] Y. Wang, A. Hu, Carbon quantum dots: synthesis, properties and applications, J. Mater. Chem. C 2 (2014) 6921-6939.

[10] L.M. Shen, J. Liu, New development in carbon quantum dots technical applications, Talanta 156-157 (2016) 245–256.

[11] M.J. Molaei, A review on nanostructured carbon quantum dots and their applications in biotechnology, sensors, and chemiluminescence, Talanta 196 (2019) 456–478.

[12] F. Gao, S. Ma, J. Li, K. Dai, X. Xiao, D. Zhao, W. Gong, Rational design of high quality citric acid-derived carbon dots by selecting efficient chemical structure motifs, Carbon 112 (2017) 131-141.

[13] B. Kong, A. Zhu, C. Ding, X. Zhao, B. Li, Y. Tian, Carbon Dot-Based Inorganic–Organic Nano system for Two-Photon Imaging and Biosensing of pH Variation in Living Cells and Tissues, Adv. Mater. 24 (2012) 5844–5848.

[14] D. Qu, M. Zheng, L. Zhang, H. Zhao, Z. Xie, X. Jing, R.E. Haddad, H. Fan, Z. Sun. Formation mechanism and optimization of highly luminescent N-doped graphene quantum dots, Sci Rep. 4 (2014) 5294 1-11.

[15] J. Wu, W. Liu, J. Ge, H. Zhang, P. Wang, New sensing mechanisms for design of fluorescent chemosensors emerging in recent years, Chem. Soc. Rev. 40 (2011) 3483–3495.

[16] F. Zu, F. Yan, Z. Bai, J. Xu, Y. Wang, Y. Huang, X. Zhou, The quenching of the fluorescence of carbon dots: A review on mechanisms and applications, Microchim. Acta 184 (2017) 1899–1914

[17] S. Chen, Y.L. Yu, J.H. Wang, Inner filter effect-based fluorescent sensing systems: A

review, Anal. Chim. Acta 999 (2018) 13-26

[18] H.W. Yang, P. Xu, B. Ding, Z.Y. Liu, X.J. Zhao, E.C. Yang, A Highly Stable Luminescent Eu-MOF Exhibiting Efficient Response to Nitrofuran Antibiotics through the Inner Filter Effect and Photoinduced Electron Transfer, Eur. J. Inorg. Chem. 2019 (2019) 5077–5084

[19] A. Cayuela, M.L. Soriano, M. Valcárcel, Reusable sensor based on functionalized carbon dots for the detection of silver nanoparticles in cosmetics via inner filter effect 872 (2015) 70-76

[20] L. Sai, X. Wang, Q. Chang, W. Shi, L. Huang, Selective determination of acetone by carbon nanodots based on inner filter effect, Spectroc. Acta Pt. A-Molec. Biomolec. Spectr. 216 (2019) 290-295

[21] H. Fan, G.Q. Xiang, Y. Wang, H. Zhang, K. Ning, J. Duan, L. He, X. Jiang, W. Zhao, Manganese-doped carbon quantum dots-based fluorescent probe for selective and sensitive sensing of 2,4,6-trinitrophenol via an inner filtering effect, Spectroc. Acta Pt. A-Molec. Biomolec. Spectr. 205 (2018) 221-226

[22] Albrecht, C. Joseph R. Lakowicz, Principles of Fluorescence Spectroscopy, 3rd Edition. Springer (2007).

[23] C.A. Parker, W.J. Barnes, Some experiments with spectrofluorimeters and filter fluorimeters, Analyst 82 (1957) 606-618.

[24] S. Zhu, Y. Song, X. Zhao, J. Shao, J. Zhang, B. Yang, The photoluminescence mechanism in carbon dots (graphene quantum dots, carbon nanodots, and polymer dots): current state and future perspective, Nano Res. 8 (2015) 355–381.

[25] F. Yuan, Z. Wang, X. Li, Y. Li, Z. Tan, L. Fan, S. Yang, Bright Multicolor Bandgap Fluorescent Carbon Quantum Dots for Electroluminescent Light-Emitting Diodes, Adv. Mater. 29 (2017) 1604436 1-6.

[26] S.K. Cushing, M. Li, F. Huang, N. Wu, Origin of Strong Excitation Wavelength Dependent Fluorescence of Graphene Oxide, ACS Nano 8 (2014) 1002-1013.

[27] Y. Zhang, R. Yuan, M. He, G. Hu, J. Jiang, T. Xu, L. Zhou, W. Chen, W. Xiang, X. Liang, Multicolour nitrogen-doped carbon dots: tunable photoluminescence and sandwich fluorescent glass-based light-emitting diodes, Nanoscale 9 (2017) 17849-17858.

[28] K. Hola, M. Sudolska, S. Kalytchuk, D. Nachtigallova, A.L. Rogach, M. Otyepka, R. Zboril, Graphitic Nitrogen Triggers Red Fluorescence in Carbon Dots, ACS Nano 11 (2017) 12402–12410.

[29] S.H. Jin, D.H. Kim, G.H. Jun, S.H. Hong, S.Jeon, Tuning the Photoluminescence of Graphene Quantum Dots through the Charge Transfer Effect of Functional Groups, ACS Nano 7 (2013) 1239-1245.

[30] Q.Q. Shi, Y.H. Li, Y. Xu, Y. Wang, X.B. Yin, X.W. He, Y.K. Zhang. High-yield and high-solubility nitrogen-doped carbon dots: formation, fluorescence mechanism and imaging application, RSC Adv. 4 (2014) 1563-1566.

[31] S. Kumar, A.K. Ojha, B. Ahmed, A. Kumar, J. Das, A. Materny, Tunable (violet to green) emission by high-yield graphene quantum dots and exploiting its unique properties towards sun-light-driven photocatalysis and supercapacitor electrode materials, Materials Today Communications 11 (2017) 76–86

[32] Y. Cai, W. Wang, L. Li, Z. Wang, S. Wang, H. Ding, Z. Zhang, L. Sun, W. Wang, Effective

Capture of Carbon Dioxide Using Hydrated Sodium Carbonate Powders, Materials 11 (2018) 183

[33] J.P. Lukaszewicz, M. Panas, J. Siedlewski, Sodium-doped carbon films for humidity sensor construction, Sens. Actuator B-Chem. 32 (1996) 221-226.

[34] D. Qu, M. Zheng, J. Li, Z. Xie, Z. Sun. Tailoring color emissions from N-doped graphene quantum dots for bioimaging applications, Light-Sci. Appl. 4 (2015) 364.

[35] Y.K. Jung, E. Shin, B.S. Kim, Cell Nucleus-Targeting Zwitterionic Carbon Dots, Sci Rep. 5 (2015) 18807

[36] C. Li, W. Liu, Y. Ren, X. Sun, W. Pan, J. Wang, The selectivity of the carboxylate groups terminated carbon dots switched by buffer solutions for the detection of multi-metal ions, Sens. Actuator B-Chem. 240 (2017) 941–948.

[37] L.Lin, M. Rong, S. Lu, X. Song, Y. Zhong, J. Yan, Y. Wanga, X. Chen, A facile synthesis of highly luminescent nitrogen doped graphene quantum dots for the detection of 2,4,6-trinitrophenol in aqueous solution, Nanoscale 7 (2015) 1872-1878.

[38] H. Zeng, G. Durocher, Analysis of fluorescence quenching in some antioxidants from non-linear Stern-Volmer plots, J. Lumines. 63 (1995) 75-84.

[39] T. Hao, X. Wei, Y. Nie, Y. Xu, Y. Yan, Z. Zhou, An eco-friendly molecularly imprinted fluorescence composite material based on carbon dots for fluorescent detection of 4-nitrophenol, Microchim. Acta 183 (2016) 2197-2203

[40] C. Li, Y. Zheng, H. Ding, H. Jiang, X. Wang, Chromium(III)-doped carbon dots: fluorometric detection of p-nitrophenol via inner filter effect quenching, Microchim. Acta 186

(2019) Article number: 384

[41] N. Xiao, S.G. Liu, S. Mo, N. Li, Y.J. Ju, Y. Ling, N.B. Li, H.Q. Luo, Highly selective detection of p-nitrophenol using fluorescence assay based on boron, nitrogen co-doped carbon dots, Talanta 184 (2018) 184–192

[42] L. Han, S.G. Liu, J.Y. Liang, Y.J. Ju, N.B. Li, H.Q. Luo, pH-mediated reversible fluorescence nanoswitch based on inner filter effect induced fluorescence quenching for selective and visual detection of 4-nitrophenol, J. Hazard. Mater. 362 (2019) 45–52.

[43] M. Tian, Y. Liu, Y. Wang, Y. Zhang, Yellow-emitting carbon dots for selective detecting 4-NP in aqueous media and living biological imaging, Spectroc. Acta Pt. A-Molec. Biomolec. Spectr. 220 (2019) 117117

[44] K. Qin, D. Zhang, Y. Ding, X. Zheng, Y. Xiang, J. Hua, Q. Zhang, X. Ji, B. Li, Y. Wei, Applications of hydrothermal synthesis of Escherichia coli derived carbon dots in in vitro and in vivo imaging and p-nitrophenol detection, Analyst 145 (2020) 177-183

[45] X. Yuan, Y. Tu, W. Chen, Z. Xu, Y. Wei, K. Qin, Q. Zhang, Y. Xiang, H. Zhang, X. Ji, Facile synthesis of carbon dots derived from ampicillin sodium for live/dead microbe differentiation, bioimaging and high selectivity detection of 2,4-dinitrophenol and Hg(II), Dyes Pigment 175 (2020) Article number: 108187

[46] A. Cayuela, M.L. Soriano, M. Valcárcel, Strong luminescence of Carbon Dots induced by acetone passivation: Efficient sensor for a rapid analysis of two different pollutants, Anal. Chim. Acta 804 (2013) 246-251.

[47] S.K. Panigrahi, A.K. Mishra, Inner filter effect in fluorescence spectroscopy: As a problem and as a solution, J. Photochem. Photobiol. C-Photochem. Rev. 41 (2019) 100318

[48] A. Kasparek, B. Smyk, A new approach to the old problem: Inner filter effect type I and II in fluorescence, Spectroc. Acta Pt. A-Molec. Biomolec. Spectr. 198 (2018) 297-303.

[49] M.R. El-Ghobashy, N.F. Abo-Tali, Spectrophotometric methods for the simultaneous determination of binary mixture of metronidazole and diloxanide furoate without prior separation, Journal of Advanced Research 1 (2010) 323-329

[50] L. Tian, D. Ghosh, W. Chen, S. Pradhan, X. Chang, S. Chen, Nanosized Carbon Particles From Natural Gas Soot, Chem. Mat. 21 (2009) 2803-2809.

[51] K. Haubner, J. Murawski, P. Olk, L.M. Eng, C. Ziegler, B. Adolphi, E. Jaehne, The Route to Functional Graphene Oxide, ChemPhysChem 11 (2010) 2131-2139.

[52] M.A. Buccheri, D. D'Angelo, S. Scalese, S.F. Spano, S. Filice, E. Fazio, G. Compagnini, M. Zimbone, M.V. Brundo, R. Pecoraro, A. Alba, F. Sinatra, G. Rappazzo, V. Privitera, Modification of graphene oxide by laser irradiation: a new route to enhance antibacterial activity, Nanotechnology 27 (2016) 245704 1-12.

Chapter 5. Summary

The properties of the CDs, such as non-toxicity and photostability are not fully understood. We mostly assume that the CDs have sp^2 clusters because they are not burnt by the electron beam when using TEM (200 kV). However, we do not know the required conditions. It is also uncertain how many aromatic clusters are needed and if their aromatic polymer structure is burnt or not. This information can only be obtained from an atomic resolution image. However, it is speculated that the CDs have a few aromatic structures and layers, such as four or five multi-layers with five aromatic rings surrounded by an aromatic short polymer chain. The aromatic part is much smaller than expected. Despite this uncertainty, the CDs have been extensively used because of their high extinction coefficient and high quantum yield. Currently, it is difficult to determine the formation and photoluminescence mechanisms. Therefore, the properties of CDs cannot be rationally designed. Consequently, the CDs always have blue emission, short wavelength, and high energy. Furthermore, the stereospecific property of the CDs is difficult to understand. The NHS-EDC coupling can be used to change the surface, such as linking phenyl boronic acid, which can interact or bond with glucose and dopamine. However, the kind of CDs that can detect glucose or dopamine is not known. We believe that a deep understanding of the organic chemistry is needed for the synthesis of the CDs from an artificial graphene layer and the production of a graphene layer using a bottom-up approach to synthesize a perfect graphene layer.

The most important advantage of fluorescence sensors is their rapid response from a short lifetime and fast light velocity. We also considered other light and matter interactions. The Raman scattering had a shorter lifetime (femto second). It is better compared to fluorescence as it has a shorter signal time and does not cause biological fluorescence in nature, such as

tryptophan fluorescence in protein. The fluorescence sensor technology should develop such that a paper (cellulose, cheap material) can be coated with a small amount of fluorescent material and then hazardous materials or diseases can be detected. In other words, cheap sensors must be developed to help the poor live longer. This is the future of fluorescence sensor technology, not phosphorescence and Raman scattering.

However, fluorescence is not always the best method. Each method is best used to detect a specific hazardous molecule or disease. Electromagnetic waves are exploited in developing property analysis using instrumental analysis. When fluorescence is not suitable, the electromagnetic waves are used to diagnose diseases through methods, such as magnetic resonance imaging (MRI), computed tomography (CT), and positron emission tomography (PET). However, the fluorescence sensor technology, which mostly uses molecular recognition techniques, can be combined with bio-instrumental analysis.

The fluorescence sensors normally exploit quenching for signaling through mechanisms, such as PET, ICT, MLCT, TICT, EET, FRET, and excimer/exciplex formation. The quenching mechanism has been extensively studied to increase the sensitivity or in other words, the quenching power. The inner-filter effect can be used for quenching and signaling. However, this is normally an instrument error, and there have been many attempts to avoid this effect. Therefore, it is important to adjust the fluorescence angle (ultimately the fluorescence field) and constitution of the instrument to optimize the signal.

In this study, we investigated the precursor design to obtain improved fluorescence properties and sensing performance. The fluorescence sensing ability could be controlled by adjusting the precursor or surface passivation in a carbon dot system. For example, indole plays an important role in the detection of thioamide and shows remarkable quenching through PET. The optical

properties (fluorescence) were highly affected by the solvent or pH and other environmental conditions, which have been systematically studied in view of physical chemistry such as solvent relaxation. A mathematical calculation was performed to prove that a signal (quenching) can be obtained through the inner-filter effect in a specific system, nitroaromatics, and CDs. The inner-filter effect was exploited for signaling. However, it is better to minimize this effect.

List of publications

1. **Hye Jin Lee**, Jayasmita Jana, Jin Suk Chung, Seung Hyun Hur, Uncovering the actual Inner-filter Effect between highly efficient carbon dots and nitroaromatics, *Spectrochimica Acta Part A: Molecular and Biomolecular Spectroscopy 236 (2020) 118342*

2. **Hye Jin Lee**, Jayasmita Jana, Jin Suk Chung, Seung Hyun Hur, Fabrication of dual emission carbon dots and its use in highly sensitive thioamide detection, *Dyes and Pigments 175 (2020) 108126*

3. **Hye Jin Lee**, Jayasmita Jana, Yen-Linh Thi Ngo, Lin Lin Wang, Jin Suk Chung, Seung Hyun Hur, The effect of solvent polarity on emission properties of carbon dots and their uses in colorimetric sensors for water and humidity, *Materials Research Bulletin 119 (2019) 110564*

4. Jayasmita Jana, **Hye Jin Lee**, Jin Suk Chung, Mun Ho Kim, Seung Hyun Hur, Blue emitting nitrogendoped carbon dots as a fluorescent probe for nitrite ion sensing and cell-imaging, *Analytica Chimica Acta 1079 (2019) pp. 212-219*